The Role of Spectrosome and Centrosome in Asymmetric Stem Cell Division

BY

CHI BANG
B.S., University of California at San Diego, 2003
M.S., City College of New York, 2006

THESIS

Submitted as partial fulfillment of the requirements
for the degree of Doctor of Philosophy in Bioengineering
in the Graduate College of the
University of Illinois at Chicago, 2015

Chicago, Illinois

Defense Committee:

Jun Cheng, Chair and Advisor
Michael Cho
David Eddington
David Featherstone, Biological Sciences
Vuk Uskoković

To my family who have provided me with unwavering support and immeasurable love.

ACKNOWLEDGEMENTS

I kindly thank you Dr. Jun Cheng for your mentorship, your time, and your genuine care as my thesis advisor. I would also like to thank you my Ph.D. committee members, Drs. Michael Cho, David Eddington, David E. Featherstone, and Vuk Uskoković for your time, support, and guidance. I am very grateful for obtaining this opportunity to have worked with you.

I sincerely thank you my collaborators and mentors who have given me valuable research experiences and mentorships, including: Drs. Liang-Wei Gong and Lihua Yao for working on the Lauridan and actin polymerization experiments; Drs. Ying Liu and Hao Shen for working on the Circumin experiments; and Dr. Jason X.-J. Yuan for being on my pre-thesis committee and giving me valuable research guidance and encouragement.

I sincerely thank the Bloomington *Drosophila* Stock Center for providing me with guidance and necessary *Drosophila* stocks and Drs. A. Spradling, Y. Cai, and J. Raff for fly stocks. I also thank the Developmental Studies Hybridoma Bank and Drs. J. Raff and M. Bienz for antibodies.

I sincerely thank all the Bioengineering staff Susan Lee, Jay Lin, Jessica Terrones, Yin Zhong, and Lukasz Zientara for your kind support. With you, my days were much brighter and my life much fuller. I give big thanks from me to you.

I sincerely thank all past and present members of Dr. Jung Cheng's laboratory, which include: Nikhil Bommakanti, Grace Brown, Shilpa Colachina, Marisa Doria, Emerald E. Fikejs, Anthony E. Fielder, Danielle Madsen, Andre D. Paredes, Wei Shen, and Zhinan Wang. It was a

pleasure getting to know each of you. Your support, friendship, intellectual discussions, and your care all have provided for an enriching and fun working environment. I wish you all best of luck in all your future endeavors.

This research was partially funded by the Chicago Biomedical Consortium with support from the Searle Funds at the Chicago Community Trust.

TABLE OF CONTENTS

TABLE OF CONTENTS (continued)

CHAPTER PAGE

TABLE OF CONTENTS (continued)

CHAPTER PAGE

TABLE OF CONTENTS (continued)

CHAPTER PAGE

LIST OF FIGURES

FIGURE PAGE

LIST OF FIGURES (continued)

FIGURE PAGE

LIST OF ABBREVIATIONS OR NOMENCLATURE

2-D	Two dimensions
3-D	Three dimensions
APC	Adenomatosis polyposis coli
APC2	Adenomatosis polyposis coli 2
aPKC	Atypical protein kinase C
BAM	Bag of marble
BAZ	Bazooka
BDSC	Bloomington *Drosophila* Stock Center
BMP	Bone morphogenetic protein
CCD	Charge coupled detector
Cdk	Cycline-dependent kinase
CHO	Chinese hamster ovary cells
CNB	Centrobin
cnn	Centrosomin
CySC(s)	Cyst stem cells
DIC	Differential Interference Contrast
DSHB	Developmental Studies Hybridoma Bank
Dvl	Dishevelled
EB1	End binding 1
ECM	Extracellular matrix
Eg5	Motor protein kinesin-5
FasIII	Fasciclin III

LIST OF ABBREVIATIONS OR NOMENCLATURE (continued)

FBS	Fetal Bovine Serum
FLP	Flippase
FRT	Flippase recombination target
GB	Gonialblast
GFP	Green fluorescent protein
GSC(s)	Germline stem cell(s)
hr	Hour
Hs	Heat shock
Hts	huli-tai shao
igG	Immunoglobulin
JAK-STAT	Janus kinase-Signal Tranducer and Actiator of Transcription
Lis1	Lissencephaly gene
MARCM	Mosaic Analysis with a Repressible Cell Marker
Mch	M-cherry
min	Minute
MT	Microtubule
MTOC	Microtubule organizing center
NA	Numerical aperture
NE-dynein	Nuclear envelope associated dynein
PACT	Pericentrin-like protein
PBS	Phosphate buffer saline
PBST	Phosphate buffer saline with Triton X-100

LIST OF ABBREVIATIONS OR NOMENCLATURE (continued)

PCM	Pericentriolar matrix
PEF	Polar-ejection force
Pen-Strep	Penicillin Streptomycin
Plk1	Polo-like kinase 1
RNAi	Interference ribonucleic acid
ROI	Region of Interest
Shadd	Short adducing
Spd-2	Spindle defective protein
UAS	Upstream activation sequence
Upd	Unpaired
UV	Ultraviolet
Wnt	Wingless
α-tub	Alpha tubulin
γ-tub	Gamma tubulin

SUMMARY

Stem cells have remarkable characteristics that allow them to maintain their population through self-renewal and allow them to replenish lost tissue/cells through both self-renewal and differentiation. These self-renewal and differentiation processes, however, are tightly regulated and balanced in the stem cell systems to maintain tissue homeostasis. It has been shown previously that asymmetric stem cell division may be one of the key regulators in balancing the self-renewal and differentiation fates (Fuller and Spradling 2007, Yamashita 2010). The idea of asymmetric stem cell division balancing the self-renewal and differentiation is simple. When the stem cells divide asymmetrically, by polar orientation, daughter cells that are displaced from the stem cell niche are differentiated, devoid of signals from the niche that instruct the stem cells to maintain their identities. There are two ways the asymmetric stem cell divisions are regulated. One way is through the influence by the external environment (extrinsic regulator), such as stem cell positioning, proximity to the stem cell niche, and interaction with the stem cell niche. Other way is through the regulation of internal cellular machinery (intrinsic regulator), such as localization of fate determinant polarity proteins and spindle orientation, which ultimately determine the cleavage plane orientation (Eggert, Mitchison et al. 2006). Our study focuses on the intrinsic regulators and how they regulate the outcome of stem cell fates (self-renewal or differentiation) in male Drosophila melanogaster germline stem cells (GSCs). It has been reported that there are many key players that influences the orienting of the mitotic spindle, which include centrosomes, spectrosomes, pericentriolar matrix (PCM), astral microtubules, Adenomatous Polyposis Coli Protein 2 (APC2), and more (Deng and Lin 1997, Yamashita, Jones et al. 2003, Inaba, Yuan et al. 2010). Spectrosome is an endoplasmic reticulum-like organelle in the female GSCs that always localized to the apical cortex of the GSCs and played a critical role

in orienting the mitotic spindle (Deng and Lin 1997). Function of PCM and astral microtubules (MT) on the spindle orientation were partly observed through a mutation of centrosomin proteins (*Cnn-mut*) (Yamashita, Jones et al. 2003, Inaba, Yuan et al. 2010). Centrosomin is a general component of the centrosome and spindle poles that may act as a scaffold during early formation of the microtubule organizing center (MTOC) (Megraw, Li et al. 1999, Vaizel-Ohayon and Schejter 1999). Adenomatous Polyposis Coli Protein 2, on the other hand, is an adhesion protein that is proposed to couple astral microtubules of the mitotic spindle pole to the apical cortex of the GSCs (Yamashita, Jones et al. 2003, Inaba, Yuan et al. 2010). Our investigation focuses are twofold: 1) to elucidate how centrosome (via DSas-4 mutation) and spectrosome (via huli-tai shao mutation) interact to regulate the asymmetric stem cell division outcome and 2) how PCM/astral MT (via cnn mutation) and APC2 (via APC2-mut) participate in the regulation of asymmetric stem cell divisions in conjunction with spectrosome and non-functional centrosomes. Using conventional immunohistochemistry, live-cell live-imaging, and particle tracking method (centrosomes and spectrosomes), dynamical data (velocity, distance, spindle angles, spindle angular velocities) and morphological data were used to address the questions raised above.

Dynamic Interplay of Spectrosome and Centrosome Organelles in Asymmetric Stem Cell Divisions

Interesting observations were made when centrosomes were knocked out using the DSas-4 mutation in male *Drosophila* GSCs. The mitotic poles of the GSCs (*DSas-4-mut*) formed independently of centrosomes and the majority of spindles were still oriented. Furthermore, the

live imaging data showed that, with the centrosome knocked out, majority of the spectrosomes switched sides from the basal cortex to the apical cortex (closer to the hub-GSC) and became immobilized. This apical localization and immobilization of spectrosome is the normal characteristics in wild type female GSCs, where it was shown that the spectrosome acts as a physical anchor between the cortex and the mitotic spindle pole. In addition, when spindles were severely misoriented (greater than 45 degrees), majority of the spectrosomes were also found in the apical region (near the hub-GSC interface). Based on these data, we hypothesized that the spectrosome acts as a fail-safe mechanism to orient the spindle when the centrosome is not present. Moreover, we found out that the spindle orientation and asymmetric GSC stem cell division is not affected when the spectrosome was knocked out. Which suggests the spectrosome is dispensable when the centrosomes are present. However, with the spectrosome knocked out dynamical changes occurred such as centrosome velocity and distance, which suggests that there are dynamical interplay occurring between the spectrosome and centrosome. During the experiments, we also found previously undiscovered migration pattern of spectrosome and distribution of spectrosome material between two divided daughter cells.

Effects of Centrosomin and Adenomatous Polyposis Coli Protein 2 on Spectrosome Recruitment and Asymmetric Stem Cell Divisions

The interplay result between the centrosome and spectrosome in the regulation of asymmetric stem cell division raised additional mechanistic questions. We wanted to know what components in the cellular machinery would recruit the spectrosome to the apical side.

Interestingly, the *cnn-mut* GSCs but not *APC2-mut* GSCs recruited the majority of the spectrosomes to the apical cortices as they were in the *DSas-4-mut* GSCs. Furthermore, similar to the *DSas-4-mut* GSCs, the spectrosomes were also immobilized to the apical cortex region in *cnn-mut* GSCs. These results suggested that it is not the lack of centrioles or the lack of spindle microtubule connections to the apical cell cortex (via APC2) that initiated the spectrosome recruitment to the apical side, but rather the missing PCM (or PCM components) and compromised mitotic MTs (astral microtubule) would initiate the spectrosome recruitment. We also found out that the spindle orientation of the *cnn-mut* and *APC2-mut* GSCs were still oriented. This result shows that spectrosome may orient the spindle in absence of PCM/astral MT. Furthermore, based on immunohistochemistry data, spectrosomes were found significantly more in the apical area when the centrosomes were misoriented and in the basal area when the centrosomes were oriented. This result suggests that spectrosome may also play a role in orienting the centrosome, but it is not known what point in time this occurs.

There were also several dynamical changes that occurred in the cnn and APC2 mutants. Firstly, the mitotic duration increased significantly for both *cnn-mut* and *APC2-mut* GSCs, which suggests that the misorientation of centrosome may delay the mitosis. Secondly, the *cnn-mut* GSCs had significantly slower spectrosome velocity and increased centrosome velocity compared to the wild type. This suggests that the spectrosome velocity is slowed due to their immobilization to the apical area and centrosome velocity is increased due to the lack of attachment to the PCM. Thirdly, the APC2-mut GSCs exhibited significantly slower centrosome velocity and slower spindle angular velocity than the wild type.

It is rather difficult to say what may cause the slowing of the centrosome velocity and spindle angular velocity. Our dissertation results can be used as a model to control the fate of other stem cell types and spill into potential applications.

I. INTRODUCTION

A. Background and significance

Stem cells have garnered much scientific and public focus due to their important characteristics such as their ability to self-renew and their potentials to differentiate into various cell types (Morrison, Shah et al. 1997, Watt, Hogan et al. 2000, Morrison and Kimble 2006, He, Nakada et al. 2009). Taking advantage of the important stem cell characteristics coupled with advancement of stem cell knowledge and molecular techniques, various uses of stem cells have been developed for further enhancing knowledge base of basic scientific inquiries to clinical stem cell therapies that can replace functions of lost cells/tissues (Nadig 2009, Trounson, Thakar et al. 2011). There are many different types of adult stem cells discovered and developed for various purposes, which include bone marrow hematopoietic stem cells, bone marrow stromal stem cells, neural stem cells, olfactory stem cells, endothelial stem cells, intestinal stem cells, limbal stem cells, skin stem cells, myogenic progenitor cells, adipose derived adult stem cells, and multipotent adult progenitor cells (Avasthi, Srivastava et al. 2008, Trounson, Thakar et al. 2011, Hsu, Li et al. 2014). According to the National Institute of Health (NIH) and EuroStemCell, potential uses of stem cells may include cell based therapies, drug testing, study of cell/tissue development, and study of diseases. In the clinical settings, there have been significant advances in stem cell based cellular therapies, which include chronic wound repair using mesenchymal stem cells, burned or injured skin repair, corneal regeneration, neurological repair (multiple sclerosis and amyotrophic lateral sclerosis), immunological disease treatment (Chronic Graft Versus Host Disease, rheumatoid arthritis, Crohn's Disease), genetic blood diseases treatment (sickle cell disease) (Chen, Przyborowski et al. 2009, Trounson, Thakar et al. 2011, Li, Wang et al. 2014, Li, Zhao et al. 2015). Despite exciting promises that stem cells offer

for future applications, there remain significant hurdles that can be overcome only through further exhaustive research.

B. Maintenance of tissue homeostasis

There have been numerous reports that the stem cells play an integral role in maintaining the tissue homeostasis (Blanpain and Fuchs 2009, Biteau, Hochmuth et al. 2011, Simons and Clevers 2011). Such as an event of tissue damage, the stem cells proliferate and differentiate to replenish the lost tissue without over proliferating and over differentiating, and thus the balance finely regulated (Biteau, Hochmuth et al. 2011, Singh 2012, Herrera, Martin et al. 2013, Rabelink and Little 2013, Zebrowski and Engel 2013). However, there are deleterious instances when the stem cells malfunction. The stem cell can become unresponsive to regulative signals and over differentiate, not proliferate, and not self-renew, which may lead to tissue degeneration/aging (Van Zant and Liang 2003, Kirkwood 2005, Brunet and Rando 2007, Liu and Rando 2011, Sacco and Puri 2015). On the contrary, excessive self-renewal of stem cells may lead to over proliferation (PARDAL, MOLOFSKY et al. 2005, Clarke and Fuller 2006) and tumor/cancer (Groden, Thliveris et al. 1991, Radtke and Clevers 2005). Further elucidation of regulative mechanisms in stem cells that balance tissue homeostasis would shed a light on tumor/cancer research.

C. Stem cell niche systems and asymmetric stem cell division

Many different stem cells reside in their respective specialized environment called the niche or microenvironment, and are affected by various dynamic signals, which can be cell-cell contact signals, cell-extracellular matrix (ECM) signals, or soluble factor signals (Watt, Hogan et

al. 2000, Morrison and Spradling 2008, Spradling, Nystul et al. 2008, Marthiens, Kazanis et al. 2010).

One intriguing question about the stem cell niche system is how the stem cells can still maintain their population while meeting demands to repopulate damaged tissue. In the stem cell niche systems, the cell-cell and cell-ECM contacts are very important to the stem cell regulation (Rattis, Voermans et al. 2004, Yamashita 2010, Chen, Chen et al. 2013, Ottone, Krusche et al. 2014). The physical adhesion of the cell-cell or cell-helps stem cells to remain within the niche (where they also receive signals) (Tanentzapf, Devenport et al. 2007, Marthiens, Kazanis et al. 2010) as well as provide polarity cues for the stem cells to divide symmetrically or asymmetrically (Yamashita, Fuller et al. 2005, Neumüller and Knoblich 2009, Raymond, Deugnier et al. 2009). Most often, the fate decisions are determined by the polarization of stem cells. In asymmetric stem cell divisions, daughter cells that are displaced from the stem cell niche by polarity orientations most often commit to differentiation, devoid of signals from the niche to maintain their identity as stem cells (Yamashita 2010, Yamashita, Yuan et al. 2010) (See Fig. 1). It has previously been shown that many mammal stem cell niche systems divide asymmetrically, which include skin stem cells, muscle satellite cells, and intestinal stem cells (Lechler and Fuchs 2005, Kuang, Kuroda et al. 2007, Quyn, Appleton et al. 2010, Yamashita 2010).

The outcome of asymmetric stem cell division is influenced by combination of extrinsic and intrinsic regulation (Xie, Kawase et al. 2005, Fuller and Spradling 2007, Yamashita, Yuan et al. 2010). The extrinsic regulator in the stem cell system is the stereotypical placement of stem cells to the niche. This arrangement creates two distinctively different microenvironments, either inside (attached and close to the hub cells and signals) or outside (displaced and away from the

hub cells and signals) of the stem cell niche. When two daughter cells form through a stem cell division, they are given an option to whether to stay inside or outside of the stem cell niche. Ultimately, this extrinsic regulation creates different fates for the daughter cells depending on which side the daughter cells are placed. On a different note, intrinsic regulators control the stem cell fate through positioning polarity proteins inside the stem cells. Typical examples of Drosophila polarity proteins include bazooka (Baz), adenomatosis polyposis coli 2 (APC2), atypical protein kinase C (aPKC), among others (Cox, Seyfried et al. 2001, Inaba, Venkei et al. 2015) (see Fig. 2). The polarity proteins in turn localize to specific regions of the stem cells (hence polarity proteins) and facilitate binding of other fate determinant proteins, centrosomes and spindle microtubules, and ultimately influences whether the stem cell would divide asymmetrically or symmetrically (Yamashita, Jones et al. 2003, Inaba, Yuan et al. 2010, Inaba, Venkei et al. 2015).

D. Drosophila melanogaster testis as a model stem cell system

The stem cells inside of *Drosophila melanogaster* testis are one of the best characterized in terms of signaling pathways and have well defined and easily identifiable anatomy (Brinster 2002, Lin 2002, Fuller and Spradling 2007, de Cuevas and Matunis 2011). The stem cell niche system is located at the tip of the *Drosophila* testis, and is composed of three main cell types, which include germline stem cells (GSCs), cyst stem cells (CySCs), and hub cells (see Fig. 3A for anatomy of the *Drosophila* testis stem cell system). Figure 3B shows fluorescent features around a GSC stem cell and sub-cellular details inside a GSC. The germline stem cells physically anchor and surround the aggregated group of hub cells. While remain attached, the GSCs receive signaling factor Unpaired (Upd) excreted by the hub cells. The hub cells' release

of Upd then activates the well-studied Janus kinase-Signal Transducer and Activator of Transcription (JAK-STAT) signaling pathway in the GSCs, which in turn, inhibits GSC differentiation via inhibition of differentiation factor bag of marble's (BAM) activity (Kiger, Jones et al. 2001, Tulina and Matunis 2001, Sheng, Posenau et al. 2009, Bausek 2013). Further studies showed that bone morphogenetic protein (BMP) works in conjunction with JAK-STAT signaling pathway to inhibit the BAM activity (Shivdasani and Ingham 2003, López-Onieva, Fernández-Miñán et al. 2008, Bausek 2013). In addition, two somatic CySCs, while acting as support cells to the GSCs, encapsulate one GSC and also anchor to the hub cells via processes. Male GSC also divides asymmetrically, and when it does, it produces a GSC that is committed for self-renewal and a gonialblast (GB) that is committed for differentiation (Yamashita, Jones et al. 2003, Spradling, Fuller et al. 2011). The gonialblast then goes through 4 stages of transit-amplification divisions to produce spermatogonia and two stages of meiosis, to produce sperm cells (Hennig 1996, Riparbelli and Callaini 2011, Fabian and Brill 2012, Demarco, Eikenes et al. 2014).

E. Centrosome and spindle orientation in asymmetric stem cell division

In the GSCs, the centrosomes are mostly found to be asymmetrically localized (one centrosome is localized to the hub-GSC interface and the other localize to the basal cortex) (Yamashita, Jones et al. 2003, Yamashita, Mahowald et al. 2007). The asymmetrically behaving centrosomes are critical in the asymmetric stem cell division outcome since the centrosomes serve as the platform for the microtubule organizing center (MTOC), guides the formation of the mitotic spindles, and determines the spindle orientation (Kellogg, Moritz et al. 1994). Finally,

the spindle orientation determines the asymmetric stem cell division outcome, since it determines the cleavage plane orientation (Eggert, Mitchison et al. 2006) (see Fig. 4).

F. Centrosomes in germline stem cells (GSCs) are inherited asymmetrically

Immortal Strand Hypothesis was first conceived by John Cairns that suggests that the original DNA copy is always retained in the original adult stem cells to limit mutations to the original DNA. Similar to this idea, some questioned whether similar "immortal" centrosomes may exist in stem cell systems that may allow cells to maintain their stem cell identities. There is no conclusive evidence that the "immortal" centrosomes maintain stem cell identities, but interestingly, there have been reports that "immortal" centrosomes are retained in some stem cell systems.

In the GSCs, Yamashita et al. carried out pulse-chase experiments with PACT-GFP to see where the centrosomes segregate to after mitosis (Yamashita, Mahowald et al. 2007). Since the pericentrin-like protein (PACT) protein localizes to the centrosome a pulse of PACT-GFP causes the centrosomes to fluoresce due to the PACT incorporation into the centrosome. The pulse is stopped and the centrioles are replicated. This causes the GSC to have one older fluorescent centrosome and a younger non-fluorescent centrosome. Later the GSC divisions are quantified to see which centrosome migrated to where. Results show that in the GSCs, old centrosomes ("mother centrosome") are retained in the daughter cell that is attached to the hub-GSC interface and younger centrosome ("daughter centrosome") are retained in the gonialblast (Yamashita, Jones et al. 2003, Yamashita, Mahowald et al. 2007). A similar study was done on neuroblasts using photo-convertible marker tagged to the PACT protein and daughter centrosome specific protein centrobin (CNB) tagged with YFP. The results show the opposite is

true for the neuroblasts as the "daughter centrosome" was retained by the neuroblast and the "mother centrosome was retained by the ganglion mother cell (GMC) (Januschke, Llamazares et al. 2011). These results show that the centrosomes are inherited asymmetrically.

G. Centrosome orientation checkpoint

Similar concept to the check points of the cell cycles such as the G1, G2, and metaphase check points, another check point called the centrosome orientation check point has been proposed by Cheng et al., 2008. The proposed idea is that there exists a novel check point system that ensures that the centrosomes are properly oriented prior to mitosis. Based on the live-imaging observation, GSCs with misoriented centrosomes did not divide for extended period of time until the centrosome were properly oriented (Cheng, Turkel et al. 2008). Based on a previous publication, Par1 is reported to be involved in the centrosome orientation checkpoint (Yuan, Chiang et al. 2012).

H. Spectrosome in asymmetric stem cell division

Spectrosome is a spherical cytoskeletal organelle originally described in female GSCs (Lin, Yue et al. 1994, Lin and Spradling 1995) in *Drosophila melanogaster*, but also found in male GSCs as well as in certain mammalian lymphocytes (Dubielecka, Stebelska et al. 2003). Spectrosome is believed to be derived from the endoplasmic reticulum but its origin is not known. Its composition includes hts (adducin homolog), ankyrin, cadherin, and spectrin. It also has binding affinities to cytoskeletal molecules, microtubule, spectrin, and actin (de Cuevas, Lilly et al. 1997, Matsuoka *, Li et al. 2000, Snapp, Iida et al. 2004, Pariser, Perez-Pinera et al. 2005, Petrella, Smith-Leiker et al. 2007, Lighthouse, Buszczak et al. 2008). Additionally, the

spectrosome is reported to carry various molecules for transport (Lighthouse, Buszczak et al. 2008, Yuan, Chiang et al. 2012). In female GSCs, the previous data shows that spectrosome plays an integral role in orienting the spindle through interactions with the apical spindle pole (Lin and Spradling 1995, Deng and Lin 1997). In female GSCs, it's been observed through the years that the spectrosome is located apically near the cap cells (de Cuevas, Lilly et al. 1997, Deng and Lin 1997). According to one study, when the spectrosome was knocked out with huli-tai shao (hts^{1}) mutation, the spindle orientation of female GSCs became completely randomized (Deng and Lin 1997). A similar spectrosome knockout study was done using the hts^{01103} mutation in male GSCs. Intriguingly, unlike the female GSCs, the male GSCs had relatively no change to the centrosome and spindle pole misorientation (Yuan, Chiang et al. 2012).

When the gonialblast divides and goes through the transit amplification process, the divided cells do not finish cytokinesis and are all inter-connected by intercellular bridges (Spradling, Fuller et al. 2011). Fusome structures (spectrosome derivative) are co-localized to the region where the intercellular bridges form. The *Drosophila* fusome is composed of polarized microtubules, cytoplasmic endomembranes, and membrane skeletal proteins (de Cuevas, Lilly et al. 1997, McKearin 1997). In the female GSCs, it was shown that the fusome structures anchor one pole of each mitotic spindle and orient the plane of cell division (Lin and Spradling 1995). Similarly, the fusome also played a role in orienting the spindle in later stage of spermatocytes (Stevens, Raposo et al. 2007).

I. Acentrosomal stem cells and asymmetric stem cell division

Centrosomes have been understood as most important organizer of cells. A centrosome is composed of a pair of centrioles and pericentriolar matrix (PCM), which organizes

microtubules through the MTOC. Contrary to the belief that centrosome are essential to cellular mitosis, there have been reports that some animal cells with their centrosomes removed via surgical procedures or laser ablation can still form bipolar spindles and go through mitosis (Khodjakov, Cole et al. 2000, Hinchcliffe, Miller et al. 2001, Basto, Lau et al. 2006).

A study was done on male GSCs to ascertain how the GSCs' asymmetric stem cell divisions are affected without centrosomes. Using the *DSas-4*^{S2214} mutation, centrosome structures including centrioles were effectively knocked out and the spindle orientation measured. Surprisingly, even without centrosomes, majority of the male GSCs' spindles were still highly oriented and went through asymmetric stem cell division (Riparbelli and Callaini 2011). Similarly, in female GSCs with same DSas-4 mutation, majority of the GSCs still went through asymmetric stem cell division (Stevens, Raposo et al. 2007). One of the most intriguing parts of the centrosome knockout through DSas-4 mutation is that spectrosome switched side from usually detected basal side to the hub-GSC interface side (apical side) (Yuan, Chiang et al. 2012).

Furthermore, effects of centrosome knockout (via DSas-4 mutation) were also observed in neuroblasts. In the neuroblasts with DSas-4 mutation, the spindles were somewhat largely misoriented, but did not orient randomly. Additionally, the neuroblasts had unreliable asymmetric stem cell division with the DSas-4 mutation (Basto, Lau et al. 2006).

J. Centrosomin (cnn) and asymmetric stem cell division

Cnn is a 150kDa centrosomal protein and is an integral component of the centrosome and a general component of the spindle poles, which is believed to act as a scaffold during the early formation of the MTOC (Megraw, Li et al. 1999, Vaizel-Ohayon and Schejter 1999, Megraw, Kilaru et al. 2002, Fu and Glover 2012). There have been several reports that cnn mutation

caused disrupted MTOC and disappearance of the CP-190, γ-tubulin proteins, and late stage astral microtubules, thus making the centrosome functionally impaired (Megraw, Li et al. 1999, Vaizel-Ohayon and Schejter 1999, Megraw, Kao et al. 2001). The *cnn-mut* GSCs have been reported to have slight centrosome and spindle misorientations, thus slightly affecting the outcome of the asymmetric stem cell division (Yamashita, Jones et al. 2003, Inaba, Yuan et al. 2010). Similarly, acentrosomal GSCs via DSas-4 mutation have shown similar slight misorientation of the centrosome and spindle, which promptly raised a possibility for the existence of fail-safe mechanisms to orient the spindle when the centrosome function is compromised (Yuan, Chiang et al. 2012, Bang and Cheng 2015).

Another study has revealed that in wild type GSCs, 92% of mother centrosomes with older and richer PCM materials were inherited by the GSCs and the 85% of daughter centrosomes with younger PCM materials were inherited by the gonialblast (Yamashita, Mahowald et al. 2007). But with cnn mutation, the mother centrosomes were equally inherited by both the GSC (44%) and the gonialblast (42%) (Yamashita, Mahowald et al. 2007). This study further confirmed the existence of distinguishable PCM structure and function in the mother centrosome compared to the daughter centrosome.

Centrosomin mutant experiments have been conducted on embryo and neuroblasts as well. Inside of a *Drosophila* embryo, centriole movements were traced for both wild type and cnn mutant to reveal that *cnn-mut* centrioles moved erratically. Furthermore, additional experiments revealed that centrioles localize to regions significantly far away from the mitotic spindle poles. Additional experiments on neuroblasts reveal that centrioles co-localize away from the center of the PCM proteins (e.g. Grip75, Aurora, D-TACC) when compared to the wild

type (Lucas and Raff 2007). These results suggest that centrioles require centrosomin to make proper connections to the PCM and have stable function.

K. Adenomatous Polyposis Coli Protein 2 (APC2) and asymmetric stem cell division

Other proposed mechanism step for regulating the stem cell asymmetric division outcome is through the cortically localized adhesion proteins in the cell-cell junction. It has been shown that APC2, β-catenin, and DE-cadherin normally localize at the cellular junctions (Hamada and Bienz 2002, Yamashita, Jones et al. 2003, Bienz and Clevers 2010, Inaba, Yuan et al. 2010). In the case of GSCs, these junctional proteins are localized between the hub-GSC interface and mainly at the GSC's apical cortex. Based on previous results, it is believed that the DE-cadherin cytoplasmic tail could provide for localized binding site for the APC2 and the Armadillo (β-catenin homologue in *Drosophila*) (Hamada and Bienz 2002, Yamashita, Jones et al. 2003, Inaba, Yuan et al. 2010). In addition, β-catenin network was severely compromised when the APC2 was knocked out (*APC2-mut*), which suggests that β-catenin interact dependently of the APC2 (Bienz and Clevers 2010). The APC2, containing the microtubule binding sites, and then act as a liaison to coordinate astral microtubule binding to the junctional proteins localized at the apical cortex of the GSCs (Yamashita, Jones et al. 2003, Inaba, Yuan et al. 2010). Previous studies have shown that *APC2-mut* causes centrosome misorientation but not spindle misorientation (Yamashita, Jones et al. 2003, Inaba, Yuan et al. 2010). In addition to the microtubule binding, it was also shown that the APC2 and Armadillo work together to tether the mitotic spindles to the cortical actin the *Drosophila* embryos (McCartney, McEwen et al. 2001).

Adenomatous Polyposis Coli Protein is widely known for the role in the (wg)/Wnt signal transduction pathway (McCartney, Dierick et al. 1999, Ahmed, Nouri et al. 2002, Akong,

Grevengoed et al. 2002). Normally, the APC is part of the Armadillo (homolog of β-catenin in drosophila)/ β-catenin destruction complex. With normal presence and function of APC in the complex, the β-catenin is targeted and destroyed via proteolysis, so the β-catenin is no longer accumulated in the cell (also in the junctional space) (Kunttas-Tatli, Zhou et al. 2012, Roberts, Pronobis et al. 2012). However, with wingless signal, the Armadillo/β-catenin destruction complex is inactivated and the β-catenin begins to accumulate in the junction and into the nucleus to promote other gene activations and transcriptions (Gumbiner 1998).

Adenomatous Polyposis Coli Protein was also shown to mediate cell migration and influence cytoskeletal dynamics in the cultured cells via interactions with end binding 1 (EB1), microtubules, and α-catenin (Munemitsu, Souza et al. 1994, Smith, Levy et al. 1994, Su, Burrell et al. 1995, Berrueta, Kraeft et al. 1998, Morrison, Wardleworth et al. 1998).

L. Mosaic Analysis with a Repressible Cell Marker (MARCM) method

The Mosaic Analysis with a Repressible Cell Marker (MARCM) method is a powerful technique used in *Drosophila* to induce controllable mutation on small population of wild type cells (these mutant cells are called clones) when given a specific cue (e.g. heat shock). Using the standard MARCM method, the clones fluoresce, so they are easily identifiable. One clear advantage for using the MARCM method to introduce mutations is that lethal mutation can be introduced without killing the organism. The Mosaic Analysis with a Repressible Cell Marker (MARCM) method utilizes the flippase (FLP) and flippase recombination target (FRT) cassette system and mitotic recombination to generate mutation in wild type cells. The flippase acts as a recombinase and recombines mutant genes with GAL80 genes right at the FRT sites. After that FLP mediated recombination, cell goes through mitosis and segregates the mutants into one cell

and GAL80 into the other cell. Moreover, GAL4 is a promoter for the upstream activation sequence (UAS) and activates a gene that comes after the UAS sequence. In this case, it is preferred that the UAS activated gene has a GFP or RFP tag for the clones to fluoresce. Additionally, GAL80 acts as a suppressor for the GAL4. Technically, with presence of GAL80, UAS cannot be activated and show no fluorescence. Since the mutant clones after mitosis are free of GAL80, they are fluoresced by the activation of UAS by GAL4 (see Fig. 5 for diagram). The non-mutant cells, containing GAL80, do not fluoresce (Lee and Luo 1999, Lee and Luo 2001, Wu and Luo 2007).

M. Ultrafast laser microsurgery

Ultrafast laser microsurgery offers relatively a novel and powerful way to study functions of subcellular structures. Similar to the genetic knockout concept, the ultrafast laser microsurgery is designed to induce "structural knockouts" to desired targets. In the absence of those structures, the function of the subcellular structures can be studied just as one can study a function of a protein after a genetic knockout. The ultrafast laser uses highly focused laser beam at femtosecond pulses to deliver critical energy levels to damage the material at the nanometer resolution (Joglekar, Liu et al. 2004). Because its damage focus is so small, the laser beam spot size for ablating cellular structures is around 100nm, and the energy peak attenuates quickly after critical threshold, damage to the cells and other structures nearby are quite minimal. In addition, the infrared range frequency allows for thicker penetration depth for easier ablation manipulations. There are several advantages of using ultrafast laser microsurgery over conventional genetic knockouts methods. Firstly, the laser structural knockout can be done autonomously, only affecting structures in the targeted cells or structures. Genetic knockouts, on

the other hand, cannot be implemented autonomously as it affects the whole organism, which can create complications in cause and effect studies. Secondly, the laser structural knockout can be implemented in any stage or anytime in the animal/cell/structural development, which can be difficult to implement in genetic knockouts. Thirdly, the laser structural knockout can delete whole structures such as organelle or complicated structural assembly, which may be quite challenging or impossible to achieve with genetic knockout methods. There are also disadvantages of using ultrafast laser microsurgery compared to using genetic knockout methods. Firstly, ultrafast laser microsurgery is done serially, so it may take considerable effort and time to ablate so many things all at once, such as ablating all the focal adhesions in groups of cells. Genetic knockout, on the other hand, affects every cell. Secondly, laser structural knockout can delete an area of localized proteins or structures, but it cannot delete cytosolic free-form proteins, which may simply replenish and reform into the deleted structures.

The applications of ultrafast laser microsurgery on subcellular structures include ablating sections of a chromosome's arm in newt lung cells (Ke, Cheng et al. 2009). This ablation decreased the polar-ejection force (PEF) and increased the oscillatory movements of mitotic chromosomes known as the "directional instability" (Ke, Cheng et al. 2009). Using live-imaging observations, the authors found a direct link between the PEF and the direction of the chromosomal movements (Ke, Cheng et al. 2009).

In other case studies, ultrafast laser microsurgery was used to ablate centrosomes on different cell types, and the ablations produced mixed results (Khodjakov, Cole et al. 2000, Khodjakov, Rieder et al. 2002). Firstly, Khodjakov in 2000 ablated centrosomes in CVG-2 clone line (monkey kidney, fibroblastic) as the cells are entering mitosis. Interestingly, even after the destruction of the centrosomes, the cells reformed functional spindle poles and successfully went

through mitosis. This group showed successful ablation of centrosome and that the cells still under go mitosis, independent of the centrosomes. The same group in 2002 laser ablated centrosomes in Chinese hamster ovary (CHO) cells during the S-phase and observed something remarkably different than their first result. The centrioles simply reformed De novo after the ablation of centrosomes and developed into functional centrosomes 24 hours later. However, the ablated cells never returned to their normal state and formed up to 14 separate centrioles per cell (mostly positioned near the nucleus area) (Khodjakov, Rieder et al. 2002). The second experiment (2002) shows that the laser ablation of centrosomes had negative impact on the CHO cells, contrary to the first experiment.

So far, there is no report of laser ablation on spectrosomes.

N. Dynamic Interplay of Spectrosome and Centrosome Organelles in Asymmetric Stem Cell Divisions

(Parts of this chapter were previously published as Bang, C. and J. Cheng (2015). "Dynamic Interplay of Spectrosome and Centrosome Organelles in Asymmetric Stem Cell Divisions." PLoS ONE 10(4): e0123294.)

Many stem cells achieve tissue homeostasis through asymmetric stem cell division, effectively balancing the self-renewal ability and differentiation potential (Morrison and Kimble 2006). In these systems, imbalance of the stem cell fates could either lead to uncontrolled tumorigenesis due to excessive self-renewal (Clarke and Fuller 2006) or tissue degeneration/aging due to excessive differentiation or reduced self-renewal ability (Brunet and

Rando 2007, He, Nakada et al. 2009). Some of these stem cells achieve this balance by residing inside a specialized micro-environment (thereafter referred as stem cell niche) that provides cues and signals necessary to the stem cells for maintaining their stem cell identity (Morrison and Spradling 2008). Cells leaving the niche, deprived of the cues and signals, would lose the stem cell identity and begin differentiating.

Drosophila male germline stem cells (GSCs) are among the best models to study stem cells inside the niche because of well-characterized signaling mechanisms as well as easily-recognized niche structure. Localized at the tip of the testis, the hub cells, residing at the center of the niche, are surrounded by GSCs and cyst stem cells (CySCs). Hub cells secrete unpaired (Upd) factor, which initiates Janus kinase–signal transducers and activators of transcription (JAK-STAT) pathway in GSCs (Kiger, Jones et al. 2001, Tulina and Matunis 2001, Fuller and Spradling 2007). GSCs undergo asymmetric stem cell divisions through stereotypically oriented mitotic spindle relative to hub cells, resulting in one attached and another detached daughter cell to the hub cells (Yamashita, Jones et al. 2003). The daughter cell attached to hub cells remains as stem cell, while the other daughter cell displaced from the hub commits to differentiation. Furthermore, the stereotypical mitotic spindle orientation is ensured by the centrosome orientation (Yamashita, Jones et al. 2003, Yamashita, Mahowald et al. 2007). Additionally, it was recently found that centrosome orientation plays an important role in the cell cycle progression. A mechanism, known as the centrosome orientation checkpoint, monitors the proper centrosome orientation (Cheng, Turkel et al. 2008). If centrosome(s) is not properly oriented, the GSC mitosis is delayed until a correction is made. Centrosomin (cnn) and *Drosophila* E-cadherin are reported to be involved in this centrosome orientation checkpoint (Inaba, Yuan et al. 2010).

Spectrosome, a spherical cytoskeletal organelle, was initially described in female GSCs in *Drosophila melanogaster* (Lin and Spradling 1995), and similar spectrosomal structure was found in certain mammalian lymphocytes (Dubielecka, Stebelska et al. 2003). Spectrosome is believed to be endoplasmic reticulum-derived although its origin is unknown. It contains proteins such as huli-tai shao (hts), ankyrin, cadherin, and spectrin that have binding affinity to microtubules and actin (de Cuevas, Lilly et al. 1997, Snapp, Iida et al. 2004, Pariser, Herradon et al. 2005, Petrella, Smith-Leiker et al. 2007, Lighthouse, Buszczak et al. 2008). In female GSCs, several reports show that the spectrosome plays an important role in orienting mitotic spindles through interaction with spindle poles (Lin and Spradling 1995, Deng and Lin 1997). Thus when the spectrosome was knocked out by huli-tai shao (hts^{1}) mutation, the spindle orientation was severely compromised and randomly oriented (Deng and Lin 1997). In addition, fusome, a derivative of the spectrosome, was also shown to orient the spindle of later stage spermatocytes (Lin and Spradling 1995, Stevens, Raposo et al. 2007).

In this study, we show that both centrosome and spectrosome are complementarily involved in the spindle orientation of the male GSCs. Our investigation stemmed from a result that the majority of the spindle was still oriented despite of the centrosome being knocked out (Riparbelli and Callaini 2011). Another clue was provided when majority of the interphase spectrosomes switched locations from basal to apical cortices in *DSas-4-mut* GSCs (Yuan, Chiang et al. 2012), where the spectrosomes were seen previously anchoring the spindle pole to orient the spindle in the wild type female GSCs. Contrary to the female GSCs, however, when the spectrosome was compromised through an *hts-mut*, male GSCs with intact centrosomes had minimally altered the centrosome and spindle orientation (Yuan, Chiang et al. 2012). We

propose that in male GSCs, spectrosome is recruited as a fail-safe mechanism to the apical cortex to facilitate proper spindle orientation when centrosome's function is compromised.

O. Effects of Centrosomin and Adenomatous Polyposis Coli Protein 2 on Spectrosome Recruitment and Asymmetric Stem Cell Divisions

Many adult stem cell types maintain tissue homeostasis through asymmetric stem cell division, which effectively balances self-renewal and differentiation processes (Morrison and Kimble 2006). In the tissue, imbalance of the stem cell fates can result in tumorigenesis due to uncontrollable self-renewal (Clarke and Fuller 2006) or tissue deterioration due to excessive differentiation or diminished self-renewal potential (Brunet and Rando 2007, He, Nakada et al. 2009). Much of the self-renewal and differential processes of the stem cells are affected by the cues and signals received from the specialized neighboring environment called the microenvironments or the stem cell niche. The stem cells that reside in the microenvironment receive proper signals to maintain their identity (Morrison and Spradling 2008), and the cells that leave the microenvironment, either through migration or asymmetric stem cell division, lose the stem cell identity, bereft of cues and signals.

Among many different stem cell types that maintain tissue homeostasis through asymmetric stem cell divisions, such as skin stem cells, satellite cells, neuronal stem cells, and intestinal stem cells (Yamashita 2010), *Drosophila* male germline stem cell (GSC) is one of the best model to study the asymmetric stem cell behavior because it is well-characterized and dwells inside of easily identifiable stem cell niche architecture. The GSC stem cell niche, which is located at the tip of the testis, is composed of cyst stem cells (CySCs) and GSCs that surround terminally differentiated somatic hub cells. The hub cells, which play critical roles in

maintaining the GSCs and CySCs, secrete unpaired (Upd) signaling molecules, which initiates Janus kinase-signal transducers and activators of transcription (JAK-STAT) signaling pathway in GSCs (Kiger, Jones et al. 2001, Tulina and Matunis 2001, Fuller and Spradling 2007). When the GSCs undergo asymmetric stem cell divisions, stereotypically oriented mitotic spindle define the direction of the division axis respective to the hub and cause one daughter cell to be displaced from the hub while the other is retained (Yamashita, Jones et al. 2003). Then the displaced daughter cell, devoid of signals from the hub cells, commits to differentiate. In addition, centrosome orientation plays a critical role in asymmetric stem cell division because the spindle formation and orientation is directed by the positioning of the centrosomes prior to mitosis. Furthermore, proper centrosome orientation is critical in the progression of mitosis. Known as the centrosome orientation check point, the cell cycle is delayed until proper centrosome orientation is achieved (Cheng, Turkel et al. 2008, Inaba, Yuan et al. 2010, Yuan, Chiang et al. 2012). There have been reports that centrosomin (cnn) and *Drosophila* E-cadherin are important for the centrosome orientation checkpoint (Inaba, Yuan et al. 2010).

Spectrosome is a spherical cytoskeletal organelles originally described in female GSCs (Lin, Yue et al. 1994, Lin and Spradling 1995) in *Drosophila melanogaster*, but also found in male GSCs as well as in certain mammalian lymphocytes (Dubielecka, Stebelska et al. 2003). Spectrosome is believed to be derived from the endoplasmic reticulum but its origin is not known. It has compositions including hts (adducin homolog), ankyrin, cadherin, and spectrin. It also have binding affinities to cytoskeletal molecules microtubule and actin (de Cuevas, Lilly et al. 1997, Snapp, Iida et al. 2004, Pariser, Perez-Pinera et al. 2005, Petrella, Smith-Leiker et al. 2007, Lighthouse, Buszczak et al. 2008). Additionally, the spectrosome is reported to carry various molecules for transport (Lighthouse, Buszczak et al. 2008, Yuan, Chiang et al. 2012). In

female GSCs, the previous data shows that the spectrosome plays an integral role in orienting the spindle through interactions with the apical spindle pole (Lin and Spradling 1995, Deng and Lin 1997). According to one study, when the spectrosome was knocked out with huli-tai shao (hts^{1}) mutation, the spindle orientation of female GSCs became completely randomized (Deng and Lin 1997). Furthermore, fusome (spectrosome derivative) also played a role in orienting the spindle in later stage of spermatocyte mitosis (Stevens, Raposo et al. 2007). Additionally, it was recently discovered that in male GSCs with centrosome knocked out through DSas-4 ($DSas\text{-}4^{S2214}$) mutation, the spectrosome switched location from the basal to the apical cortex, to an intermediary position stereotypically seen in female GSCs. It was postulated that, with additional dynamic evidences, the spectrosome play a complementary role in orienting the spindle when the centrosome is compromised (Yuan, Chiang et al. 2012, Bang and Cheng 2015).

Mechanistically, there are several steps how the asymmetric stem cell division can be regulated have been proposed. One such mechanism step is through the interaction of intact PCM/astral microtubules that includes cnn, CP190, CP60, and γ-tubulin (Megraw, Li et al. 1999). Electron microscope studies show that centrosome is primarily made up of a pair of centrioles that are surrounded by shapeless, electron-dense PCM (Rattner and Phillips 1973). The pericentriolar matrix containing microtubules would search out and bind to the adhesion proteins localized to the apical cortex and orient the spindle. There have been several reports that cnn mutation caused disrupted MTOC and disappearance of the CP-190, γ-tubulin proteins, and late stage astral microtubules, thus making the centrosome functionally impaired (Megraw, Li et al. 1999, Vaizel-Ohayon and Schejter 1999, Megraw, Kao et al. 2001). Centrosomin is a 150kDa centrosomal protein and is an integral component of the centrosome and a general component of the spindle poles, which is believed to act as a scaffold during the early formation of the MTOC

(Megraw, Li et al. 1999, Vaizel-Ohayon and Schejter 1999). The centrosomin mutant GSCs have been reported to have slight centrosome and spindle misorientations, thus slightly affecting the outcome of the asymmetric stem cell division (Yamashita, Jones et al. 2003, Inaba, Yuan et al. 2010). Similarly, acentrosomal GSCs via *DSas-4*^{S2214} mutation have shown similar slight misorientation of the centrosome and spindle, which promptly raised a possibility for the existence of fail-safe mechanisms to orient the spindle when the centrosome function is compromised (Yuan, Chiang et al. 2012, Bang and Cheng 2015). Other proposed mechanism step for regulating the stem cell asymmetric division outcome is through the cortically localized adhesion proteins in the cell-cell junction. It has been shown that APC2, β-catenin, and DE-cadherin normally localize at the cellular junctions (Hamada and Bienz 2002, Yamashita, Jones et al. 2003, Bienz and Clevers 2010, Inaba, Yuan et al. 2010). In the case of GSCs, these junctional proteins are localized between the hub-GSC interface and mainly at the GSC's apical cortex. Based on previous results it is believed that the DE-cadherin cytoplasmic tail could provide for localized binding site for the APC2 and the Armadillo (β-catenin homologue in *Drosophila*) (Hamada and Bienz 2002, Yamashita, Jones et al. 2003, Inaba, Yuan et al. 2010). In addition, β-catenin network was severely compromised when the APC2 was knocked out (*APC2-mut*), which suggests that β-catenin interact dependently of the APC2 (Bienz and Clevers 2010). The Adenomatous Polyposis Coli Protein 2, containing the microtubule binding sites, then act as a liaison to coordinate astral microtubule binding to the junctional proteins localized at the apical cortex of the GSCs. Previous studies have shown that *APC2-mut* causes centrosome misorientation but not spindle misorientation (Yamashita, Jones et al. 2003, Inaba, Yuan et al. 2010).

In this current study, we show that both PCM (cnn) and cortical adhesion proteins (APC2) are involved in the centrosome and spindle orientation regulation in the male GSCs. Our investigation stemmed from a result that acentrosomal GSCs have spectrosome switch localization from the basal to apical regions, which is proposed to act as a back-up mechanism to correct the spindle misorientation when the centrosome is compromised. Our interest in this study is to 1) ascertain whether the PCM or the cortical adhesion proteins is responsible for the spectrosome recruitment to the apical cortex and 2) investigate how the compromised PCM (*cnn-mut*) and cortical adhesion proteins (*APC2-mut*) affect the dynamics associated with asymmetric GSC divisions.

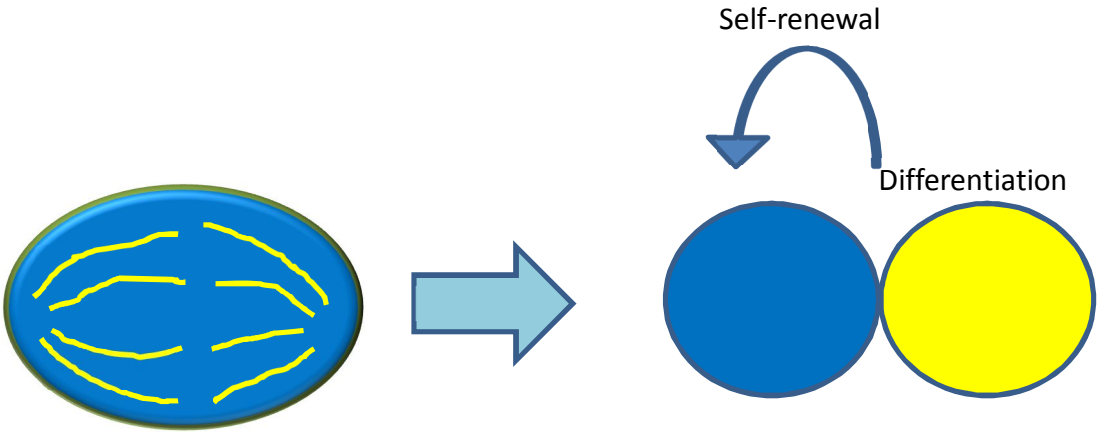

Figure 1: Concept of asymmetric stem cell division. When the stem cells divide, due to their polarity orientation to the stem cell niche, one daughter is self-renewed and the other daughter cell that is differentiated.

Figure 2: Mechanism of asymmetric stem cell division. (A) Extrinsic regulation occurs when external environment influences the outcome of the stem cell fate. The stem cell proximity, stem cell placement inside the niche, and stem cell placement configuration influences the outcome of the stem cells. (B) Intrinsic regulation occurs when internal machinery inside the stem cell influences the outcome of the stem cell outcome. When the stem cell divides, fate determinant polarity proteins guide the orientation of the dividing daughter cells, which can be asymmetric or symmetric.

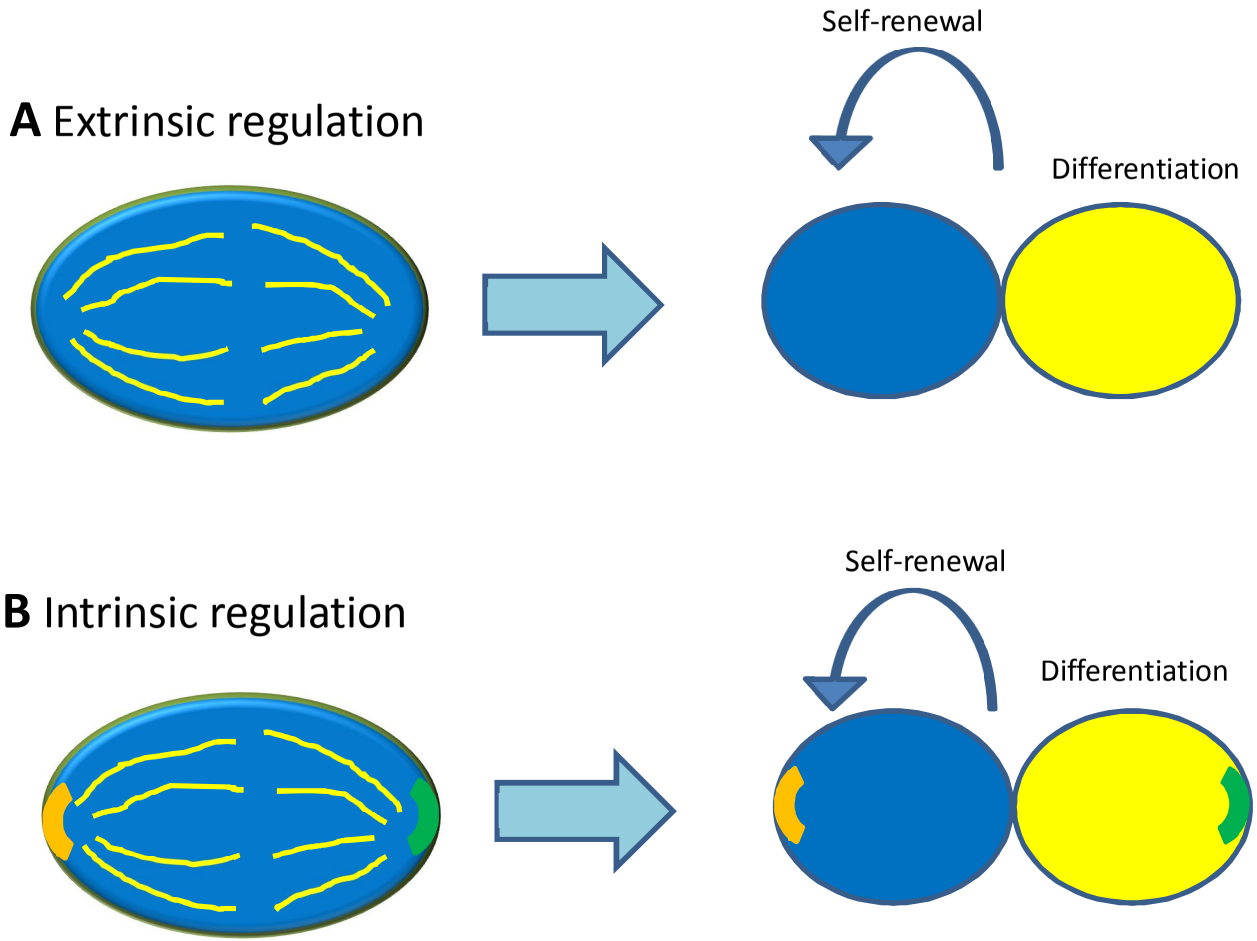
A Extrinsic regulation
Self-renewal
Differentiation
B Intrinsic regulation
Self-renewal
Differentiation

Figure 3: Anatomy of *Drosophila* Stem cell niche system inside of a testis. (A) Anatomical features of stem cell niche system inside *Drosophila* testis are shown. **(B)** Fluorescent image of the stem cell niche is shown. White dotted line: hub cells. Yellow dotted line: a germline stem cell.

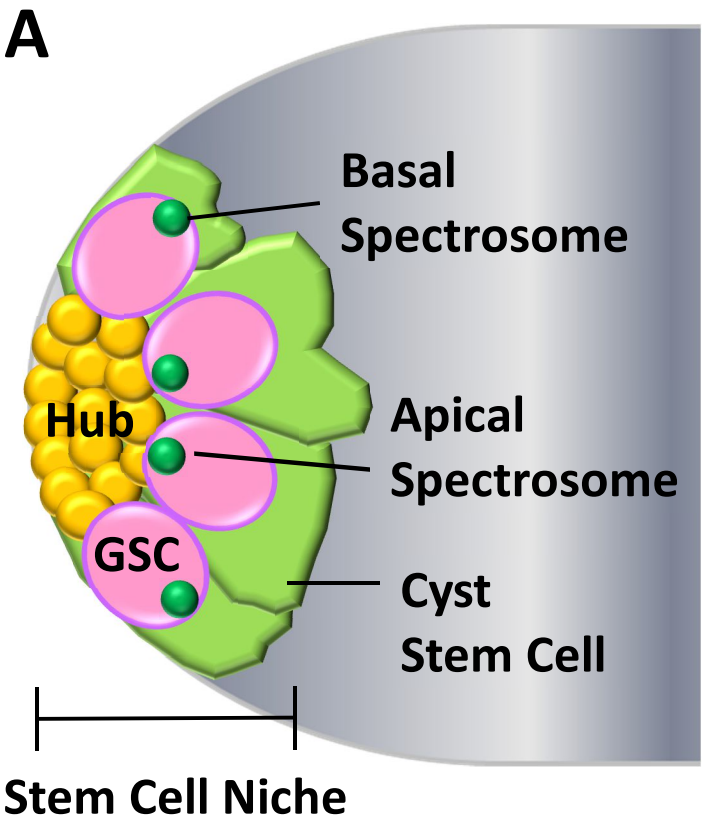
A
Basal
Spectrosome
Hub
Apical
Spectrosome
GSC
Cyst
Stem Cell
Stem Cell Niche

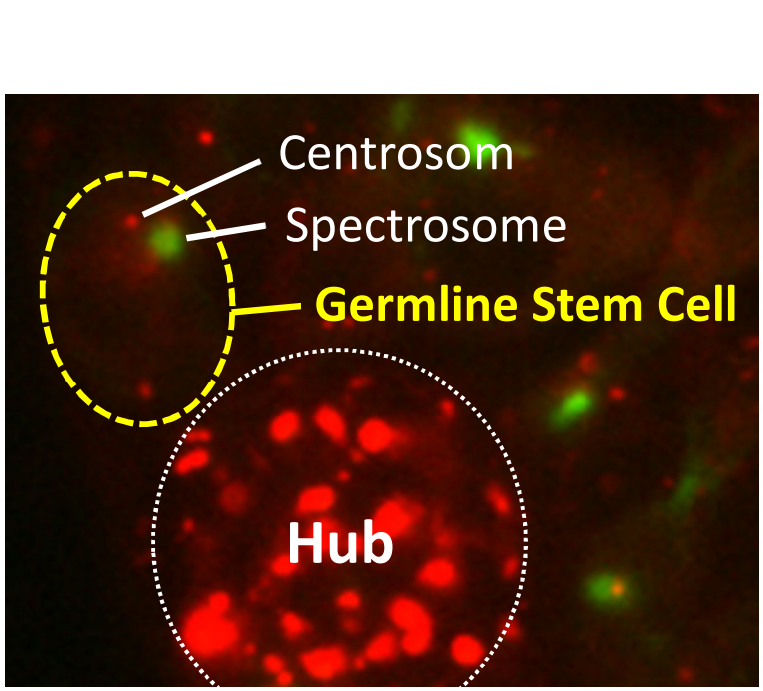
B
Centrosom
Spectrosome
Germline Stem Cell
Hub

Figure 4: Stem cell fate is determined by centrosome and spindle orientations in male *Drosophila* GSCs. Example of asymmetric stem cell division and the fate of two daughter cells. Oriented centrosomes orient the mitotic spindle perpendicular to the hub-GSC interface. The stem cell divides asymmetrically and gives rise to one GSC and one gonialblast. The gonialblast that express BAM are differentiated.

Asymmetric stem cell division

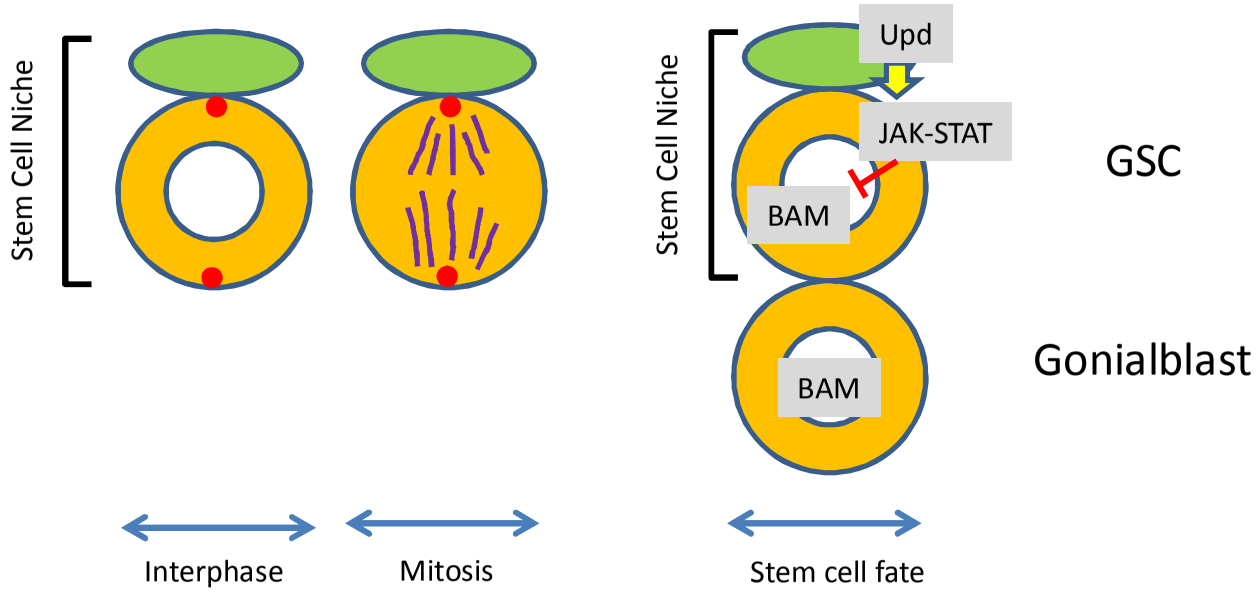

Figure 5: Schematics of MARCM method in GSCs. Using the FLP-FRT cassette system and mitotic recombination, DSas-4 mutations are introduced into a group of wild type GSCs via controllable cues (e.g. heat shock). The final product of the MARCM system is the creation of fluorescing GSCs that contain the DSas-4 mutations (mutant clone

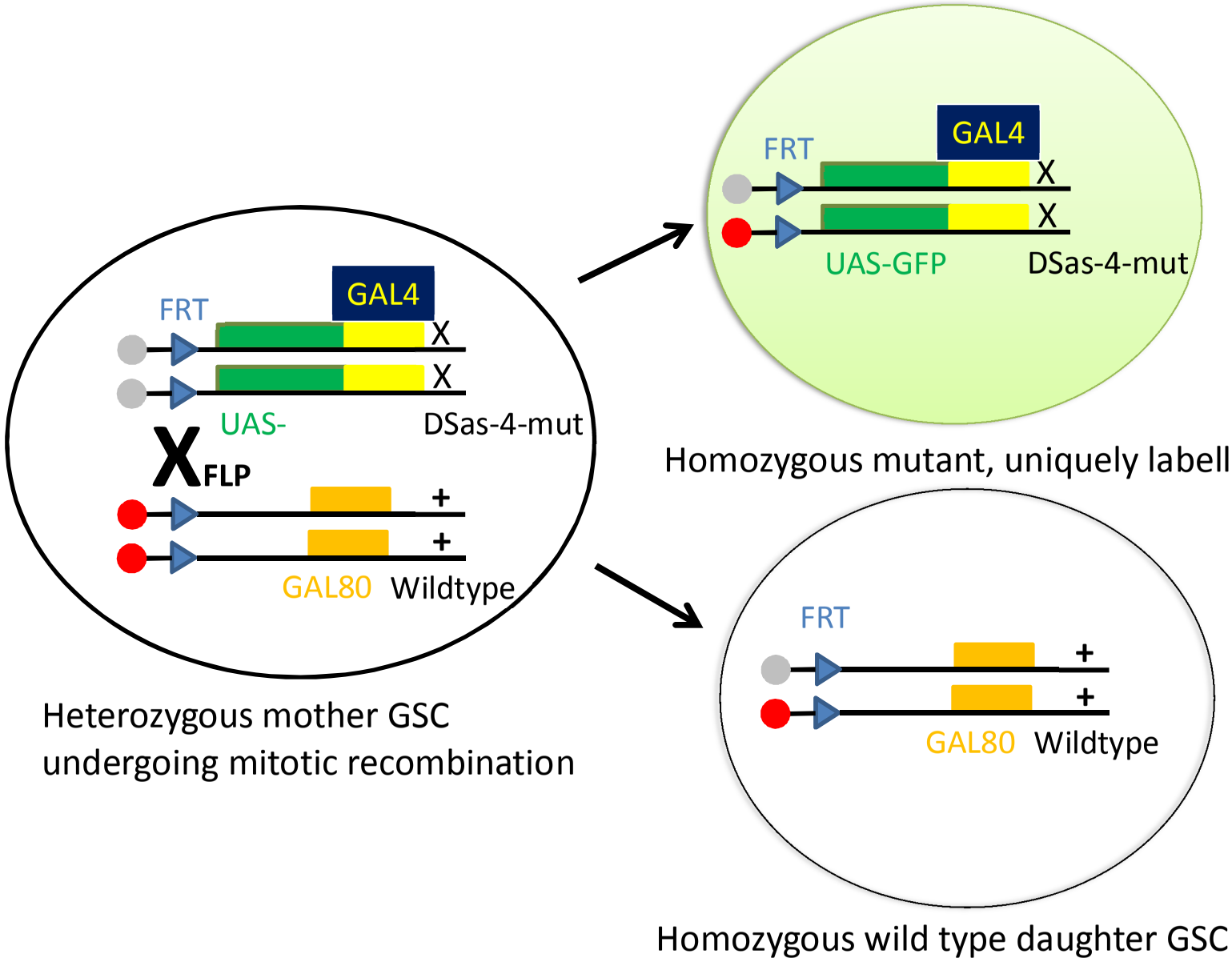

Heterozygous mother GSC undergoing mitotic recombination

Homozygous mutant, uniquely labelled

Homozygous wild type daughter GSC

II. METHODS

A. Dynamic Interplay of Spectrosome and Centrosome Organelles in Asymmetric Stem Cell Divisions

(Parts of this chapter were previously published as Bang, C. and J. Cheng (2015). "Dynamic Interplay of Spectrosome and Centrosome Organelles in Asymmetric Stem Cell Divisions." PLoS ONE 10(4): e0123294.)

1. Fly husbandry and strains

All fly stocks were raised on standard Bloomington medium and inside of an environmental chamber (25°C; standard 24 hour dark-light cycle (12:12); controlled humidity). Fly stocks used were: Ubi-Short Adducin-GFP (Shadd-GFP; obtained from Dr. Spradling's Laboratory); Ubi-α-tubulin-GFP (Ubi-α-tub-GFP); Ubi-Sas6-mcherry (Sas6-mch); Df(2R)BSC26 (Df(2R)); hts^{01103}; DSas-4^{S2214}; FRT82B, DSas-4^{S2214}(Stevens, Raposo et al. 2007); UAS-mCD8-GFP, hs-FLP; GAL4.nos.NGT40 (nos-GAL4), hts^{01103}; FRT82B, GAL80LL3 (FRT82B,TubP-GAL80). Stocks were obtained from the Bloomington Drosophila Stock Center at Indiana University unless otherwise noted. Following genotypes were generated and used for our live-imaging and fixed experiments:

$$\frac{Ubi{-}\propto{-}tub-GFP}{Y};\frac{Shadd-GFP}{Shadd-GFP};\frac{\text{DSas}-4^{S2214}}{\text{DSas}-4^{S2214}}$$

$$\frac{Ubi{-}\propto -tub-GFP}{Y};\frac{Shadd-GFP}{Shadd-GFP};\frac{\mathrm{DSas}-4^{S2214}}{+}$$

$$\frac{Ubi{-}\propto -tub-GFP}{Y};\frac{hts^{01103}}{Df(2R)};\frac{Sas6-mch}{Sas6-mch}$$

$$\frac{Ubi{-}\propto -tub-GFP}{Y};\frac{hts^{01103}}{+};\frac{Sas6-mch}{Sas6-mch}$$

The homozygote mutant genes $\frac{\mathrm{DSas}-4^{S2214}}{\mathrm{DSas}-4^{S2214}}$ will be hence forth be referred *DSas-4-mut* and the heterozygote deleterious and mutant genes $\frac{hts^{01103}}{Df(2R)}$ will hence forth be referred as *hts-mut*. The geneotypes with + are the respective control to those mutants. The *DSas-4-mut* genotype were too weak to eclose on their own, so their eclosions were manually assisted on day 10 to 11 after mating with a pair of size 5 forceps (Stevens, Raposo et al. 2007). Normal sized third-instar (L3) larvae were selected (non-mutants had TM6B balancers, which were much shorter) and placed on top of damped cloths inside of 10cm petri dishes on day 5 to 6 and allowed the larvae to transform into pupas the following day. After the eclosion, the flies were selected against the TM6B balancer phenotypes (shorter length and missing humerus bristles) to ensure the selection of *DSas-4-mut* flies. For the *hts-mut* flies, newly eclosed adult flies with any balancer phenotypes (curly wings and TM6B) were discarded to select for the mutants. The mutant of hts fly generations were verified through the short adducin antibody stain; the spectrosome and fusome structures were not detected in *hts-mut* flies as was previously reported (de Cuevas, Lilly et al. 1997, de Cuevas and Spradling 1998).

2. Meiotic recombination

Using meiotic recombination, different genes (mutants, transgenes, and tagged) from each parent were recombined via chromosomal crossover during meiosis so that both genes can exist in offspring's chromosome. Using a simple crossing technique (Greenspan 2004), the following genes were successfully recombined: nos-GAL4, hts^{01103}. The recombined genes were validated by crossing with a Df(2R) gene and stained with short adducing antibody to show the absence of spectrosome and fusome structures. The existence of nos-GAL4 was confirmed by crossing with a fly containing the UAS-mCD8-GFP, which specifically fluoresced on GSCs' membranes. Nos is a marker specific to germ cells; mCD8-GFP localizes to the membrane; and GAL4 activates the upstream activation sequence (UAS). The necessary number (N) of progeny lines required to probablistically obtain the recombined genes was calculated using the Mather's formula and how much map units the genes were apart:

$$N = \frac{\log(1-p)}{\log(1-f)} * 2$$

,where p is the confidence interval (e.g. 95% assurance of outcome) and the f is the probability for the meiotic recombination (also referred to as a map unit number) of the two genes to occur. The two is multiplied by two for conservative purposes.

$$N = \frac{\log(1-0.95)}{\log(1-0.33)} * 2$$

$$N = 15$$

All of the 15 lines generated were tested for the existence of the nos-GAL4 and the hts^{01103} genes as stated above. This recombined gene was made to be used for the MARCM experiment (see section A, subsection 10 for more information).

3. Tissue preparation and time-lapse live-cell imaging

The following protocol is an adaptation to the methods previously used (Cheng and Hunt 2009). Prior to the dissection, all the dissecting equipment were sterilized using 70% ethanol or sterilized under UV for at least one hour. Newly eclosed *DSas-4-mut* and *hts-mut* adult flies (0-1 day old) flies were selected from the stock and placed on a carbon dioxide pad (10 lbs/in^2) to administer anesthesia (see Fig. 6A). Under 5x magnification on a Leica stereomicroscope, *Drosophila* testes were isolated while submerged under 0.5ml of sterile Schneider's Complete *Drosophila* medium (Schneider's *Drosophila* medium, 10% fetal bovine serum (FBS), 1% penicillin streptomycin (Pen-Strep)) with two size 5 dissection tweezers (Dumont) inside a sterile 10 well glass plate (see Fig. 6B). The isolated testes were then transferred into the adjacent well of the glass plate containing 0.5 ml of Schneider's Complete *Drosophila* medium to be cut. Using a size 10 scalpel blade, the tips of the testes were cut from the remainder of the testes and were selected for live-imaging. Removing much of the testes muscles minimized movement for live-imaging. On average per imaging session, about 10-15 testes tips were cut.

The cut testes tips were then transferred into a sterile glass bottom petri dish (MatTek, 35mm glass with 20mm microwell) using a 10µl pipette (sterile). The excess Schneider's Complete *Drosophila* medium from the glass bottom petri dish was removed with a tweezer's tip using capillary force. The testes were then evenly arranged on the glass bottom petri dish's surface and covered with a 5/8 inch regenerated cellulose membrane (Spectrum Lab), which was used to immobilize the testes tips. The regenerated cellulose membranes were cut with a 5/8 inch hole puncher when dry, and then soaked in sterile Schneider's Complete *Drosophila*

medium overnight at 4 degrees Celsius prior to application. After covering the testes tips with the cellulose membrane, several drops of Schneider's Complete *Drosophila* medium were added on top of the membrane to prevent testes dehydration during imaging. Additional medium were added around the edges of the glass bottom petri dish away from the microwell. The glass bottom petri dish is then lidded and wrapped along the side with a piece of parafilm to prevent spillage and further dehydration (see Fig. 6C).

The testes containing glass bottom petri dish was then loaded onto the Zeiss Axio Observer.Z1 (see Fig. 6D) and visualized with Plan-Apochromat 63x oil emersion objective with numerical aperture (NA) of 1.4. All the live-imaging sequence frames were recorded using the Hamamatsu charge coupled detector (CCD) camera at 512 by 512 resolution and the Zeiss Axiovision software for up to 8 hours with 1 to 2 minute time intervals. To capture the movement patterns of spectrosomes, centrosomes, and the mitotic spindles with optimal photobleaching effects, three z-scans were made with 3µm sections per time frame. Consistent fluorescence exposure times were used throughout the experiments. Following fluorescence markers were used for the live-imaging: Ubi-α-tub-GFP (mitotic spindle visualization); Shadd-GFP (spectrosome organelle visualization); Sas6-mch (centrosome organelle visualization).

For the longer live-imaging (longer than 8hrs) sessions that span up to 24 hours to visualize the spectrosome dynamics throughout the whole GSC cell cycle, the Schneider's Complete *Drosophila* medium was replenished every 7-8 hours to maintain cellular activity. Results show that all cellular activities halt if the medium is not replenished past those time intervals. Similar to the shorter time-lapse imaging sessions, three z-scans were made with 3µm sections per time frame, but the time sequence interval increased to 8 minutes.

4. Quantification of GSCs' spindle orientation, centrosome misorientation, pro-metaphase to anaphase duration, and spectrosome orientation

Spindle orientation (spindle angle) was measured manually during Anaphase using the built in angle measurement add-on in Zeiss Axiovision software. The angle measured is the acute angle between the spindle axis and a line that passes through the hub-GSC interface and the center of the spindle length. Then the spindle angle measurements were divided into 0-30, 30-60, and 60-90 degree groups and their respective frequencies (%) reported.

Centrosome misorientation was quantified from all the sequence frames (across 3 z-stacks) taken from live-imaging of the GSCs that eventually divided. The criterion for correctly oriented centrosome was to have at least one centrosome localize to the quarter circle region that is connected to the hub-GSC interface. When one centrosome appeared misoriented but the other centrosome could not be found, the frame was not quantified to prevent false positives. Centrosomes were counted as misoriented when both centrosomes were outside the quarter circle region that is connected to the hub-GSC interface.

Pro-mephase to anaphase duration was recorded in minutes by subtracting the two times in which anaphase and pro-metaphase occur. Due to the Ubi-α-tub-GFP, the spindle formation and separation of the GSCs were clearly observed and stages of mitosis were easily distinguishable. Visually, we were able to observe the nuclear envelope break down by looking at the dark nuclear area being filled by non-specific cytosolic fluorescence. This can be observed in both red and green channels as trace amounts of cytosolic free form of Shadd-GFP and Sas6-mch fill the darker void. Specifically, we referred this point in time as the pro-metaphase stage of the mitosis. Anaphase time was recorded by observing the beginning of the spindle separation towards the mitotic spindle poles.

Spectrosome orientation was quantified as either apical or basal, and was decided to be apical or basal during the last 30 minutes prior to mitosis (before the nuclear envelope breakdown or before pro-metaphase). Most of the spectrosomes in the last 30 minutes of the interphase stayed either in the apical or the basal area (with movement generally possible in the basal area), except a few instances, which will be elaborated further in the next section. The spectrosome was quantified to be apical if the spectrosome resided in the apical part of the GSC's hemisphere and basal if the spectrosome resided in the basal part of the GSC's hemisphere.

5. Quantification of GSCs' Mobile vs Stationary Spectrosome and spectrosome movement pattern

Spectrosomes were quantified as either mobile or stationary during interphase. Generally, in wild type GSCs, it has been previously observed that spectrosome can migrate around the cell during interphase. We have quantified the spectrosome to be stationary, regardless of whether it is located apically or basally, if the spectrosome remained in the same area (usually around the basal or apical cortex regions) with very subtle to no movement for longer than 30 minutes prior to mitosis (before the nuclear break down or pro-metaphase). On the other hand, spectrosome was quantified as mobile if the spectrosome moved significantly more than its diameter (particularly outside the cortex region is most obvious) within 30 minutes prior to mitosis.

On several occasions, we have observed spectrosome migrating from apical cortex region of the GSCs to the basal cortex suddenly within the 30 minutes prior to mitosis. We have

presented this spectrosome movement in the Apical→Basal category and reported its occurrence frequency (%).

6. GSC Dynamics quantification

Please see Chapter II: Methods, section C: Subcellular organelle tracking, image processing, and dynamics quantification for more information.

7. Tissue preparation and Immunohistochemistry

Newly eclosed *DSas-4-mut* and *hts-mut* adult flies (0-1 day old) flies were selected from the stock and placed on a carbon dioxide pad (10 lbs/in^2) to administer anesthesia. Under 5x magnification on a Leica stereomicroscope, *Drosophila* testes were isolated while submerged under 0.5ml of 1x phosphate buffer saline (PBS) with two size 5 dissection tweezers (Dumont) inside a sterile 10 well glass plate. The isolated testes were then transferred into a 1.5 ml centrifuge tube containing 4% paraformaldehyde in PBS and fixated away from light for 30 minutes at room temperature (25 degrees Celsius), rocking on a nutator. The paraformaldehyde was then removed and the samples were rinsed two times and washed for 30 minutes with PBST (1x PBS+0.1% Triton X-100), rocking on a nutator at room temperature.

The following primary antibodies were used: Goat-anti-Vasa polyclonal igG (immunoglobulin) [1:80; dc-13; Santa Cruz Biotechnology] was used to identify germ cells (including GSC); mouse anti-γ-tub monoclonal igG (1:80; GTU-88; Sigma) was used to identify centrosomes; mouse anti-Fasciclin III igG [1:80; obtained from the Developmental Studies

Hybridoma Bank (DSHB)] was used to identify hub cells and hub-GSC interface; mouse anti-Adducin-like monoclonal (1:100; obtained from DSHB); rabbit-anti-α-tub polyclonal (1:100; ab18251; Abcam). In addition, the following secondary antibodies were used to capture the primary antibodies: Alex Fluor ® [350 or 488 or 568] donkey anti-[goat or rabbit or mouse] igG (1:100). The primary antibodies were diluted into an antibody buffer (3% Bovine serum albumin+ 0.1% Trion-X 100 in PBS) at proper concentrations and inserted into the centrifuge tubes containing the testes with the supernatant already removed. Then the testes were allowed to incubate overnight (between 16-24hrs) at 4 degree Celsius, rocking and away from light. The following day, the testes were rinsed two times with PBST and washed additionally with PBST three times (each wash: 10minutes on nutator at room temperature). The secondary antibodies were then diluted into an antibody buffer (3% Bovine serum albumin+ 0.1% Trion-X 100 in PBS) at proper concentrations and inserted into the centrifuge tubes containing the testes with the supernatant already removed. Again, the testes were allowed to incubate overnight (between 16-24hrs) at 4 degree Celsius, rocking and away from light. Finally, on the third day, the testes were rinsed two times and washed three times for 10 minutes with PBST on a nutator at room temperature.

The supernatants were then removed after the final wash and a single drop of Vectashield® Mounting Media was added into the centrifuge tube containing the testes. Under the Leica stereo microscope at 5x magnification, the testes and the Vectashield® Mounting Media were transferred on top of a glass slide using a 200µl pipette. The testes were then gently arranged on the glass slide and size 1 glass coverslip (0.15mm thickness) was applied on top of the testes. A care was used to prevent introducing bubbles on the testes. Furthermore, excess mounting medium between the glass slide and the glass cover slip was removed by placing a

paper towel on top of the glass cover slip and gently applying uniform pressure onto the glass cover slip. After the most of the excess moisture has been removed, nail polish was used to seal off the testes sample to prevent tissue dehydration from the environment. The prepared tissue samples were then stored at 4 degrees Celsius in the dark for future use.

8. Fluorescence microscopy

The glass slide containing the stained testes was then loaded onto the Zeiss Axio Observer.Z1 and visualized with Plan-Apochromat 63x oil emersion objective with numerical aperture (NA) of 1.4 or Plan-Neofluar 40x air objective with NA of 0.75. Fluorescence images were recorded using the Hamamatsu CCD camera at 512 by 512 resolution and the Zeiss Axiovision software. All the fixed samples were imaged using the Apotome add-on module by Zeiss, which has confocal capability and is designed to create optical sections of the fluorescent samples. Depending on the size of the subcellular structures, the optical section thickness was varied from 0.24μm to 1μm sections. By default, minimum optical section thickness of 0.24 μm was used for imaging centrosomes and spectrosomes. For other quantification such as counting GSCs (about 10um in diameter), up to 1μm optical section size was used. For each testis, all the spaces between two testes walls were imaged, which sometime was as thick as 25μm in height. For all the fixed fluorescence magnitude insensitive experiments, auto exposure (built-in) option in Axiovision was used set the initial exposure time for all the red, green, and blue channels. For taking multi-channel and multi-optical section images, optical section scans were completed for each channel instead of taking all the channel images (changing reflectors at each height) per each optical section for faster imaging acquisition time.

9. Quantification of GSC count

Germline stem cells were counted using the Vasa and FasIII staining. Since Vasa proteins localize to the cytoplasm of all the germ cells and FasIII proteins localize to the junction spaces of the hub cells, we only counted germ cells that are immediately adjacent to the FasIII staining (above, below, or next to the FasIII). Germline stem cells were not counted when slightest space between the hub cells and the GSCs were detected.

10. Mosaic Analysis with a Repressible Cell Marker Method

a. Final genotype generation

This method utilizes mitotic recombination to instantly induce desired mutation in a wild type fly via a controllable cue such as heat shock. Because previous attempt to conventionally generate a double knockout of centrosome (*DSas-4-mut*) and spectrosome (*hts-mut*) has failed due to lethality of both knockouts, MARCM method was a promising alternate genetic manipulation technique. Our approach was designed to induce a *DSas-4-mut* on a fly that has conventional *hts-mut* background, thus effectively creating a double mutant. The rational for choosing the *hts-mut* as the conventional background was due to the fact that *DSas-4-mut* is a much sicker fly that can only live couple of days after eclosion. On the other hand, the *hts-mut* flies are much more robust, surviving for weeks. To generate the final genotype for the MARCM experiment, we used combination of meiotic recombination mating and conventional mating methods. It took us longer than a year to produce the desired genotype and validate its functionality. The stocks we used to generate the final genotype were: Df(2R)BSC26 (Df(2R)); hts^{01103}; FRT82B, $DSas\text{-}4^{S2214}$(Stevens, Raposo et al. 2007); UAS-mCD8-GFP, hs-FLP;

GAL4.nos.NGT40 (nos-GAL4), hts^{01103}; FRT82B, GAL80LL3 (FRT82B,TubP-GAL80). Stocks were obtained from the Bloomington Drosophila Stock Center at Indiana University unless otherwise noted.

The final genotype generated is shown below:

$$\frac{\text{UAS} - \text{mCD8} - \text{GFP}, \text{hs} - \text{FLP}}{Y}; \frac{\text{nos} - \text{GAL4},\ \text{hts}^{01103}}{Df(2R)}; \frac{FRT82B, TubP - GAL80}{\text{FRT82B}, \text{DSas} - 4^{S2214}}$$

b. Heat shock

After mating the parental fly to generate the desired final genotype, the parental flies were discarded and the food vials containing the L3 larvae and pupa were submerged under water inside a water bath at 37 degree Celsius (heat shock treatment) for two hours for three consecutive days. The flies were then collected as soon as they eclosed on day 10 to 11. The eclosed flies were further selected against balancer phenotypes (e.g. Curly O wings and TM6B) to obtain the desired genotype.

c. Immunohistochemistry and microscopy

MARCM adult flies (up to 3 days old) flies were selected from the stock and placed on a carbon dioxide pad (10 lbs/in^2) to administer anesthesia. Under 5x magnification on a Leica stereomicroscope, *Drosophila* testes were isolated while submerged under 0.5ml of 1x phosphate buffer saline (PBS) with two size 5 dissection tweezers (Dumont) inside a sterile 10 well glass plate. The isolated testes were then transferred into a 1.5 ml centrifuge tube containing 4% paraformaldehyde in PBS and fixated away from light for 30

minutes at room temperature (25 degrees Celsius), rocking on a nutator. The paraformaldehyde was then removed and the samples were rinsed two times and washed for 30 minutes with PBST (1x PBS+0.1% Triton X-100), rocking on a nutator at room temperature. Because the number of desired genotype flies were very scarce, the newly eclosed flies were immediately fixed and stored at 4 degrees Celsius in PBS away from light (wrapped in aluminum foil) for a few days but not exceeding one week for the collective immunostaining.

The following primary antibodies were used: Goat-anti-Vasa polyclonal igG (immunoglobulin) [1:100; dc-13; Santa Cruz Biotechnology] was used to identify germ cells (including GSC); mouse anti-γ-tub monoclonal igG (1:70; GTU-88; Sigma) was used to identify centrosomes; mouse anti-Fasciclin III igG [1:70; obtained from the Developmental Studies Hybridoma Bank (DSHB)] was used to identify hub cells and hub-GSC interface; rabbit-anti-α-tub polyclonal (1:100; ab18251; Abcam). In addition, the following secondary antibodies were used to capture the primary antibodies: Alex Fluor ® 350 donkey anti-mouse igG (1:70), Alex Fluor ® 568 donkey anti-goat igG (1:100), and Alex Fluor ® 568 donkey anti-rabbit igG (1:300). The primary antibodies were diluted into a stringent antibody buffer (3% Bovine serum albumin+ 1% Trion-X 100 in PBS) at proper concentrations and inserted into the centrifuge tubes containing the testes with the supernatant already removed. Then the testes were allowed to incubate overnight (between 16-24hrs) at 4 degree Celsius, rocking and away from light. The following day, the testes were rinsed two times with PBST and washed additionally with PBST three times (each wash: 10minutes on nutator at room temperature). The secondary antibodies were then diluted into a stringent antibody buffer (3% Bovine serum albumin+ 1% Trion-X 100 in PBS) at proper concentrations and inserted into the centrifuge tubes containing the testes with the supernatant already removed. Again, the testes were allowed to incubate overnight (between

16-24hrs) at 4 degree Celsius, rocking and away from light. Finally, on the third day, the testes were rinsed two times and washed three times for 10 minutes with PBST on a nutator at room temperature.

The supernatants were then removed after the final wash and a single drop of Vectashield® Mounting Media was added into the centrifuge tube containing the testes. Under the Leica stereo microscope at 5x magnification, the testes and the Vectashield® Mounting Media were transferred on top of a glass slide using a 200µl pipette. The testes were then gently arranged on the glass slide and size 1 glass coverslip (0.15mm thickness) was applied on top of the testes. A care was used to prevent introducing bubbles on the testes. Furthermore, excess mounting medium between the glass slide and the glass cover slip was removed by placing a paper towel on top of the glass cover slip and gently applying uniform pressure onto the glass cover slip. After the most of the excess moisture has been removed, nail polish was used to seal off the testes sample to prevent tissue dehydration from the environment. The prepared tissue samples were then stored at 4 degrees Celsius in the dark for future use.

The glass slide containing the stained testes was then loaded onto the Zeiss Axio Observer.Z1 and visualized with Plan-Apochromat 63x oil emersion objective with numerical aperture (NA) of 1.4. Fluorescence images were recorded using the Hamamatsu CCD camera at 512 by 512 resolution and the Zeiss Axiovision software. All the fixed samples were imaged using the Apotome add-on module by Zeiss. Minimum optical section thickness of 0.24 µm was used as to include all the centrosomes and all the spaces between two walls of the testes were imaged. The UAS-mCD8-GFP signal compared to other GFP or mcherry signal was extremely faint, so particularly longer exposure time was required. Best exposure time was around 1-1.5

seconds per image frame from the X-Cite® 120 lamp set at medium brightness. Higher brightness setting decreased the sample exposure time, but it created photobleaching problems.

d. Verification

We have ascertained whether we correctly created the desired genotype and the genes function as intended. Firstly, we tested the $\frac{\text{nos}-\text{GAL4,hts}^{01103}}{Df(2R)}$ or *hts-mut* background condition by staining with adducin-like antibody to look for spectrosome and fusome structures. It was verified that that the fusome and spectrosomes were successfully knocked out. Secondly, we tested if the nos-GAL4 is present and can effectively activate the UAS-mCD8-GFP (membrane protein-GFP). By observing green florescence only in the germ cells (also GSCs') and their membranes (after heat shock), it was verified that both UAS-mCD8-GFP and nos-GAL4 were present and working properly. Thirdly, we checked for the presence of tubP-GAL80 and its function. GAL80 gene is supposed to suppress the function of GAL4. In the genotype setup, without heat shock (i.e. without activating the hs-FLP), both GAL80 and GAL4 were expected to co-exist in the GSCs, so technically the GSCs were expected not to show any fluorescence because UAS-mCD8-GFP gene cannot be activated due to the suppression of GAL4. Based on our testing, without heat shock, no fluorescence was detected, which verifies the existence and intended function of GAL80. Next, we checked to see whether the hs-FLP and the FRT cassette system was working properly. In our MARCM set-up, the heat shock was expected to cause FLP to recombine the FRT region and cause mitotic recombination. In turn, the mitotic recombination was expected to generate GSCs with homozygote mutant genes without GAL80 genes (GSC clones) and other GSCs with homozygote GAL80 genes without

mutant genes. Technically, the GSC clones should fluoresce and have reduced centrosome number while the other GSCs should not fluoresce and have normal centrosome number. This was verified by two observations: 1) after applying heat shock, fluorescing GSC clones were observed; 2) centrosome stains (γ-tubulin stain) showed significantly reduced centrosomes in the fluorescing GSC clones compared to non-fluorescing GSCs. These results showed that the FLP-FRT cassette system was working properly. Finally, all the verification showed that our MARCM method was successful in generating double knockout (centrosome and spectrosome) GSC clones.

11. Statistical Analysis

Student's t-test was used to calculate the p-values to determine significant differences between groups. The histograms were generated by selecting a fixed number of bins that covers the range of 0 to maximum values in groups. Bin sizes used for the centrosome velocity and centrosme distance were 0.15μm/min and 0.84μm, respectively. Wilcoxon rank sum test (also called Mann–Whitney U test) was used to calculate the p-values to determine significant differences in groups that did not follow normal distributions. Standard deviations were used for the error bars on the bar charts.

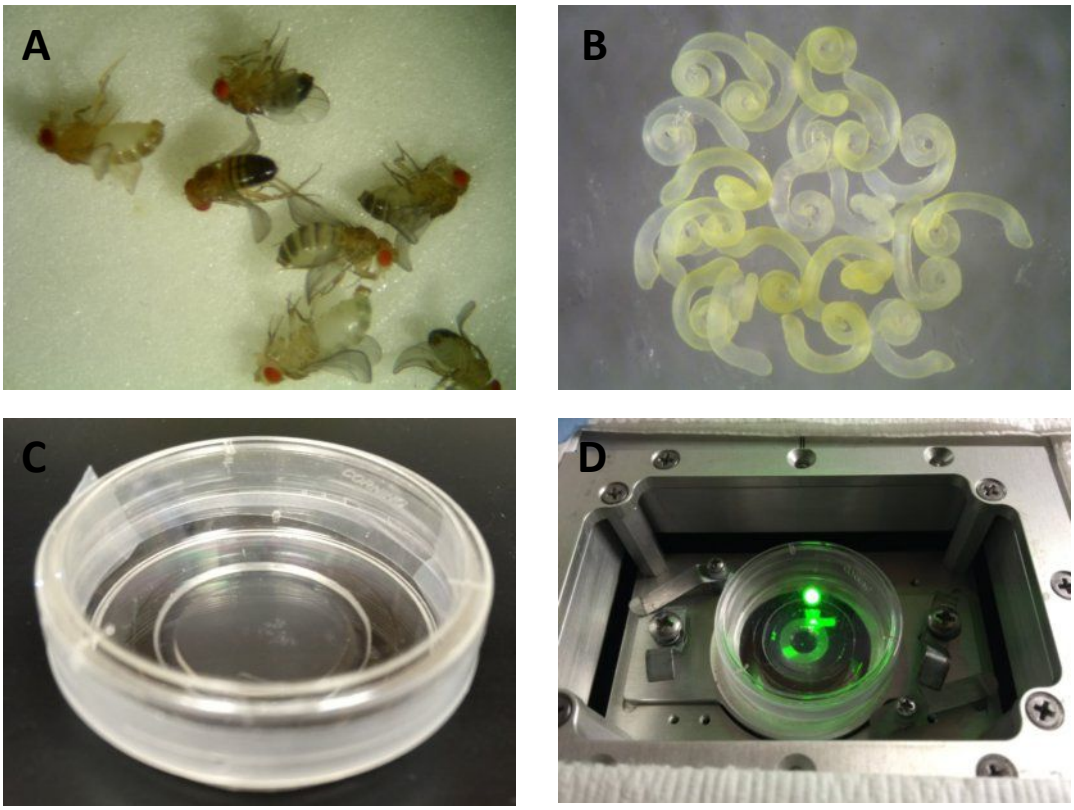

Figure 6: Tissue preparation and time-lapse live-cell imaging. (A) *Drosophila* was anesthetized using carbon dioxide on a fly pad. **(B)** *Drosophila* testes were then collected using surgical tweezers under a stereomicroscope. **(C)** Glass bottom petri dish has been loaded with cut testes, cellulose membrane to immobilize the testes, and *Drosophila* medium for nutrition, and is ready for imaging. **(D)** The glass bottom petri dish loaded onto the high magnification Zeiss microscope.

B. Effects of Centrosomin and Adenomatous Polyposis Coli Protein 2 on Spectrosome Recruitment and Asymmetric Stem Cell Divisions

(Parts of this chapter were previously published as Bang, C. and J. Cheng (2015). "Dynamic Interplay of Spectrosome and Centrosome Organelles in Asymmetric Stem Cell Divisions." PLoS ONE 10(4): e0123294.)

1. Fly husbandry and strains

All fly stocks were raised on standard Bloomington medium and inside of an environmental chamber (25°C; standard 24 hour dark-light cycle (12:12); controlled humidity). Fly stocks used were: Ubi-Short Adducin-GFP (Shadd-GFP; obtained from Dr. Spradling's Laboratory); Ubi-Sas6-mcherry (Sas6-mch) both on second and third chromosomes; $APC2^{N175K}$; $APC2^{\Delta S}$; cnn^{HK21}; cnn^{mfs7}. Stocks were obtained from the Bloomington Drosophila Stock Center at Indiana University unless otherwise noted. Following genotypes were generated and used for our live-imaging and fixed experiments:

$$\frac{X}{Y}; \frac{Shadd-GFP, cnn^{mfs7}}{cnn^{HK21}}; \frac{\text{Sas6}-\text{mch}}{\text{Sas6}-\text{mch}}$$

$$\frac{X}{Y}; \frac{Shadd-GFP, cnn}{+}; \frac{\text{Sas6}-\text{mch}}{\text{Sas6}-\text{mch}}$$

$$\frac{X}{Y}; \frac{Shadd-GFP, Sas6-mch}{Shadd-GFP, Sas6-mch}; \frac{APC2^{N175K}}{APC2^{\Delta S}}$$

$$\frac{X}{Y}; \frac{Shadd-GFP, Sas6-mch}{Shadd-GFP, Sas6-mch}; \frac{APC2}{+}$$

$$\frac{X}{Y}; \frac{Shadd-GFP}{Shadd-GFP}; \frac{\text{Sas6}-\text{mch}}{\text{Sas6}-\text{mch}}$$

The heterozygote mutant genes $\frac{cnn^{mfs7}}{cnn^{HK21}}$ will be hence forth be referred *cnn-mut* and the heterozygote mutant genes $\frac{APC2^{N175K}}{APC2^{\Delta S}}$ will hence forth be referred as *APC2-mut*. Both *cnn-mut* and *APC2-mut* flies did not require any manual assistance during the eclosion process. The geneotypes with + are the respective control to those mutants. Finally the last genotype is a wild type control that was used as live-imaging controls. The Ubi-α-tub-GFP was taken out so the spectrosomes can be observed clearly without Ubi-α-tub-GFP obscuring views in the green channel. Importantly, in both cnn-mut and APC2-mut genotypes generated, there were orange and red eyed flies, and only the orange eye flies were selected for our studies. Main reason for this was because the red eye flies contained hazy testes walls that made live-imaging not very clear. Interestingly, however, the haziness disappeared after fixating with paraformaldehyde and permeabilizing with PBST.

The existences of Shadd-GFP and Sas6-mch in our generated flies were easily verified by observing their signals under the fluorescence microscope. Furthermore, the existence of *cnn-mut* in our generated flies was firstly prescreened by observing the balancer to non-balancer ratio and increased presence of abnormal onion stage spermatocytes and was later verified by quantifying functional characteristics, such as centrosome and spindle misorientation as previously shown (Yamashita, Jones et al. 2003, Inaba, Yuan et al. 2010). Furthermore, the existence of *APC2-mut* in our generated flies was also verified by quantifying functional characteristics, such as centrosome and spindle misorientation as previously shown (Yamashita,

Jones et al. 2003, Inaba, Yuan et al. 2010). In addition, the existence of *APC2-mut* gene was further verified by staining with a rabbit-APC2 antibody (1:100; gift from the Bienz laboratory, UK), which did not localize to the hub-GSC interface as shown previously (Inaba, Yuan et al. 2010).

2. Meiotic recombination

Using meiotic recombination, different genes (mutants, transgenes, and tagged) from each parent were recombined via chromosomal crossover during meiosis so that both genes can exist in offspring's chromosome. Using a simple crossing technique (Greenspan 2004), the following genes were successfully recombined: Shadd-GFP, cnn^{mfs7} and Shadd-GFP, Sas6-mch. Presences of Shadd-GFP and Sas6-mch in the recombined genes were easily identified via a fluorescence microscope. However, identifying the presence of the cnn^{mfs7} gene was not straight forward as the antibody for *Drosophila* cnn^{mfs7} was not available commercially. We firstly prescreened for the cnn^{mfs7} gene by observing the balancer to non-balancer ratio (it's a lethal mutation for homozygotes) and looking for increased presence of abnormal onion stage spermatocytes. Then, we verified the presences of cnn^{mfs7}gene by quantifying functional characteristics, such as centrosome and spindle misorientation as reported previously. The necessary number (N) of progeny lines required to probabilistically obtain the recombined genes was calculated using the Mather's formula and how much map units the genes were apart:

$$N = \frac{\log(1-p)}{\log(1-f)} * 2$$

,where p is the confidence interval (e.g. 95% assurance of outcome) and the f is the probability for the meiotic recombination (also referred to as a map unit number) of the two genes to occur. The two is multiplied by two for conservative purposes.

N value for the *cnn*^{mfs7}, Shadd-GFP:

$$N = \frac{\log(1 - 0.95)}{\log(1 - 0.18)} * 2$$

$$N = 31$$

However, we generated 37 lines just in case. All of the 37 lines generated were tested for the existence of the *cnn*^{mfs7} and Shadd-GFP genes as stated above. Additionally, N value for the Shadd-GFP, Sas6-mch could not be calculated since the Sas6-mch chromosome insertion sites were multiple and were unknown. There was also no additional information about the gene insertion sites in the Flybase.org. So, we arbitrarily used N=40, generated 40 lines, and verified those lines for the existence of both Shadd-GFP and Sas6-mch. Surprisingly, there were quite a few lines that contained both genes.

3. Tissue preparation and time-lapse live-cell imaging

The following protocol is an adaptation to the methods previously used (Cheng and Hunt 2009). Prior to the dissection, all the dissecting equipment were sterilized using 70% ethanol or sterilized under UV for at least one hour. Newly eclosed *cnn-mut* and *APC2-mut* adult flies (0-1 day old) flies were selected from the stock and placed on a carbon dioxide pad (10 lbs/in^2) to administer anesthesia. Under 5x magnification on a Leica stereomicroscope, *Drosophila* testes were isolated while submerged under 0.5ml of sterile Schneider's Complete *Drosophila* medium (Schneider's *Drosophila* medium, 10% fetal bovine serum (FBS), 1% penicillin streptomycin (Pen-Strep)) with two size 5 dissection tweezers (Dumont) inside a sterile 10 well glass plate. The isolated testes were then transferred into the adjacent well of the glass plate containing 0.5 ml of Schneider's Complete *Drosophila* medium to be cut. Using a size 10

scalpel blade, the tips of the testes were cut from the remainder of the testes and were selected for live-imaging. Removing much of the testes muscles minimized movement for live-imaging. On average per imaging session, about 10-15 testes tips were cut.

The cut testes tips were then transferred into a sterile glass bottom petri dish (MatTek, 35mm glass with 20mm microwell) using a 10µl pipette (sterile). The excess Schneider's Complete *Drosophila* medium from the glass bottom petri dish was removed with a tweezer's tip using capillary force. The testes were then evenly arranged on the glass bottom petri dish's surface and covered with a 5/8 inch regenerated cellulose membrane (Spectrum Lab), which was used to immobilize the testes tips. The regenerated cellulose membranes were cut with a 5/8 inch hole puncher when dry, and then soaked in sterile Schneider's Complete *Drosophila* medium overnight at 4 degrees Celsius prior to application. After covering the testes tips with the cellulose membrane, several drops of Schneider's Complete *Drosophila* medium were added on top of the membrane to prevent testes dehydration during imaging. Additional medium were added around the edges of the glass bottom petri dish away from the microwell. The glass bottom petri dish is then lidded and wrapped along the side with a piece of parafilm to prevent spillage and further dehydration.

The testes containing glass bottom petri dish was then loaded onto the Zeiss Axio Observer.Z1 and visualized with Plan-Apochromat 63x oil emersion objective with numerical aperture (NA) of 1.4. All the live-imaging sequence frames were recorded using the Hamamatsu charge coupled detector (CCD) camera at 512 by 512 resolution and the Zeiss Axiovision software for up to 3 hours with 1 minute time intervals. To capture the movement patterns of spectrosomes, centrosomes, and the mitotic spindles with minimal photobleaching effects but capturing adequate movement space, three z-scans were made with 3µm sections per time frame.

Consistent fluorescence exposure times were used throughout the experiments. Following fluorescence markers were used for the live-imaging: Shadd-GFP (spectrosome organelle visualization); Sas6-mch (centrosome organelle visualization).

4. Quantification of GSCs' spindle orientation, spectrosome orientation, and pro-metaphase to telophase duration

Spindle orientation (spindle angle) was measured manually during Anaphase using the built in angle measurement add-on in Zeiss Axiovision software. Since there was no Ubi-α-tub-GFP in the generated GSCs, apical and basal centrosome positions (Sas6-mch) were used to calculate the spindle angles. The angle measured is the acute angle between a line that passes through the apical and basal centrosomes and a line that passes through the hub-GSC interface and the center of the two centrosomes. Then the spindle angle measurements were divided into 0-30, 30-60, and 60-90 degree groups and their respective frequency (%) reported.

Centrosome misorientation was quantified from all the sequence frames (across 3 z-stacks) taken from live-imaging of the GSCs that eventually divided. The criterion for correctly oriented centrosome was to have at least one centrosome localize to the quarter circle region that is connected to the hub-GSC interface. When one centrosome appeared misoriented but the other centrosome did not come into view, the frame was not quantified to prevent false positives. Centrosomes were counted as misoriented when both centrosomes were outside the quarter circle region that is connected to the hub-GSC interface.

Pro-mephase to telophase duration was recorded in minutes by subtracting the two times in which telophase and pro-metaphase occur. Due to the absence of Ubi-α-tub-GFP, the spindle formation and separation of the GSCs could not be observed. In addition, other stages of mitosis

such as metaphase and anaphase could only be inferred through cellular shape change. Thus, the most distinguishable stages of the mitosis were pro-metaphase and telophase, so we quantified the pro-metaphase to telophase duration instead of using pro-metaphase to anaphase duration as used previously. Visually, we were able to observe the nuclear envelope break down by looking at the dark nuclear area being filled by non-specific cytosolic fluorescence. This can be observed in both red and green channels as trace amounts of cytosolic free form of Shadd-GFP and Sas6-mch fill the darker void. Specifically, we referred this point in time as the pro-metaphase stage of the mitosis.

Spectrosome orientation was quantified as either apical or basal, and was decided to be apical or basal during the last 30 minutes prior to mitosis (before the nuclear envelope breakdown or before pro-metaphase). Most of the spectrosomes in the last 30 minutes of the interphase stayed either in the apical or the basal area (with movement generally possible in the basal area), except a few instances, which will be elaborated further in the next section. The spectrosome was quantified to be apical if the spectrosome resided in the apical part of the GSC's hemisphere and basal if the spectrosome resided in the basal part of the GSC's hemisphere.

5. Quantification of GSCs' Mobile vs Stationary Spectrosome and spectrosome movement pattern

Spectrosomes were quantified as either mobile or stationary during interphase. Generally, in wild type GSCs, it has been previously observed that spectrosome can migrate around the cell during interphase. We have quantified the spectrosome to be stationary, regardless of whether it is located apically or basally, if the spectrosome remained in the same

area (usually around the basal or apical cortex regions) with very subtle to no movement for longer than 30 minutes prior to mitosis (before the nuclear break down or pro-metaphase). On the other hand, spectrosome was quantified as mobile if the spectrosome moved significantly more than its diameter (particularly outside the cortex region is most obvious) within 30 minutes prior to mitosis.

On several occasions, we have observed spectrosome migrating from apical cortex region of the GSCs to the basal cortex suddenly within the 30 minutes prior to mitosis. We have presented this spectrosome movement in the Apical→Basal category and reported its occurrence frequency (%).

6. GSC Dynamics quantification

Please see Chapter II: Methods, section C: Subcellular organelle tracking, image processing, and dynamics quantification for more information.

7. Tissue preparation and Immunohistochemistry

Newly eclosed *cnn-mut* and *APC2-mut* adult flies (0-1 day old) flies were selected from the stock and placed on a carbon dioxide pad (10 lbs/in^2) to administer anesthesia. Under 5x magnification on a Leica stereomicroscope, *Drosophila* testes were isolated while submerged under 0.5ml of 1x phosphate buffer saline (PBS) with two size 5 dissection tweezers (Dumont) inside a sterile 10 well glass plate. The isolated testes were then transferred into a 1.5 ml centrifuge tube containing 4% paraformaldehyde in PBS and fixated away from light for 30 minutes at room temperature (25 degrees Celsius), rocking on a nutator. The paraformaldehyde

was then removed and the samples were rinsed two times and washed for 30 minutes with PBST, rocking on a nutator at room temperature.

To visualize onion-stage spermatocytes to prescreen for the *cnn*^{mfs7} GSCs, live testes were placed with PBS on a glass slide and gently lidded with a number 1 sized cover slip. Then the testes were sealed off using a nail polish. The samples were only viable for up to only one hour to hour and a half.

The following primary antibodies were used for the *cnn-mut*: Goat-anti-Vasa polyclonal igG (immunoglobulin) [1:100; dc-13; Santa Cruz Biotechnology] was used to identify germ cells (including GSC); rabbit-anti-Spd-2 igG (1:500; gift from the Raff Laboratory, UK) was used to identify centrosomes; mouse anti-Fasciclin III igG [1:700; obtained from the Developmental Studies Hybridoma Bank (DSHB)] was used to identify hub cells and hub-GSC interface. Spd-2 antibody was used instead of γ-tubulin because γ-tubulin expression is drastically reduced in *cnn-mut* GSCs. Spd-2 is a centrosomal protein that was shown to recruit PCM to the sperm centriole (Dix and Raff 2007). In addition, the following secondary antibodies were used to capture the primary antibodies: Alex Fluor ® 568 donkey anti-mouse igG (1:200); Alex Fluor ® 568 donkey anti-goat igG (1:100); and Alex Fluor ® 350 donkey anti-rabbit igG (1:100). The following primary antibodies were used for the *APC2-mut*: Goat-anti-Vasa polyclonal igG (immunoglobulin) [1:80; dc-13; Santa Cruz Biotechnology] was used to identify germ cells (including GSC); mouse anti-γ-tub monoclonal igG (1:80; GTU-88; Sigma) was used to identify centrosomes; mouse anti-Fasciclin III igG [1:80; obtained from the Developmental Studies Hybridoma Bank (DSHB)] was used to identify hub cells and hub-GSC interface. In addition, the following secondary antibodies were used to capture the primary antibodies: Alex Fluor ® 350 donkey anti-mouse igG (1:50) and Alex Fluor ® 568 donkey anti-goat igG (1:100).

The primary antibodies were diluted into an antibody buffer (3% Bovine serum albumin+ 0.1% Trion-X 100 in PBS) at proper concentrations and inserted into the centrifuge tubes containing the testes with the supernatant already removed. Then the testes were allowed to incubate overnight (between 16-24hrs) at 4 degree Celsius, rocking and away from light. The following day, the testes were rinsed two times with PBST and washed additionally with PBST three times (each wash: 10minutes on nutator at room temperature). The secondary antibodies were then diluted into an antibody buffer (3% Bovine serum albumin+ 0.1% Trion-X 100 in PBS) at proper concentrations and inserted into the centrifuge tubes containing the testes with the supernatant already removed. Again, the testes were allowed to incubate overnight (between 16-24hrs) at 4 degree Celsius, rocking and away from light. Finally, on the third day, the testes were rinsed two times and washed three times for 10 minutes with PBST on a nutator at room temperature.

The supernatants were then removed after the final wash and a single drop of Vectashield® Mounting Media was added into the centrifuge tube containing the testes. Under the Leica stereo microscope at 5x magnification, the testes and the Vectashield® Mounting Media were transferred on top of a glass slide using a 200µl pipette. The testes were then gently arranged on the glass slide and size 1 glass coverslip (0.15mm thickness) was applied on top of the testes. A care was used to prevent introducing bubbles on the testes. Furthermore, excess mounting medium between the glass slide and the glass cover slip was removed by placing a paper towel on top of the glass cover slip and gently applying uniform pressure onto the glass cover slip. After the most of the excess moisture has been removed, nail polish was used to seal off the testes sample to prevent tissue dehydration from the environment. The prepared tissue samples were then stored at 4 degrees Celsius in the dark for future use.

8. Fluorescence and phase contrast microscopy

The glass slide containing the stained testes was then loaded onto the Zeiss Axio Observer.Z1 and visualized with Plan-Apochromat 63x oil emersion objective with numerical aperture (NA) of 1.4. Fluorescence images were recorded using the Hamamatsu CCD camera at 512 by 512 resolution and the Zeiss Axiovision software. All the fixed samples were imaged using the Apotome add-on module by Zeiss, which has confocal capability and is designed to create optical sections of the fluorescent samples. Size 0.24µm optical section thickness was used for imaging *cnn-mut* and *APC2-mut* testes. For each testis, all the spaces between two testes walls were imaged, which sometime was as thick as 25µm in height. For all the fixed fluorescence magnitude insensitive experiments, auto exposure (built-in) option in Axiovision was used set the initial exposure time for all the red, green, and blue channels. For taking multi-channel and multi-optical section images, optical section scans were completed for each channel instead of taking all the channel images (changing reflectors at each height) per each optical section for faster imaging acquisition time.

To visualize onion-stage spermatocytes to prescreen cnn^{mfs7} GSCs, the live testes inside of glass slide were loaded onto the Zeiss Axio Observer.Z1 and visualized with Plan-Apochromat 63x oil emersion objective. Then, differential interference contrast (DIC) and phase contrast methods were selected to visualize the onion-stage spermatocytes. Additionally, the DIC and phase contrast images were recorded using the Hamamatsu CCD camera at 512 by 512 resolution and the Zeiss Axiovision software.

9. Quantification of spectrosome localization categories, centrosome misorientation, and GSC count.

Spectrosome localization categories from a previous study (Yuan, Chiang et al. 2012) was used to represent all the possible spectrosome localization configurations in fixed GSCs. Therefore, all the GSCs in the testes (if quantifiable), which also meant all the cell cycle stages of the GSCs, were quantified for the spectrosome localization. Thus, all optical sections of the testes (from one testes wall to the other) were inspected. Spectrosome apical or basal localizations were decided based on which side of the center line of the GSC the spectrosome was placed.

Centrosome misorientation was quantified from the fixed GSCs, which included all the GSCs in all the stages of the cell cycles. All the optical sections were thoroughly examined to check for the centrosome locations. The criterion for correctly oriented centrosome was to have at least one centrosome localize to the quarter circle region that is connected to the hub-GSC interface. When one centrosome appeared misoriented but the other centrosome could not be found, the frame was not quantified to prevent false positives. Centrosomes were counted as misoriented when both centrosomes were outside the quarter circle region that is connected to the hub-GSC interface. In addition to quantifying the total centrosome misorientation, centrosome misorientation to each spectrosome localization categories was also quantified.

Germline stem cells were counted using the Vasa and FasIII staining. Since Vasa proteins localize to the cytoplasm of all the germ cells and FasIII proteins localize to the junction spaces of the hub cells, we only counted germ cells that are immediately adjacent to the FasIII staining (above, below, or next to the FasIII). GSCs were not counted when slightest space between the hub cells and the GSCs were detected.

10. Ultrafast laser microsurgery

a. Set-up

The fempto-second ultra-fast fiber laser (PolarOnyx) with maximum output of 5W and 1035nm wavelength with repetition rate of 30-40 kHz was used. The laser path was then created (see schematics in Fig. 7) from the fiber laser to the Zeiss Observer.Z1 microscope, using mirrors to control the directionality and lenses to control the beam size. Fine control and safety mechanisms were also put in place such as the Faraday Isolator to prevent back reflections to the laser, neutral density filter to control the laser intensity into the samples, and laser shutter to control the laser exposure time to ablate the samples. The laser was then routed to the Plan-Apochromat 63x oil emersion objective, then onto the samples. For safety concerns, the system was designed so that when the fluorescence is being used, laser is blocked off, and vice versa, which could be even fast as a fraction of a second between the switches. The ablation was controlled by a Three Axis Nanopositioners (Mad City Labs) that can precisely move nano meter distance in the x, y, and z directions.

b. Ablation programs and parameters

The Three Axis Nanopositioners, laser and fluorescence shutters, CCD camera, reflectors, the ablation parameter controls, and image acquisitions were all controlled by an in-house developed (via Visual Basic) program. The ablation program for centrosome and spectrosome works as follows. Firstly, the user selects a centrosome or spectrosome to ablate and creates a circle (region of interest (ROI)) around it, then the program takes 7 z-stacks images above and below the chosen ROI and selects the best focus (i.e. center of the centrosome

in z) using the variance algorithm. Then, the program executes the ablation algorithms, opens the laser shutter, relays coordinates for the Three Axis Nanopositioners to follow, and ablates the sample, covering all the selected ROI as well as the z-height equivalent to the ROI diameter. The selection and ablation occurs within few seconds, so the centrosome and spectrosome drifts were not much of a concern. To verify successful ablation, we test cut sperm tails in few testes and verified through DIC microscopy that the cut region had indents and that the sperm tails have drifted away. When ablating centrosomes and spectrosomes, ablations destroyed the centrosomes' and spectrosomes' fluorescence and created cytosolic debris around the ablated sites. We found that 80 mW laser before entering the microscope was adequate enough to ablate centrosomes and spectrosomes successfully without much visible damage to the GSCs. We believe that at the sample level, the power of laser would taper off significantly below the 80mW power measured at the entrance of the microscope. The laser beam spot-size is around 100 nm.

11. Statistical Analysis

Sudent's t-test was used to calculate the p-values to determine significant differences between groups. The histograms were generated by selecting a fixed number of bins that covers the range of 0 to maximum values in groups. Bin sizes used for the histograms are: spectrosome distance to hub-GSC interface (0.92 μm), spectrosome velocity (0.23 μm/min), GSC-inherited centrosome distance to hub-GSC interface (0.79 μm), GB-inherited centrosome distance to hub-GSC interface (0.95 μm), GSC-inherited centrosome velocity (0.21 μm/min), GB-inherited centrosome velocity (0.26 μm/min), spindle angle (6 degrees), spindle angular velocity (4 degrees/min). Wilcoxon rank sum test (also called Mann–Whitney U test) was used

to calculate the p-values to determine significant differences in groups that did not follow normal distributions. Standard deviations were used for the error bars on the bar charts.

C. Subcellular organelle tracking, image processing, and dynamics quantification

(Parts of this chapter were previously published as Bang, C. and J. Cheng (2015). "Dynamic Interplay of Spectrosome and Centrosome Organelles in Asymmetric Stem Cell Divisions." PLoS ONE 10(4): e0123294.)

1. Transforming 3-Dimensional images to trackable 2-D images

For tracking centrosomes and spectrosomes in 2-Dimensions (2-D), time-lapse live-image sequences recorded in 3-Dimensions (3-D) were overlaid (each pixel intensities from the optical section images were averaged using Matlab) and contrasted to yield 2-D image sequences. Three dimensional tracking was not a feasible option granted the optical sections were too sparsely taken during live-imaging to prevent photobleaching. Written with Matlab, the users have the options to include and exclude any optical sections while overlaying to create crisper 2-D images.

2. Development of the tracking software with Labview and submodule Labview Vision

Tracking program to track the centrosome and spectrosome was developed in-house using the Labview software and its submodule Labview Vision. Labview Vision has a proprietary pattern matching function built-in to its library. Selecting a specific shape using the

ROI selector, the pattern matching function remembers that selected ROI and attempts to match many like it in the image. The matching scores can be adjusted to decrease the false positive matching, but at the price of possibly having no match. Also, there is an option to set the number of matching to user's desire. In our case, since we were matching the centrosome/spectrosome organelle in the next time sequence with a ROI template from the previous time sequence, increasing matching scores and setting the matching number to one or two provided the best result. The Labview program was built around the Labview Vision's pattern match function and has many necessary components to make it user friendly, including: 1) Load and open image sequences subroutine, 2) Image learn and image crop subroutine, 3) pattern matching subroutine that includes the pattern matching function, 4) previous, current, and next image sequence browsing subroutines, 5) record and save center coordinate of the matching image with the ROI template subroutine, 6) overlay and visualize pattern matched coordinate subroutine, 7) text file output subroutine containing all the pattern matched coordinates, and 8) verification of pattern matched coordinate subroutine.

3. Tracking centrosomes, spectrosomes, and the hub-GSC interface and verification of coordinates

Tracking starts with loading an image and selection of centrosome/spectrosome with an ROI selector and feed the ROI template to the pattern matching function. The function then learns the ROI template image and attempt to match the ROI in the next sequence image. The function then guesses and displays overlaying red dots on the locations of matching. User then confirms the correctness of the matching and moves onto the next image sequence by clicking on the next image button. If the matching is wrong, then the user reselects the ROI

template for the function to relearn and move onto the next image sequence. The process continues until the last image sequence is matched. Every time when the user confirms the matching or reselects the ROI template for the function to learn, the function outputs a center coordinate (x,y) of the matched image or learned ROI. Finally the coordinates for each time sequence are collected and saved as a text file (see the program interface in Fig. 8).

There is one additional sub-routine program written to double check if the tracking (pattern matching) was correct. This subroutine program allows the user to reload the coordinate systems from a saved text file and displays a red dot on top of the tracked centrosome/spectrosome (See interface in Fig. 8, enclosed by a blue rectangular box). There is also a time browsing button (-1 for previous and +1 for next image sequence) so the user can browse through all the tracked image sequences and verify the correctness of tracking through observing where the red dot is placed. If the tracked coordinate is found to be wrong, then the user can either restart the tracking process for that particular GSC or simply open up the text file and update the coordinates manually. The coordinates of the open image is shown if user places a cross-hair on top of the image. Using the tracking (pattern matching) methods as described above, hub-GSC interface coordinates, spectrosome coordinates, and apical and basal centrosome coordinates were obtained.

4. Quantification of spectrosome velocity

To quantify the spectrosome velocity, a Matlab program was written to calculate the velocity using the hub-GSC interface coordinates and spectrosome coordinates with sequential time points. Firstly, to take account of tissue movements affecting the spectrosome velocity (which can become quite large), local spectrosome coordinates with respect to the hub-

GSC were calculated by subtracting the spectrosome coordinates from the hub-GSC coordinates. This effectively makes the hub-GSC coordinates as the new origin (0, 0). Then, to calculate the spectrosome velocity, distance formula and the local spectrosome coordinates were used to calculate the spectrosome movement distance from the previous time point to the next. The distance was simply divided by the time interval to produce velocity. The procedure was repeated for all subsequent time points to obtain total n-1 velocity values, given n is the total number of time points. Spectrosome velocities from many GSCs were pooled together to generate a histogram for each experimental and control groups.

5. Quantification of spectrosome distance to the hub-GSC interface

To quantify the spectrosome distance to the hub-GSC interface, a Matlab program was written to calculate the distance using the hub-GSC interface coordinates and spectrosome coordinates. For each time point, the distance was calculated using the distance formula. The procedure was repeated for all subsequent time points. Spectrosome distances from many GSCs were pooled together to generate a histogram for each experimental and control groups.

6. Quantification of apical and basal centrosome velocity

The procedure to calculate the apical centrosome velocity is exactly same as the procedure to calculate the basal centrosome velocity, so specific description apical or basal will not be mentioned. To quantify the centrosome velocity, a Matlab program was written to calculate the velocity using the hub-GSC interface coordinates and centrosome coordinates with sequential time points. Firstly, to take account of tissue movements affecting the centrosome velocity (which can become quite large), local centrosome coordinates with respect to the hub-

GSC were calculated by subtracting the centrosome coordinates from the hub-GSC coordinates. This effectively makes the hub-GSC coordinates as the new origin (0, 0). Then, to calculate the centrosome velocity, distance formula and the local centrosome coordinates were used to calculate the centrosome movement distance from the previous time point to the next. The distance was simply divided by the time interval to produce velocity. The procedure was repeated for all subsequent time points to obtain total n-1 velocity values, given n is the total number of time points. Centrosome velocities (both apical and basal) from many GSCs were pooled together to generate a histogram for each experimental and control groups.

7. Quantification of apical and basal centrosome distance to hub-GSC interface

The procedure to calculate the apical centrosome distance to the hub-GSC interface is exactly same as the procedure to calculate the basal centrosome distance to the hub-GSC interface, so specific description apical or basal will not be mentioned. To quantify the centrosome distance to the hub-GSC interface, a Matlab program was written to calculate the distance using the hub-GSC interface coordinates and centrosome coordinates. For each time point, the distance was calculated using the distance formula. The procedure was repeated for all subsequent time points. Centrosome (both apical and basal) distances from many GSCs were pooled together to generate a histogram for each experimental and control groups.

8. Quantification of spindle separation velocity

To quantify the spindle separation, a Matlab program was written to calculate the velocity using both apical and basal centrosome coordinates with sequential time points (only

during mitosis). Firstly, for each time point, distance formula was used to calculate how far the two centrosomes are apart. Then, the distance from the next time point was subtracted from the previous time point, and the difference was divided by time the point interval to obtain the spindle separation velocity. Negative spindle separation velocity is directed inward towards the GSC equator and positive spindle separation velocity is directed outwards. Spindle separation velocities from many GSCs were pooled together to generate a histogram for each experimental and control groups.

9. Quantification of spindle angle

A Matlab program was written to calculate the spindle angle using the apical and basal centrosome coordinates as well as the hub-GSC interface coordinates. Firstly, the angle system was defined from 0 to 180 degrees (in the first and second quadrants) and from 0 to -180 degrees (in the third and fourth quadrants). The angles at -180 degrees and 180 degrees were overlapping on top of each other (See Fig. 9). We have adopted this angle system so we can use the calculated angles to calculate the angular velocity (shown in the next section). The angle measured is the angle between a vector that passes through the apical and basal centrosomes and a vector that passes through the hub-GSC interface and the center of the two centrosomes. All angles belonging to the respected time points were calculated. In addition, when pooling different GSCs' angles together, we calculated the average angle for each GSC and multiplied the GSC's angle matrix by negative one if the average angle was negative. This was done to make the all different GSCs' angles aligned before pooling; since we were not sure during the time of live imaging whether the GSCs were being viewed from the bottom or the top. Finally, after all the angles from different GSCs were pooled together, all the negative angles were

converted to absolute values, since there was no biological significance of reporting negative angle values. All the pooled angle data was represented as a histogram for experimental and control groups.

10. Quantification of spindle angular velocity

A Matlab program was written to calculate the spindle angular velocity using the angles calculated on the 0 to 180 degrees and 0 to -180 degrees system. To calculate the spindle angular velocity, angle calculated in the previous time point was subtracted from the angle calculated in the next time point, and the angle difference was divided by the time interval of the two time points. All the spindle angular velocities were then converted to positive values. Finally all the spindle angular velocities from different GSCs were pooled together to generate a histogram for experimental and control groups.

11. Verification of dynamics quantification

All the Matlab programs written to calculate the distances, velocities, spindle angles, and spindle angular velocities were robustly tested with all possible known values, and was verified to be working properly.

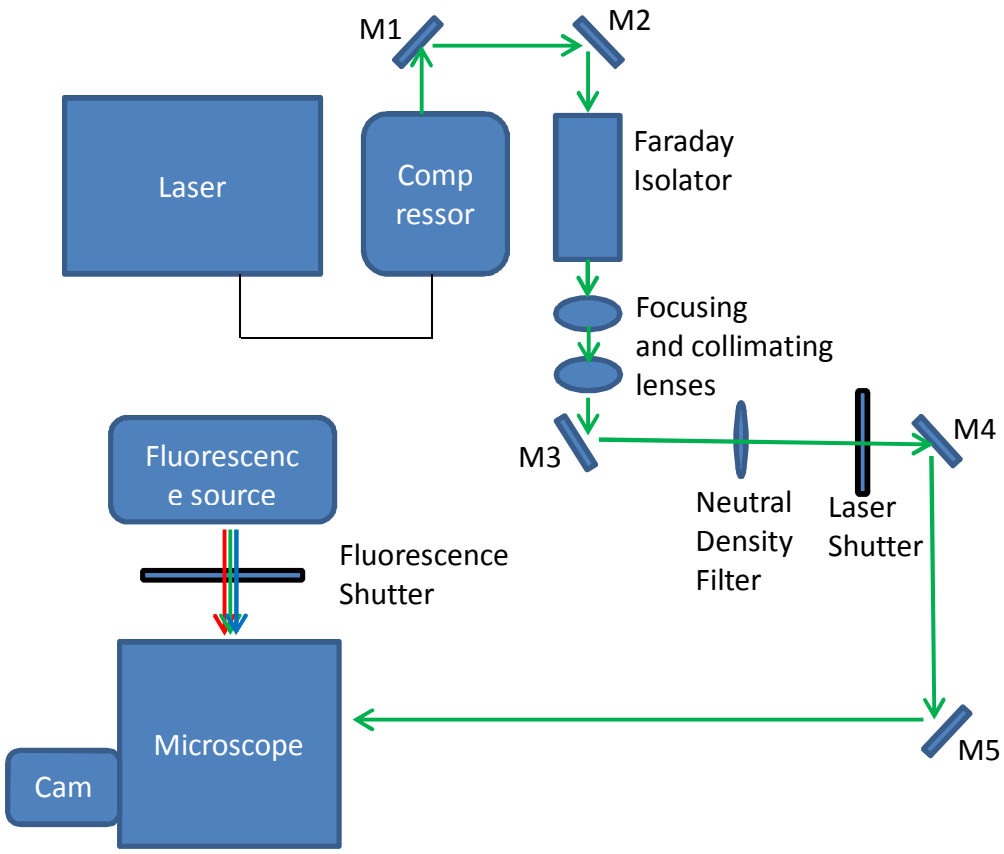

Figure 7: Schematics of an ultrafast-laser microsurgery system. The schematics show how the ultrafast laser is delivered to the microscope objective to perform microsurgery. Laser is amplified in the compressor, and then it is passed down to the Faraday Isolator to prevent beam reflections back to the compressor. The laser beam size is then modified through the lenses and passed down to the neutral density filter, which can control the beam intensity. Finally the laser is delivered to the microscope and then to the objective when the laser shutter opens via the control software. M1-M5: Mirror number 1 through 5.

Figure 8: Tracking program interface developed using Labview and Labview Vision.
The interface for the tracking program via pattern matching is shown. Currently, it is tracking and recording coordinates of an apical centrosome inside a GSC. Various modules and functions are highlighted by different colored rectangular box.
Orange rectangular box: program loading module
Yellow rectangular box: coordinate saving button
Red rectangular box: pattern matching criteria and settings module
Blue rectangular box: tracking coordinate verification module
Purple rectangular box: learn template and pattern matching controls module

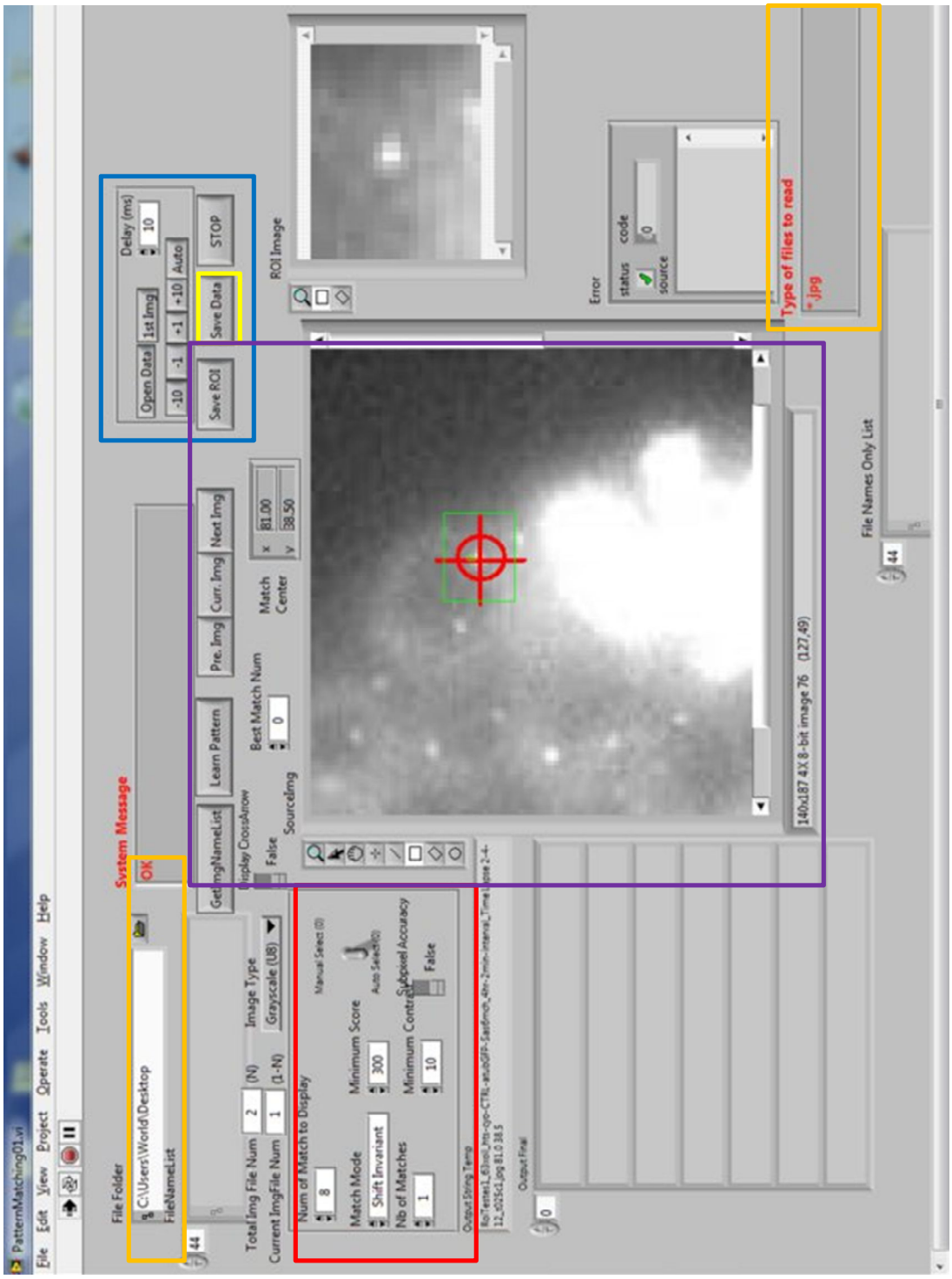
PatternMatching01.vi
File Edit View Project Operate Tools Window Help
File Folder
C:\Users\World\Desktop
FileNameList
System Message
OK
Delay (ms)
10
Open Data
1st Img
-10
-1
-1
-10
Auto
Save ROI
Save Data
STOP
ROI Image
Error
status
code
0
source
Type of files to read
*.jpg
GetImgNameList
Learn Pattern
Pre. Img
Curr. Img
Next Img
Display CrossArrow
False
SourceImg
Best Match Num
0
Match Center
x 81.00
y 38.50
140x187 4X 8-bit image 76 (127,49)
File Names Only List
Total Img File Num
2
(N)
Current ImgFile Num
1
(1-N)
Image Type
Grayscale (U8)
Num of Match to Display
8
Match Mode
Shift Invariant
Nb of Matches
1
Minimum Score
300
Minimum Contrast
10
Subpixel Accuracy
False
Output String Temp
Output Final
0

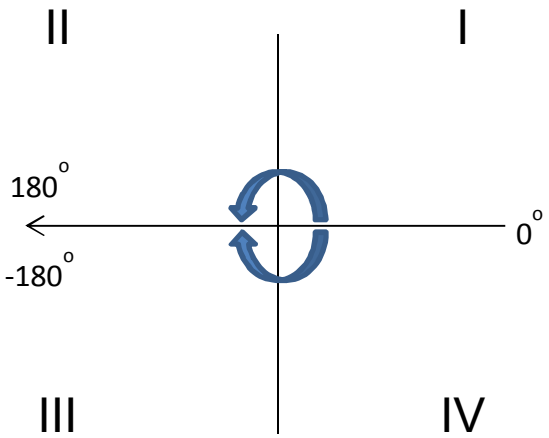

Figure 9: Schematics of the angle system used in Matlab. The angles calculated in Matlab was based on the 0 to 180 degrees (quadrant I and II) and 0 to -180 degrees (quadrants III and IV) system. Eventually, the angle calculation was converted to positive acute angles, but this system was necessary to calculate the angular spindle velocity. The roman numerals represent the quadrants.

III. RESULTS

A. Dynamic Interplay of Spectrosome and Centrosome Organelles in Asymmetric Stem Cell Divisions

(Parts of this chapter were previously published as Bang, C. and J. Cheng (2015). "Dynamic Interplay of Spectrosome and Centrosome Organelles in Asymmetric Stem Cell Divisions." PLoS ONE 10(4): e0123294.)

1. Spindle orientation is maintained in most male GSCs without centrosomes

Previous literature has reported that centrosomes in *Drosophila* appear to have mixed roles for some types of stem cells in maintaining asymmetric stem cell divisions. A neuroblast without centrosome due to *DSas-4-mut* displays asymmetric division defects (Basto, Lau et al. 2006), but most male and female GSCs in *DSas-4-mut* can still maintain asymmetric stem cell division with proper spindle alignment (Stevens, Raposo et al. 2007, Riparbelli and Callaini 2011). Consistently, we found that most acentrosomal GSCs with *DSas-4-mut* maintained proper orientation (Fig. 10A: 63% at 0-30 degrees, 20% at 30-60 degrees, and 17% at 60-90 degrees) compared to wild type (83% at 0-30 degrees, 17% at 30-60 degrees, and 0% at 60-90 degrees). Additionally, by counting the GSC numbers per testis, we found that there is no significant difference (t-test: $p>0.69$) of GSC number per testis in *DSas-4-mut* (8.8±1.2 GSCs, n=26 testes) and wild type (8.8±1.0 GSCs, n=25 testes) (Fig. 10B). To further gain an insight of spindle dynamics during mitosis, time-lapse live-cell imaging (hence forth referred as live

imaging) microscopy was utilized to examine the mitotic spindle morphology and movement in GSCs. We were able to compare the effect of centrosome knockout on mitotic duration by measuring the time from the onset of nuclear envelope break down (pro-meta phase) to the beginning of spindle elongation (anaphase). Our results showed that the time in *DSas-4-mut* GSCs (11.8±2.9 minutes, n=26) was significantly longer (t-test:$p<0.02$) compared to that in wild type GSCs (10.0±2.1 minutes, n=22) (Fig. 10C). These results suggest that although centrosomes are not required to maintain proper asymmetric GSC divisions, centrosomes play a role in facilitating GSC mitosis.

2. Spectrosome migration pattern changes in acentrosomal GSCs

Although previous fixed sample study showed that the spectrosome in male GSCs had higher frequency localizing at the apical cortex in *DSas-4-mut* than that in wild type (Yuan, Chiang et al. 2012), the migration pattern of spectrosome remain unknown. To better understand the migration of the spectrosome, live imaging study was used to examine the movement pattern of spectrosome. Firstly, results from the live imaging show that spectrosome frequently localized to the apical region when the centrosome was knocked out in *DSas-4-mut* (67 ± 12%, n = 24) compared with wild type (33 ± 14 %, n = 23) (Fig. 11A). Additionally, live imaging revealed previously undiscovered dynamic movement of spectrosome (a typical *DSas-4-mut* GSC is shown in Fig. 11B). Spectrosomes in both wild type and *DSas-4-mut* were mobile during interphase and became immobilized prior to entering mitosis. In wild type (n=23) GSCs, mobile and basally positioned spectrosomes composed 39%, while stationary and apically positioned spectrosomes composed 26% (Fig. 11C). In *DSas-4-mut* (n=24) GSCs, stationary and apically positioned spectrosomes composed majority at 54%, while mobile and basally positioned

spectrosomes composed 17%. Spectrosome was counted as stationary when it stays at either basal or apical ends for 30 minutes or longer. Furthermore, spectrosomes are highly positioned at the apical region (75%, 3 out of 4 GSCs) in the very rare and severely misoriented spindles in *DSas-4-mut* GSCs, while only 54% (13 out of 24 GSCs) positioned at apical region in *DSas-4-mut* GSCs with the properly oriented spindles. On few occasions, the apically located spectrosomes quickly migrated over to the basal location prior to mitosis (wild type: 4%, *DSas-4-mut*: 13%) (Fig. 11D). These results demonstrate that without centrosome, majority of spectrosomes position at the apical end of the GSC and become immobilized.

3. Spectrosome material transfers between daughter cells during asymmetric GSC divisions

Next, we investigated, during asymmetric GSC division, how the spectrosome is dynamically transferred among the two daughter cells. Prior to completion of cytokinesis, spectrosome can initially be received by either stem cell daughter (i.e., GSC) or the differentiating daughter cell (i.e., gonialblast or GB) depending on the positioning of the spectrosomes (apically or basally) at the onset of mitosis. The dynamic spectrosome material transfer process can be illustrated in a typical example shown in Fig. 12. Prior to and during mitosis, spectrosome in wild type GSC generally remained stationary at the basal end of the GSC, as shown in Fig. 12 (0 min, prior to mitosis and 24 min, metaphase). At the end of mitosis (1hr 12 mins), the spectrosome moved to and localized at the bridge between two daughter cells, presumably co-localized with the intercellular bridge known as ring canal. On wild type spectrosome live-imaging sessions, the spectrosome, whether received by the GSC or the gonialblast during mitosis, in almost all cases conjoined to the ring canal and formed a complex.

Many hours later, smaller tail region of the ring canal and spectrosome complex grew and further extended into the daughter GSC (Fig. 12, 6hr 16min). Finally, the ring canal and spectrosome complex structure broke apart and was transferred to both the daughter GSC and the gonialblast when the gonialblast and the GSC detached from each other (Fig. 12, 15hr 20 min). Typical counts of spectrosome like structures in the GSC (Fig. 12, 15hr 20 min) vary from one to multiple. Based on many observations, the gonialblast appeared to inherit larger portions of the spectrosome. The GSC and its spectrosome size further grew while the gonialblast slightly separated away from the stem cell niche (Fig. 12, 20hr 40 min). These results demonstrate that ring canal plays an important role in facilitating the spectrosome transfer between the two daughter cells (GSC and gonialblast) regardless of the initial spectrosome position prior to mitosis.

4. Hu-li tai shao does not affect centrosome orientation or mitotic spindle orientation

Utilizing time-lapse live-cell imaging, we investigated the centrosome and spindle orientation when spectrosome was knocked out. Firstly, consistent with reported results based on fixed sample studies, *hts-mut* does not affect either the interphase centrosome orientation (t-test:$p>0.5$) (Fig. 13A) or the mitotic spindle orientation, as 95% spindles in *hts-mut* were still properly oriented (Fig. 13B). Moreover, the *hts-mut* does not significantly affect mitosis duration either (Fig. 13C: from nuclear envelope break time to the onset of anaphase, t-test:$p>0.06$); wild type GSCs were 9.5±1.5min (n=21) and *hts-mut* GSCs were 8.5±1.7min (n=21). We found that wild type GSC count per testis (8.3±0.9 GSCs, n=20 testes) and *hts-mut* GSC counts per testis

(7.9±0.6 GSCs, n=18 testes) were not significantly different (t-test:$p>0.23$), (Fig. 13D). These results demonstrate that the spectrosome does not affect the centrosome and spindle orientation.

5. Hu-li tai shao affects centrosome migration velocity and centrosome position in GSCs

Although spectrosome knockout does not affect centrosome or spindle orientation, further analysis of dynamic migration pattern show the centrosome migration pattern does change. Our live imaging results showed that the motility of GSC-inherited centrosomes during interphase is significantly slower than that of GB-inherited centrosomes in *hts-mut* (Wilcoxon rank sum test:$p<0.001$). Quantitatively, in wild type, the GSC-inherited centrosome velocity is 0.53±0.38μm/min (n=639) while the GB-inherited velocity is 0.57±0.34μm/min (n=654); and in *hts-mut*, the GSC-inherited centrosome velocity is 0.35±0.3μm/min (n=716) and GB-inherited velocity is 0.47±0.32μm/min (n=734) (Fig. 14A). Furthermore, GSCs in *hts-mut* flies have both less motile GSC-inherited and GB-inherited centrosomes than that in wild type (Wilcoxon rank sum test:$p<0.001$). Interestingly, we also found that GSC-inherited centrosomes in wild type throughout the interphase were located significantly further away from the hub-GSC interface than that in *hts-mut* (Wilcoxon rank sum test:$p<0.001$) (Fig. 14B). The results reveal the previously undiscovered dynamic interplay of centrosome and spectrosome. The velocity mean values (μm/min) and mean distance values (μm) were merely calculated to show whether the experimental groups have greater or smaller distribution than the control, but were not in any way used for the Wilcoxon rank sum test to obtain the p-values.

6. Centrosome and Spectrosome double knock out using Mosaic Analysis with a Repressible Cell Marker (MARCM) Method

To further study the potential interactive roles of centrosome and spectrosome, we tried to double knockout both centrosomes and spectrosome. Because the *DSas-4-mut* and *hts-mut* double mutation is lethal, MARCM method was adapted to generate *DSas-4-mut* GSC clones on *hts-mut* background. Using the MARCM method, we successfully obtained double mutant clones, however no mitotic double mutant clone was observed (out of 65 double mutant clones). Considering the typical frequency of observing mitotic GSCs in wild type is about 1 per 5 testes, this result suggest that the mitotic activity is significantly suppressed when centrosomes and spectrosomes both malfunction.

Figure 10: Most spindle orientation at anaphase and stem cell number are maintained in GSCs without centrosomes. **(A)** Live imaging reveals that most *DSas-4-mut* GSCs maintain their spindle orientation compared to the wild type. **(B)** There is no significant difference of GSC number per testes in *DSas-4-mut* and wild type flies. **(C)** The mitosis duration from pro-metaphase to anaphase in *DSas-4-mut* GSCs is significantly longer than that in wild type.

A

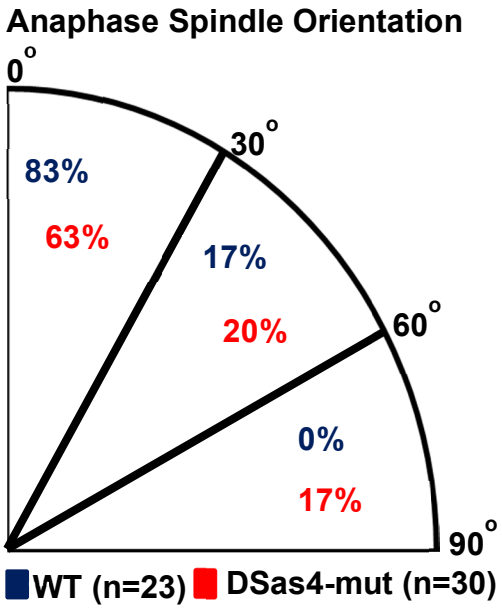
Anaphase Spindle Orientation
0°
30°
60°
90°
83%
63%
17%
20%
0%
17%
WT (n=23)
DSas4-mut (n=30)

B

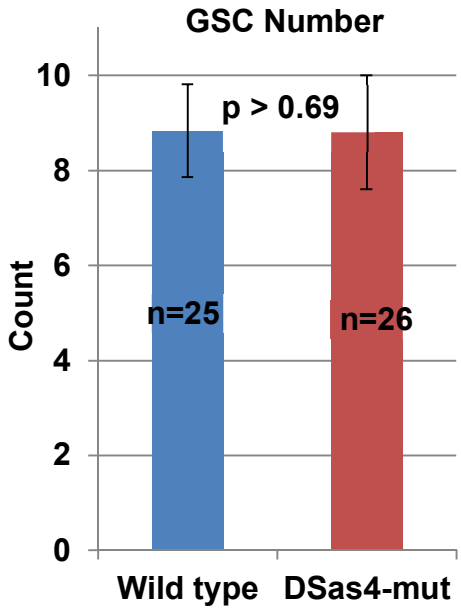
GSC Number
p > 0.69
Count
10
8
6
4
2
0
n=25
n=26
Wild type
DSas4-mut

C

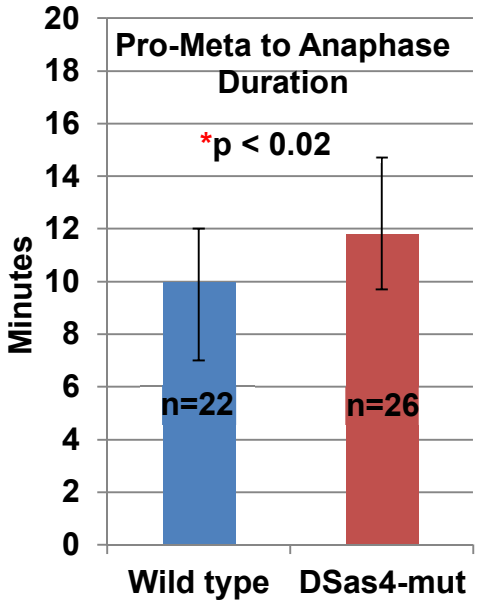
Pro-Meta to Anaphase Duration
*p < 0.02
Minutes
20
18
16
14
12
10
8
6
4
2
0
n=22
n=26
Wild type
DSas4-mut

Figure 11: Dynamic migration patterns of spectrosomes are quantified utilizing time-lapse live-imaging. (A) Spectrosome localization in *DSas-4-mut* becomes predominantly apical compared to wild type. #: $p<0.05$. **(B)** Live image sequences shows apically (to the hub cells) migrating spectrosome in a dividing *DSas-4-mut* GSC. Arrowhead: spectrosome. *: hub cells. Yellow dash-line: GSC. **(C)** In wild type GSCs, large majority of spectrosomes were mobile and located basally (39%) during interphase. In *DSas-4-mut* GSCs, majority of spectrosomes were stationary and located apically (54%). Wild type: n=23, *DSas-4-mut*: n=24. **(D)** *DSas-4-mut* GSCs had higher percentage of spectrosomes migrating from apical to the basal side prior to mitosis. Spectrosome switches are categorized as such if they migrate within 30 mins prior to mitosis (identified by nuclear envelope breakdown).

A

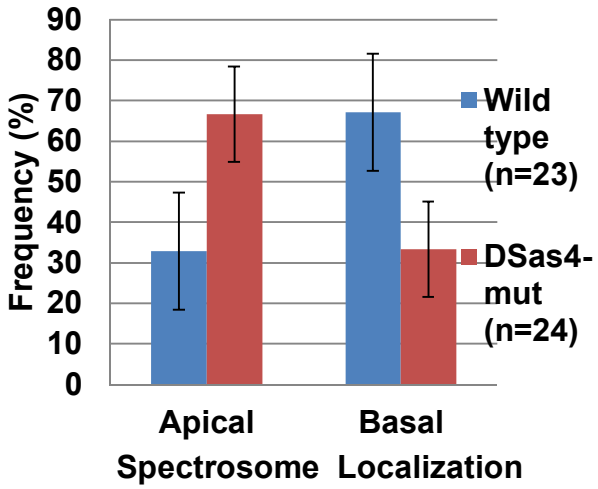
90
80
70
60
50
40
30
20
10
0
Frequency (%)
Wild type (n=23)
DSas4-mut (n=24)
Apical Spectrosome
Basal Localization

B

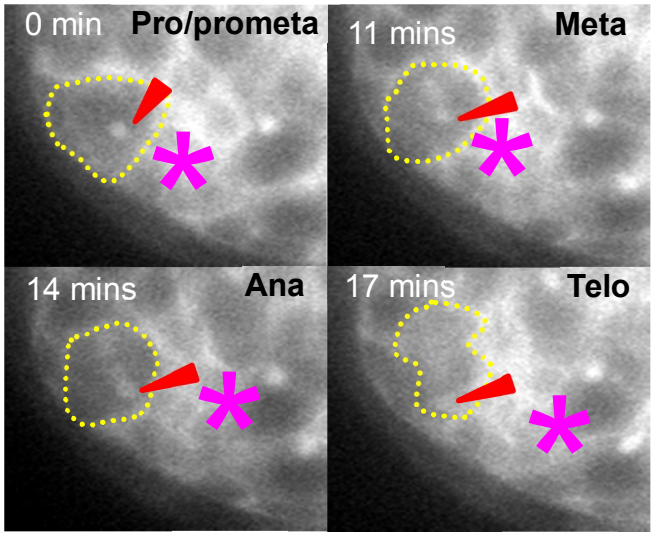
0 min
Pro/prometa
11 mins
Meta
14 mins
Ana
17 mins
Telo

C

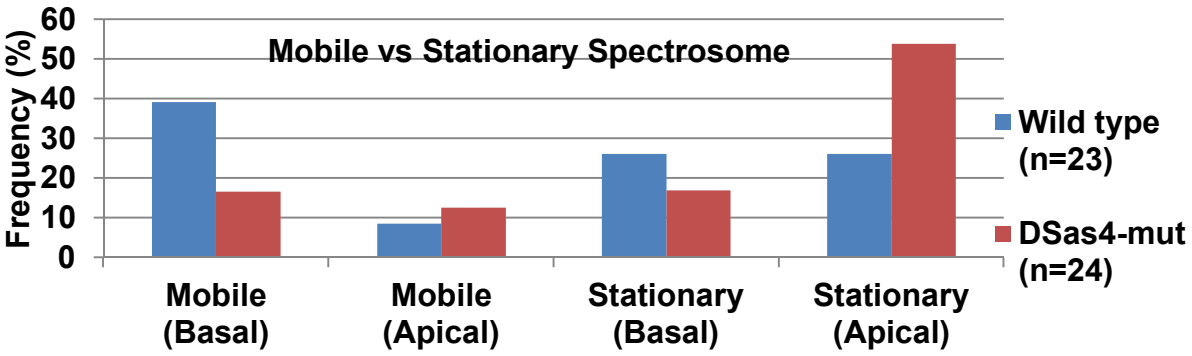
Mobile vs Stationary Spectrosome
Frequency (%)
60
50
40
30
20
10
0
Mobile (Basal)
Mobile (Apical)
Stationary (Basal)
Stationary (Apical)
Wild type (n=23)
DSas4-mut (n=24)

D

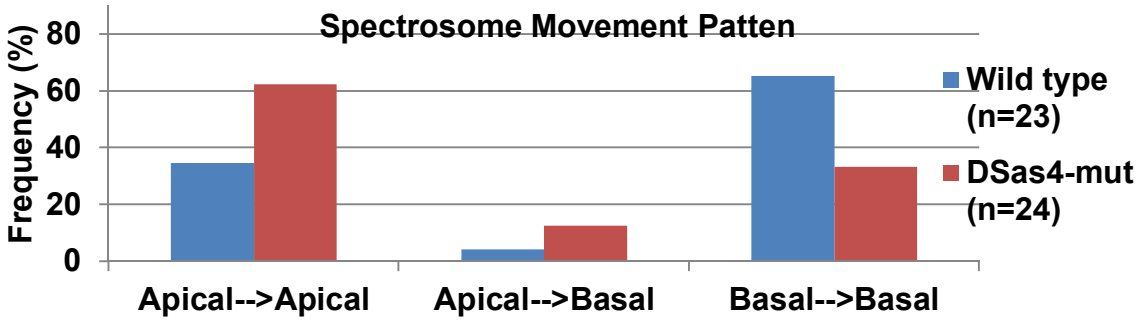
Spectrosome Movement Patten
Frequency (%)
80
60
40
20
0
Apical-->Apical
Apical-->Basal
Basal-->Basal
Wild type (n=23)
DSas4-mut (n=24)

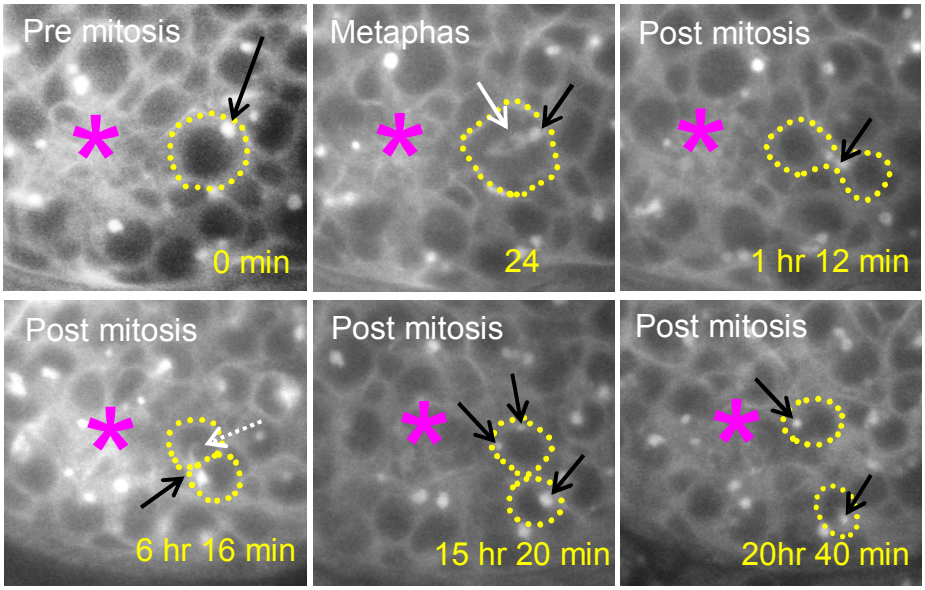

Figure 12: Spectrosome material is transferred via ring canal in GSCs. Spectrosome (Short Adducin-GFP) in wild type GSC is located in the basal position (0 min: interphase and 24min: metaphase). At 1hr 12min, spectrosome is co-localized with the ring canal structure. Spectrosome, together with ring canal structure, grows into the stem cell daughter at 6hr 16min, segregates into both daughter cells and form spectrosome-like structure again at 15hr 20 min. At 20hr 40 min, spectrosomes in both GSC and gonialblast further develop, and the gonialblast separates from GSC. Cellular boundaries and mitotic spindle are visualized with α-tub-GFP. Black arrow: spectrosome. White dash-arrow: spectrosome and/or ring canal tail. *: hub cells. Yellow dash-line: GSC or gonialblast boundary. Solid white arrow: mitotic spindle.

Figure 13: Spectrosome knockout minimally affects centrosome orientation, spindle orientation, mitosis duration, and stem cell numbers in male GSCs. **(A)** Centrosome misorientation during interphase was analyzed from time lapse image sequences, and there is no significant difference between the *hts-mut* and the wild type. **(B)** There is minimal change in the spindle orientation between the *hts-mut* and the wild type. **(C)** Mitosis duration is not affected in *hts-mut* compared to the wild type when measured from nuclear envelope breakdown time to anaphase. **(D)** There is no significant difference for GSC number per testis in hts-mut and wild type flies.

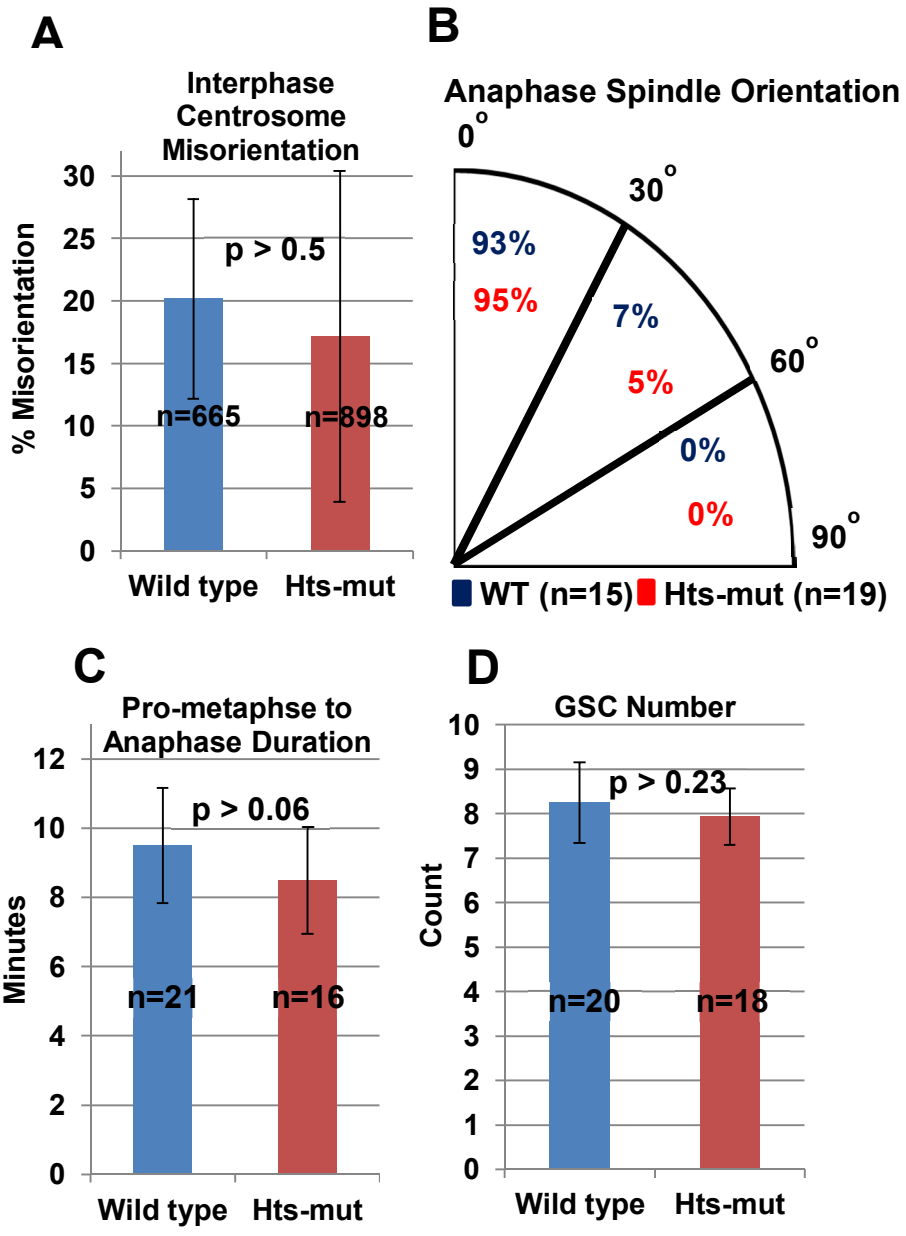
A
Interphase Centrosome Misorientation
% Misorientation
30
25
20
15
10
5
0
p > 0.5
n=665
n=898
Wild type
Hts-mut
B
Anaphase Spindle Orientation
0°
30°
60°
90°
93%
95%
7%
5%
0%
0%
WT (n=15)
Hts-mut (n=19)
C
Pro-metaphse to Anaphase Duration
Minutes
12
10
8
6
4
2
0
p > 0.06
n=21
n=16
Wild type
Hts-mut
D
GSC Number
Count
10
9
8
7
6
5
4
3
2
1
0
p > 0.23
n=20
n=18
Wild type
Hts-mut

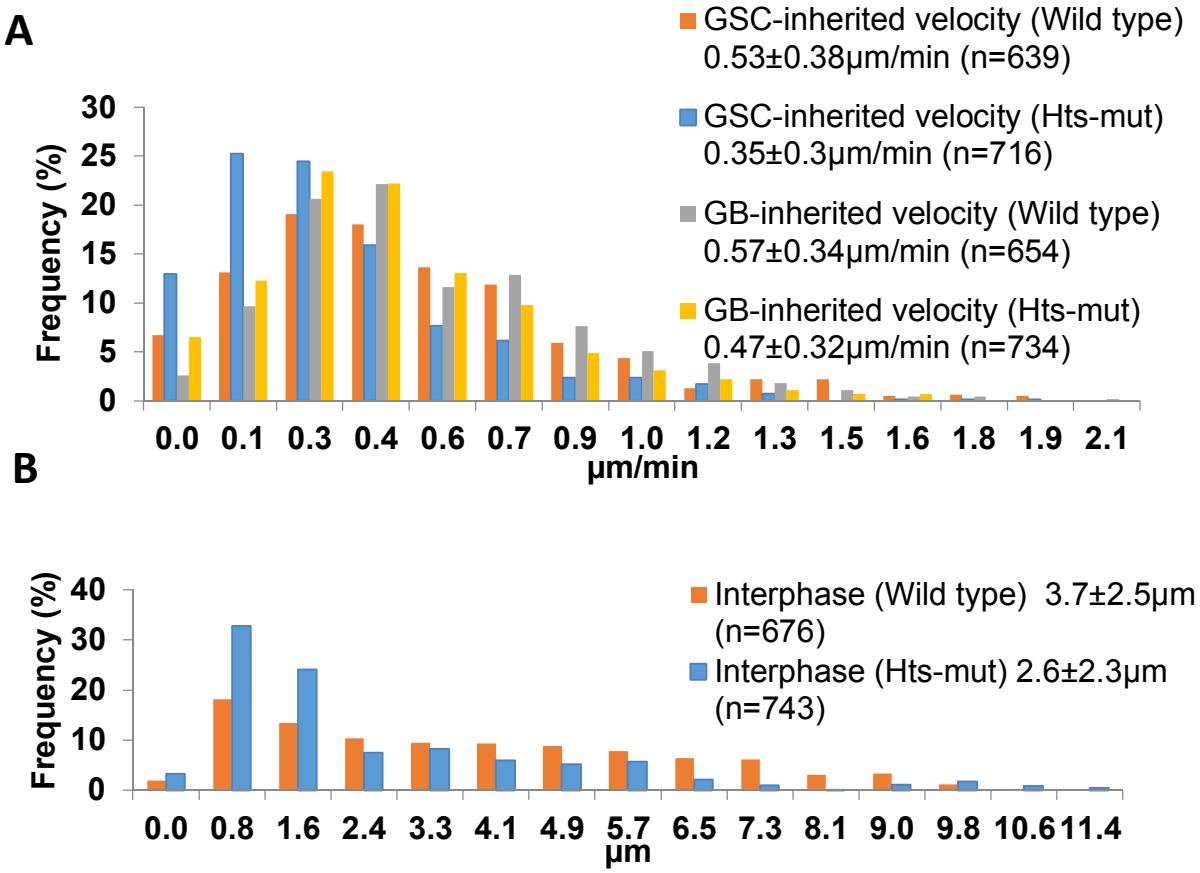

Figure 14: Centrosome velocity and distance to hub-GSC interface change in *hts-mut* GSCs. Based on the centrosome tracking analysis of live-image sequences, the **(A)** Interphase centrosome velocities are shown for both *hts-mut* GSCs and wild type GSCs ($p<0.001$ between *hts-mut* and wild type for both GSC-inherited and GB-inherited centrosomes), and the **(B)** GSC-inherited centrosome distance to the hub-GSC interphase histograms are shown for both *hts-mut* and wild type GSCs ($p<0.001$). The p-values in **(A)** and **(B)** were obtained using the Wilcoxon rank sum test.

B. Effects of Centrosomin and Adenomatous Polyposis Coli Protein 2 on Spectrosome Recruitment and Asymmetric Stem Cell Divisions

1. Spindle orientation is maintained in most male GSCs with non-functional centrosomes (*cnn-mut*) and compromised microtubule binding protein APC2 (*APC2-mut*).

Previous study by Lucas et al (2007), has reported that the *cnn-mut* neuroblasts seemed to have their centrioles lost connection to the mitotic spindle poles, attenuated astral microtubule formation, and misoriented spindles. Similarly, in GSCs, it was reported that the astral microtubule attenuated and the mitotic spindle misorientation also increased, but most of the GSCs divided asymmetrically (Yamashita, Jones et al. 2003, Inaba, Yuan et al. 2010). Consistently, we found that most GSCs with non-functional centrosomes with *cnn-mut* maintained proper orientation despite misorientation in about 1/3 of the GSCs (Fig. 15A: 63% at 0-30 degrees, 32% at 30-60 degrees, and 5% at 60-90 degrees) compared to wild type (84% at 0-30 degrees, 16% at 30-60 degrees, and 0% at 60-90 degrees). Similarly, most APC2-mut GSCs maintained proper orientation (61% at 0-30 degrees, 19% at 30-60 degrees, and 0% at 60-90 degrees) similar to the wild type. Centrosome orientation was also quantified due to its important role in mediating as the microtubule organizing center and defining spindle positions. The *cnn-mut* GSCs (Fig. 15B) had significantly increased centrosome misorientation (t-test:$p<0.01$) than its control, and interestingly, the *APC2-mut* GSCs also had significantly increased misorientation (t-test:$p<0.026$) despite its highly oriented spindles, which were consistent with data previously reported (Yamashita, Jones et al. 2003, Inaba, Yuan et al. 2010). Furthermore, we counted GSC number per testis to observe how the *cnn-mut* and *APC2-mut*

affect stem cell homeostasis. We found the GSC number per testis (Fig. 15C) has increased significantly (t-test:$p<0.001$) for the *cnn-mut* (9.9±1.6 GSCs, n=33 testes) compared to the control (7.9±0.9 GSCs, n=35 testes). Similarly, we also found significant increase (t-test:$p<0.001$) in the GSC number per testis for the *APC2-mut* (9.1±1.5 GSCs, n=56 testes) compared to the control (8.1±1.0 GSCs, n=51 testes).

To quantify dynamic occurrences such as spindle dynamics, centrosome dynamics, spectrosome dynamics, and mitotic duration of GSCs, we utilized time-lapse live-cell imaging to investigate. We were able to compare the effect of *cnn-mut* and *APC2-mut* on mitotic duration by measuring the time from the onset of nuclear envelope break down (pro-meta phase) to the onset of telophase. Nuclear envelope break down was observed through darker background of the nucleus region spontaneously brightening as cytosolic short-adducin-GFP freely entered the nucleus region and telophase was visualized through short-adducin-GFP delineating the GSC-GB membrane. Our results showed that the mitotic duration in *cnn-mut* GSCs (18.2±2.7 minutes, n=19) and the *APC2-mut* GSCs were significantly longer (both t-test:$p<0.001$) than the wild type GSCs (12.5±2.8 minutes, n=22). In addition, *cnn-mut* GSCs' mitotic duration was also significantly (t-test:$p<0.001$) longer than the *APC2-mut* GSCs. These results suggests that centrosomin and APC2 are not required to maintain proper asymmetric GSC divisions, but the microtubule and the microtubule binding protein are necessary in proper GSC mitosis.

2. Spectrosome migration pattern of *cnn-mut* GSCs change but *APC2-mut* GSCs' migration pattern remains similar to the wild type.

In previous fixed sample studies and live imaging studies, spectrosome in male acentrosomal GSCs via *DSas-4-mut* had higher frequency localizing to the apical cortex than that

in the wild type (Yuan, Chiang et al. 2012, Bang and Cheng 2015). To better understand the migration of the spectrosome in *cnn-mut* and *APC2-mut*, we have utilized the same live imaging protocol as used previously (Cheng and Hunt 2009, Bang and Cheng 2015). First of all, results from the live imaging show that spectrosomes frequently localized to the apical region in *cnn-mut* GSCs (69 ± 11%, n = 19) compared to the wild type (17 ± 12 %, n = 24) (Fig. 16A, t-test:$p<0.01$), which is similar to the localization of spectrosome in acentrosomal (*DSas-4-mut*) GSCs previously reported (Yuan, Chiang et al. 2012, Bang and Cheng 2015). On the other hand, spectrosome localization to the apical region remained relatively unchanged in *APC2-mut* GSCs (30 ± 10%, n = 27) compared to the wild type (Fig. 16B, t-test:$p>0.2$). Stereotypical positioning of spectrosomes during the GSC mitosis is shown for the *cnn-mut* and *APC2-mut* in Fig. 16C; spectrosome in the *cnn-mut* GSCs localize at the apical cortex during interphase and mitosis, while *APC2-mut* GSCs localize at the basal cortex during interphase and mitosis. Additionally, live imaging revealed little-known dynamic movement of spectrosome in *cnn-mut* and *APC2-mut* GSCs. Spectrosomes in *cnn-mut*, *APC2-mut*, and wild type GSCs were mobile during interphase and became immobilized prior to entering mitosis. In wild type GSCs (n=24), mobile and basally positioned spectrosomes composed 42%, while stationary and apically positioned spectrosomes composed 12% (Fig. 16D). In *cnn-mut* GSCs (n=19), stationary and apically positioned spectrosomes composed majority at 47%, while mobile and basally positioned spectrosomes composed 26%. On the other hand, *APC2-mut* GSCs (n=26) showed similar trend as the wild type, having much greater mobile and basally positioned spectrosomes (31%) compared to the stationary and apically positioned spectrosomes (8%); however, APC2-mut GSCs had much greater stationary and basally positioned spectrosomes (39%) compared to the wild type (21%). Spectrosome was counted as stationary when it stayed at either basal or apical

ends for 30 minutes or longer. In small number of the GSCs, the apically located spectrosome rushed over to the basal location prior to mitosis (wild type: 0%, *cnn-mut*: 16%, *APC2-mut*: 19%). These results demonstrate that in *cnn-mut* GSCs, majority of spectrosomes position at the apical end of the GSCs and become immobilized, however in the APC2-mut GSCs, the spectrosome behave similar to the wild type.

3. Spectrosome localizations change drastically in *cnn-mut* GSCs but minimally in *APC2-mut* GSCs, and centrosome misorientation to the spectrosome positions also change in both mutant GSCs.

We have investigated spectrosome and centrosome localizations in fixed *cnn-mut* and *APC2-mut* GSCs, quantifying various fixed stages of the cell cycle. Based on our quantification, we segregated the spectrosome localization into five categories: basal localization, apical localization, ring canal localization, apical and ring canal localization, and GSC spanning and ring canal localization. Examples of all the spectrosome localization categories are shown in Fig. 17A (1-5), and further represented cartoons in the orientation data. When comparing the frequency of occurrence of the *cnn-mut* GSCs (n=275) to the respective control GSCs (n=214), changes in all the localization categories were all statistically significant (t-test:$p<0.02$ for all categories) (Fig. 17B). On the contrary, *APC2-mut* GSCs (n=292) changed significantly in the apical and ring canal localization category (t-test:$p<0.04$) to its respective control GSCs (n=326); all other localizations remained similar to the respective control GSCs (Fig. 17C). In addition to the spectrosome localization, we quantified how the centrosomes are misoriented in those respective categories for both *cnn-mut* and *APC2-mut* GSCs. In the *cnn-mut* GSCs, the centrosome misorientation (46±15%, n=17) was significantly changed (t-

test:$p<0.04$) from the respective control (4±6%, n=58) in the ring canal localization category (Fig. 17D). Furthermore, in the *APC2-mut* GSCs, the centrosome misorientation (15±2.4%, n=108) was significantly changed (t-test:$p<0.01$) from the respective control (5±1.4%, n=97) in the ring canal localization category (Fig. 17E). These results demonstrate that *cnn-mut* significantly alters the spectrosome localization patterns, while the *APC2-mut* minimally alters the spectrosome localization patterns; but both mutants alter centrosome orientations in some spectrosome localization categories.

4. Centrosomin mutant affects spectrosome migration velocity and spectrosome position in GSCs.

Utilizing our live imaging techniques, we have quantified previously unexplored dynamic migration pattern of spectrosome in both *cnn-mut* and *APC2-mut* GSCs. In *cnn-mut* GSCs, the average spectrosome velocity at interphase was significantly slower (Wilcoxon rank sum test:$p<0.01$) than wild type GSCs (Fig. 18A). Quantitatively, in wild type GSCs, the spectrosome velocity is 0.61±0.45 μm/min (n=689) while the *cnn-mut* spectrosome velocity is 0.56±0.49 μm/min (n=1239). Contrarily, the *APC2-mut* GSC spectrosome velocity was not statistically different compared to the wild type GSCs. The APC2-mut GSC spectrosome velocity is 0.61±0.42 μm/min (n=845). In addition, we found that wild type GSC spectrosomes were, on average, found significantly (Wilcoxon rank sum test:$p<0.001$) further away from the hub-GSC interface than the *cnn-mut* GSC spectrosomes (Fig. 18B). The average spectrosome distance to the hub-GSC interface for the wild type GSC is 6.2±3.1 μm (n=716), for the *cnn-mut* GSCs is 4.3±2.4 μm (n=1265), and for the *APC2-mut* GSCs is 6.5±2.4 μm (n=882). These results further disclose previously undiscovered dynamic interactions of spectrosome to cnn.

The mean velocity values (μm/min) and mean distance values (μm) were merely calculated to show whether the experimental groups have greater or smaller distribution than the control, but were not in any way used for the Wilcoxon rank sum test to obtain the p-values.

5. Centrosomin mutant affects centrosome migration velocity and both *cnn-mut* and *APC2-mut* affect centrosome position in GSCs.

Dynamic centrosome migration pattern for the *cnn-mut* and *APC2-mut* were also explored in addition to spectrosome migration pattern, utilizing same quantification methods as discussed previously in *hts-mut* GSCs (Bang and Cheng 2015). Our live imaging revealed that in wild type, the motility of GSC-inherited centrosomes during interphase is significantly slower (Wilcoxon rank sum test:$p<0.028$) than that of *cnn-mut* GSC-inherited centrosomes, but significantly faster than that of *APC2-mut* GSC-inherited centrosomes (Wilcoxon rank sum test:$p<0.001$) (Fig. 19A). Quantitatively, average GSC-inherited wild type centrosome velocity is 0.64±0.46μm/min (n=609), while the average GSC-inherited *cnn-mut* centrosome velocity is 0.70±0.49μm/min (n=499); and the average GSC-inherited APC2-mut centrosome velocity is 0.54±0.44μm/min (n=690). Next, we have discovered that the motility of GB-inherited wild type GSC centrosomes during interphase were significantly slower (Wilcoxon rank sum test:$p<0.001$) then the *cnn-mut* GSC centrosomes (Fig. 19B). The average GB-inherited wild type centrosome velocity is 0.71±0.49μm/min (n=516), while the average GB-inherited *cnn-mut* centrosome velocity is 0.83±0.58μm/min (n=543). Amid quantifying the centrosome velocities, we have also analyzed centrosome distance to the hub-GSC interface. Interestingly, we have found that the GSC-inherited centrosomes in wild type GSCs throughout the interphase were located significantly further away from the hub-GSC interface than the *APC2-mut* GSCs

(Wilcoxon rank sum test:$p<0.001$) (Fig. 19C), but found no difference in *cnn-mut* GSCs. The wild type average GSC-inherited centrosome distance to the hub-GSC interface is 3.8±1.9μm (n=666) and the *APC2-mut* average GSC-inherited centrosome distance to the hub-GSC interface is 2.8±1.7μm (n=743). In addition, we have also discovered that GB-inherited centrosomes in wild type GSCs during interphase were located significantly closer to the hub-GSC interface than both *cnn-mut* and *APC2-mut* GSCs (Wilcoxon rank sum test:$p<0.001$, Wilcoxon rank sum test:$p<0.001$, respectively) (Fig. 19D). Numerically, the wild type average GB-inherited centrosome distance to the hub-GSC interface is 7.6±1.6μm (n=561); the *cnn-mut* average GB-inherited centrosome distance to the hub-GSC interface is 7.9±2.2μm (n=652); and the *APC2-mut* average GB-inherited centrosome distance to the hub-GSC interface is 8.5±1.5μm (n=772). These results further reveal novel dynamic interactions of centrosomes to cnn and APC2. The velocity mean values (μm/min) and mean distance values (μm) were merely calculated to show whether the experimental groups have greater or smaller distribution than the control, but were not in any way used for the Wilcoxon rank sum test to obtain the p-values.

6. Centrosomin mutant affects spindle angle and *APC2-mut* affects spindle angular velocity.

We were able to quantify the spindle angle and the spindle angular velocity by tracking the centrosomes and the hub-GSC interface during mitosis. Pro/prometaphase of mitosis was visible through observing nuclear envelope breakage, where soluble Sas6-mcherry spontaneously increased the background of the previously dark nuclear region by filling the void. Telophase was observed by visualizing the GSC shape through the faint short-adducin-GFP signal localizing to the cortex of the plasma membrane. Our results show that average spindle angle for the wild type GSCs was significantly smaller (Wilcoxon rank sum test:$p<0.001$) than

the *cnn-mut* GSCs (Fig. 20A); however the average *APC2-mut* GSC spindle angle was not significantly different. Numerically, the average spindle angle for the wild type GSCs is 11±10 degrees (n=272), whereas the average spindle angle for the *cnn-mut* GSCs is 29±25 degrees (n=99). This result is consistent with the previously discussed fixed spindle angle in Fig. 15A for both *cnn-mut* and *APC2-mut* GSCs. Moreover, we have also analyzed spindle angular velocity and found that in wild type, the average spindle angular velocity was significantly faster (Wilcoxon rank sum test:$p<0.026$) than *APC2-mut* GSCs (Fig. 20B). The wild type GSC spindle angular velocity is 4.9±4.8 degrees/min (n=236); whereas the *cnn-mut* GSC spindle angular velocity is 7.1±8.6 degrees/min (n=72); and the *APC2-mut* GSC spindle angular velocity is 4.0±4.0 degrees/min (n=256). These new results reveal how cnn and APC2 interact and alter dynamics of spindle movement and orientation. The mean spindle angle values (degrees) and mean spindle angular velocity values (degrees/min) were merely calculated to show whether the experimental groups have greater or smaller distribution than the control, but were not in any way used for the Wilcoxon rank sum test to obtain the p-values.

Figure 15: Most spindle orientation at anaphase is maintained in *cnn-mut* and *APC2-mut* GSCs, but GSC numbers are significantly higher in the mutants than the wild type. (A) Live imaging reveals that most *cnn-mut* and *APC2-mut* GSCs maintain their spindle orientation compared to the wild type. **(B)** Centrosome misorientation frequency is significantly higher in both *cnn-mut* and *APC2-mut* GSCs compared to their respective controls. **(C)** There are significantly increased GSC numbers per testes for both *cnn-mut* and *APC2-mut* flies compared to wild type flies. **(D)** The mitosis duration from pro-metaphase to telophase in both *cnn-mut* and *APC2-mut* GSCs are significantly longer than the wild type, with *cnn-mut* having the longest mitosis duration.

A

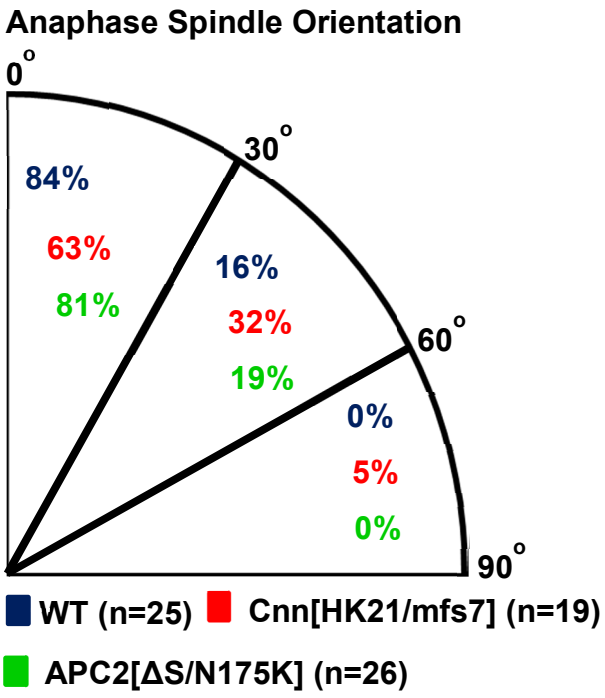
Anaphase Spindle Orientation
0°
30°
60°
90°
84%
63%
81%
16%
32%
19%
0%
5%
0%
WT (n=25)
Cnn[HK21/mfs7] (n=19)
APC2[ΔS/N175K] (n=26)

B

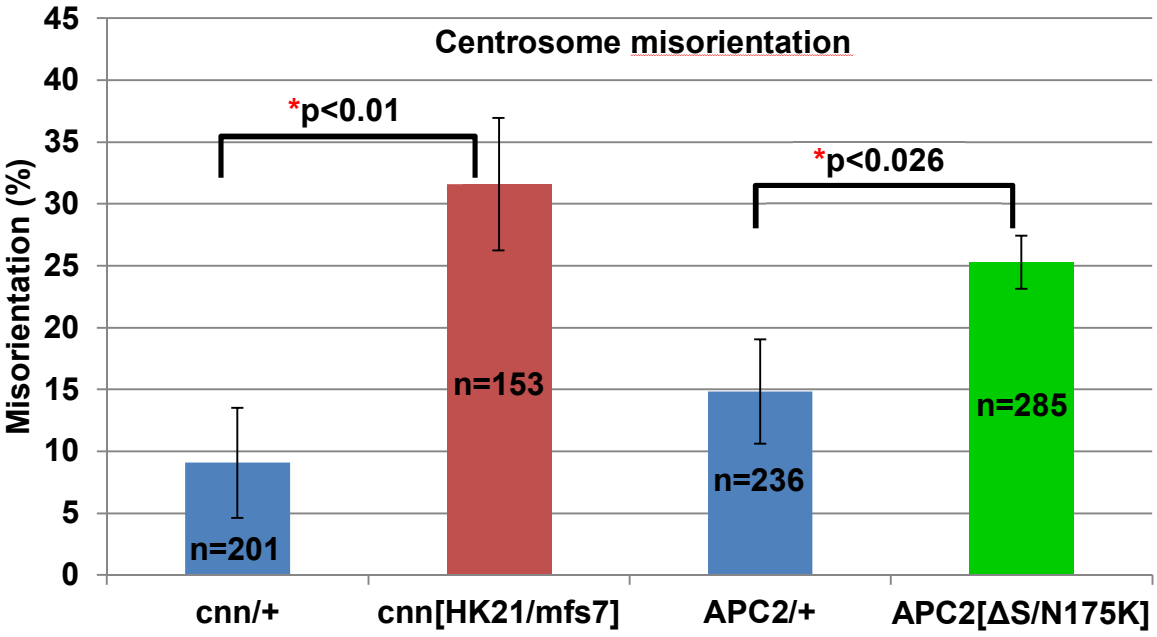
Centrosome misorientation
Misorientation (%)
45
40
35
30
25
20
15
10
5
0
*p<0.01
*p<0.026
n=201
n=153
n=236
n=285
cnn/+
cnn[HK21/mfs7]
APC2/+
APC2[ΔS/N175K]

C

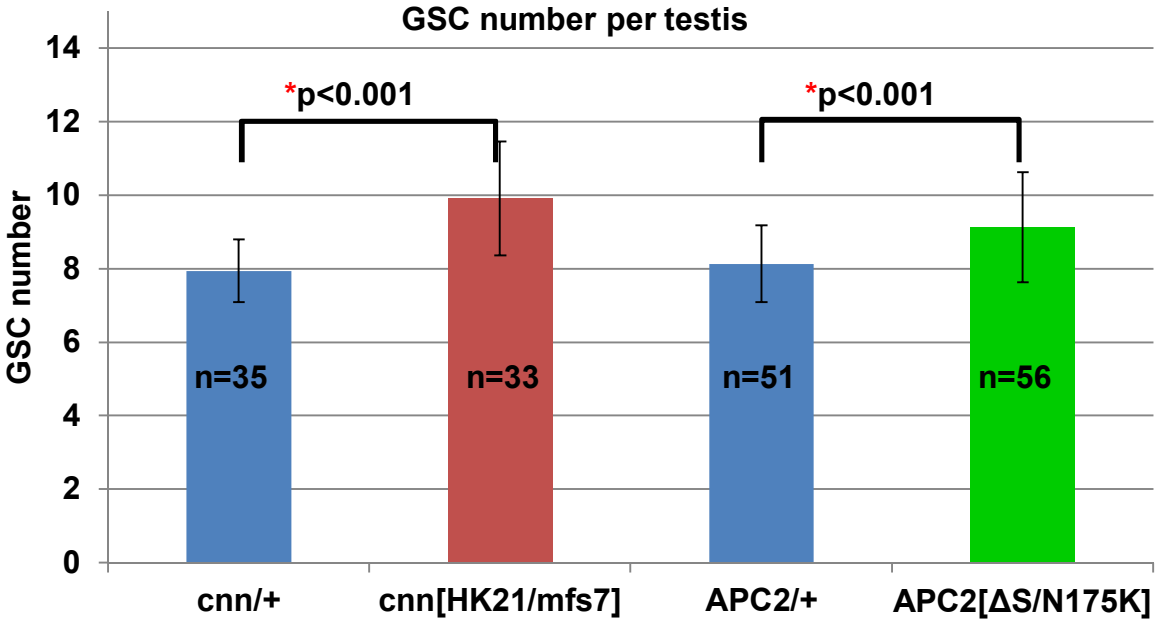
GSC number per testis
GSC number
14
12
10
8
6
4
2
0
*p<0.001
*p<0.001
n=35
n=33
n=51
n=56
cnn/+
cnn[HK21/mfs7]
APC2/+
APC2[ΔS/N175K]

D

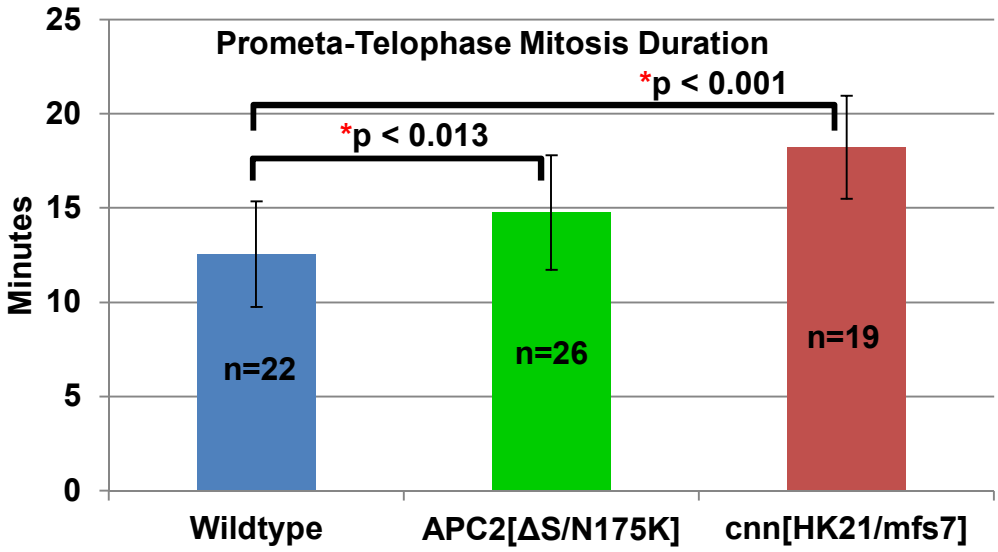
Prometa-Telophase Mitosis Duration
Minutes
25
20
15
10
5
0
*p < 0.001
*p < 0.013
n=22
n=26
n=19
Wildtype
APC2[ΔS/N175K]
cnn[HK21/mfs7]

Figure 16: Dynamic migration patterns of spectrosomes were quantified utilizing time-lapse live-imaging. **(A)** Spectrosome localization in *cnn-mut* becomes predominantly apical compared to wild type. $p<0.01$. **(B)** Spectrosome localization in *APC2-mut* is similar compared to wild type. $p<0.19$. **(C)** Live image sequences shows apically (to the hub cells) migrating spectrosome in dividing *cnn-mut* and *APC2-mut* GSCs. Arrowhead: spectrosome. *: hub cells. Yellow dash-line: GSC. **(D)** In wild type GSCs, large majority of spectrosomes were mobile and located basally (42%) during interphase. In *cnn-mut* GSCs, majority of spectrosomes were stationary and located apically (47%). In *APC2-mut* GSCs, majority of spectrosomes were stationary and located basally (39%). Wild type: n=24, *cnn-mut*: n=19, *APC2-mut*: n=26. **(E)** Both *cnn-mut* and *APC2-mut* GSCs had higher percentage of spectrosomes migrating from apical to the basal side prior to mitosis. Spectrosome switches are categorized as such if they migrate within 30 mins prior to mitosis (identified by nuclear envelope breakdown).

A

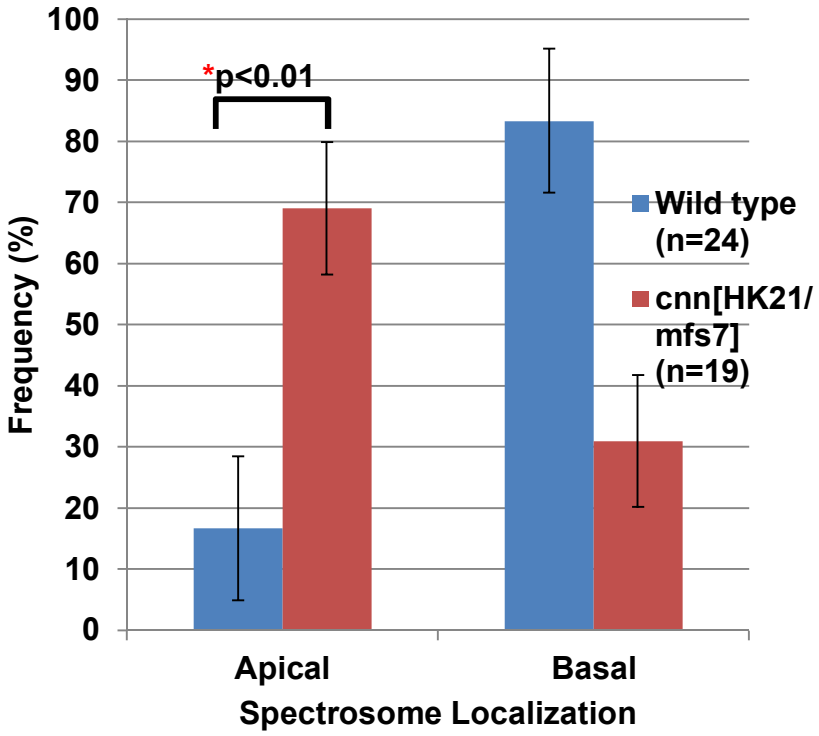
100
90
80
70
60
50
40
30
20
10
0
Frequency (%)
*p<0.01
Wild type (n=24)
cnn[HK21/ mfs7] (n=19)
Apical
Basal
Spectrosome Localization

B

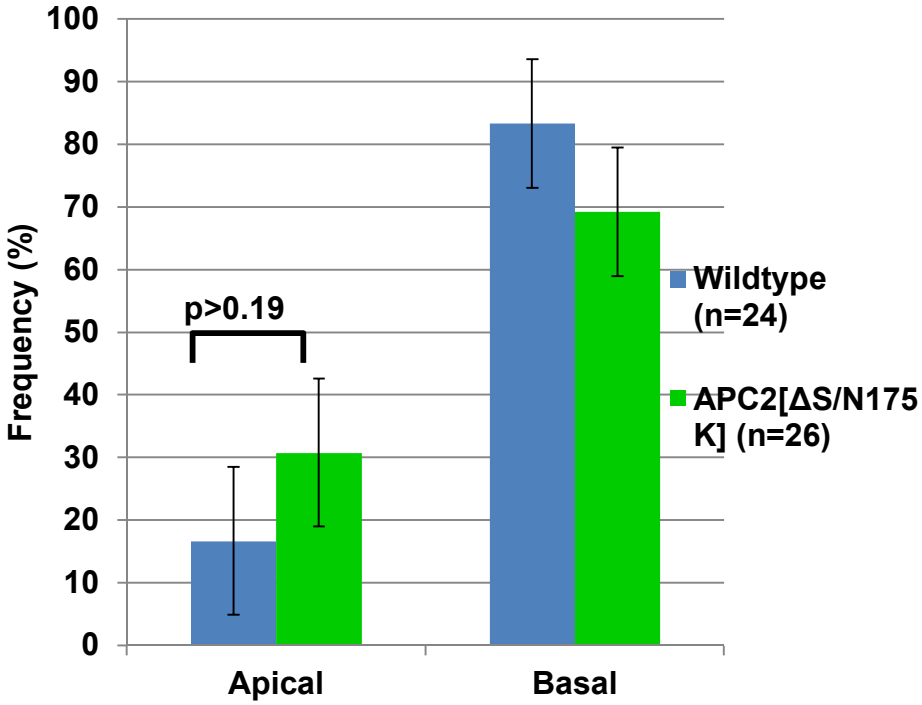
100
90
80
70
60
50
40
30
20
10
0
Frequency (%)
p>0.19
Wildtype (n=24)
APC2[ΔS/N175 K] (n=26)
Apical
Basal

C

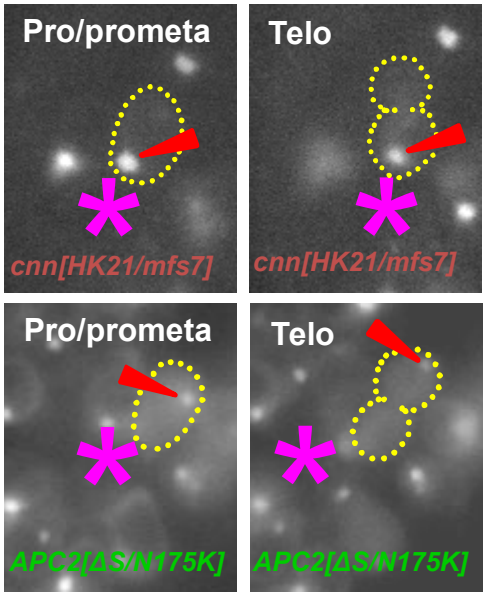
Pro/prometa
Telo
cnn[HK21/mfs7]
cnn[HK21/mfs7]
Pro/prometa
Telo
APC2[ΔS/N175K]
APC2[ΔS/N175K]

D

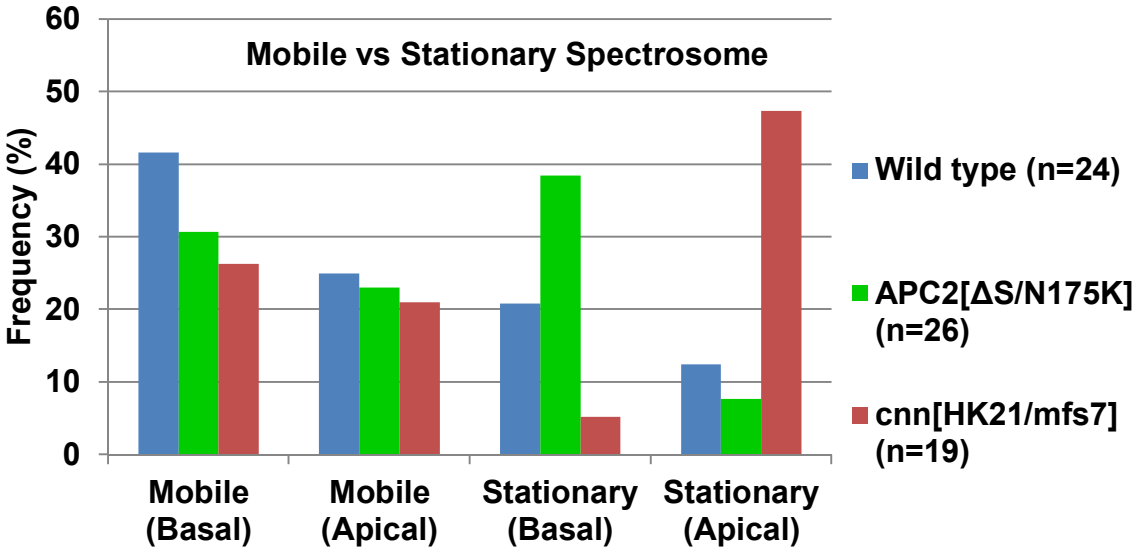
Mobile vs Stationary Spectrosome
Frequency (%)
60
50
40
30
20
10
0
Mobile (Basal)
Mobile (Apical)
Stationary (Basal)
Stationary (Apical)
Wild type (n=24)
APC2[ΔS/N175K] (n=26)
cnn[HK21/mfs7] (n=19)

E

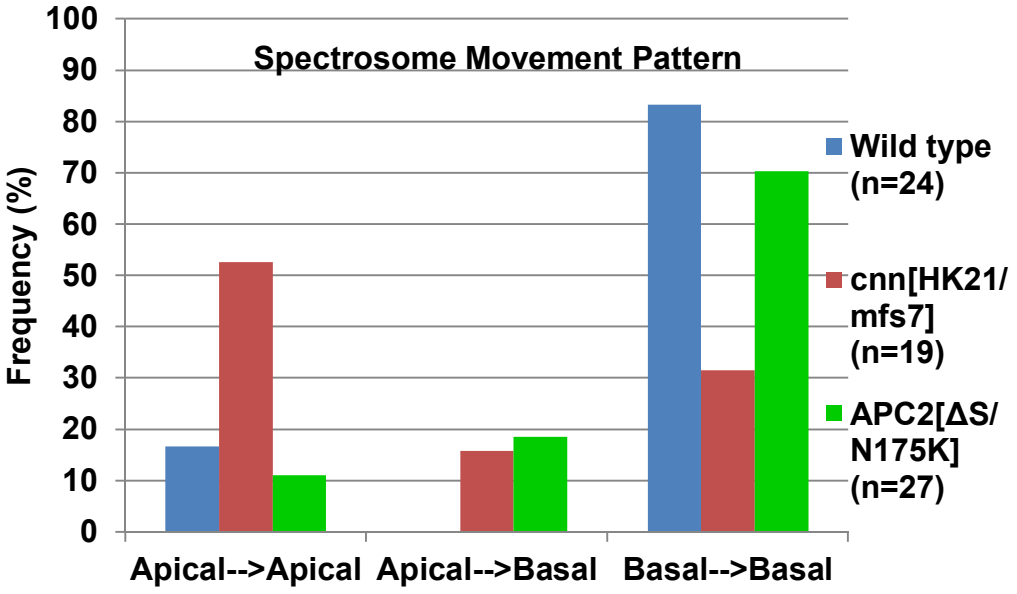
Spectrosome Movement Pattern
Frequency (%)
100
90
80
70
60
50
40
30
20
10
0
Apical-->Apical
Apical-->Basal
Basal-->Basal
Wild type (n=24)
cnn[HK21/ mfs7] (n=19)
APC2[ΔS/ N175K] (n=27)

Figure 17: Spectrosome localization categories and the centrosome misorientations to those categories were quantified. **(A)** Five separate spectrosome localization category images are shown using conventional immunostaining methods. The spectrosome localization categories are (1) basal localization, (2) apical localization, (3) ring canal localization, (4) apical and ring canal localization, and (5) GSC spanning and ring canal localization. Arrowhead: spectrosome. *: hub cells. Yellow dash-line: GSC. Red channel: anti-FasIII and anti-Vasa. Green channel: Shadd-GFP. Blue channel: anti-Spd-2. **(B)** Spectrosome localization category frequencies are shown for the *cnn-mut* GSCs. Each category shows significant difference compared to the control (cnn/+: n=214, *cnn-mut*: n=275]. **(C)** Spectrosome localization category frequencies are shown for the *APC2-mut* GSCs. Spectrosome Apical and ring canal localization category shows significant difference compared to the control (APC2/+: n=292, *APC2-mut*: n=326). **(D)** Centrosome misorientations (%) in all the spectrosome localization categories are shown for the *cnn-mut* GSCs. Misorientation difference is significant in the ring canal localization category for the *cnn-mut* compare to the control (cnn/+: n=58, *cnn-mut*: n=17). **(E)** Centrosome misorientations (%) in all the spectrosome localization categories are shown for the *APC2-mut* GSCs. Misorientation difference is significant in the basal localization category for the *APC2-mut* compare to the control (APC2/+: n=97, *APC2-mut*: n=108).

A

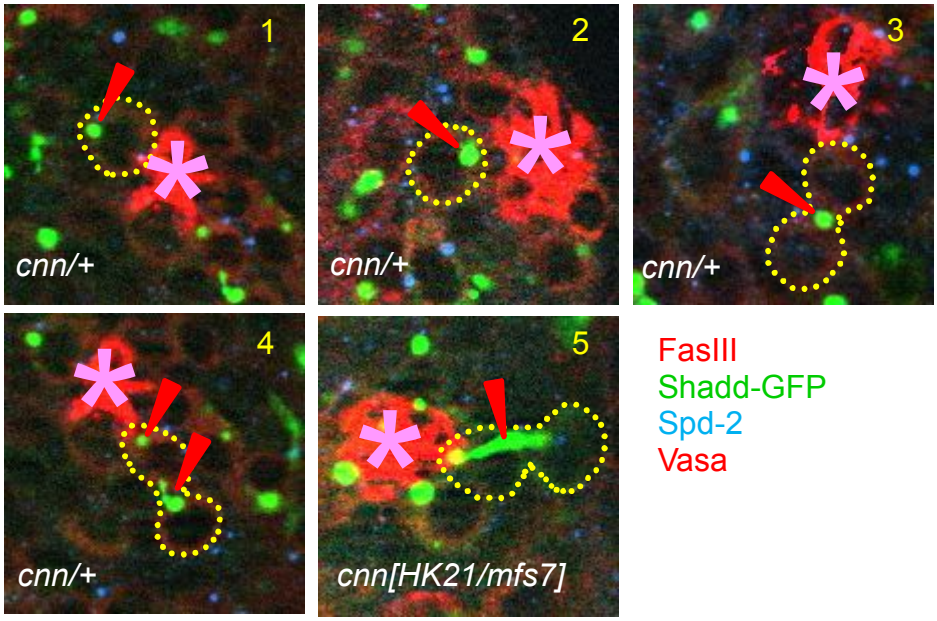
1
2
3
4
5
cnn/+
cnn/+
cnn/+
cnn/+
cnn[HK21/mfs7]
FasIII
Shadd-GFP
Spd-2
Vasa

B

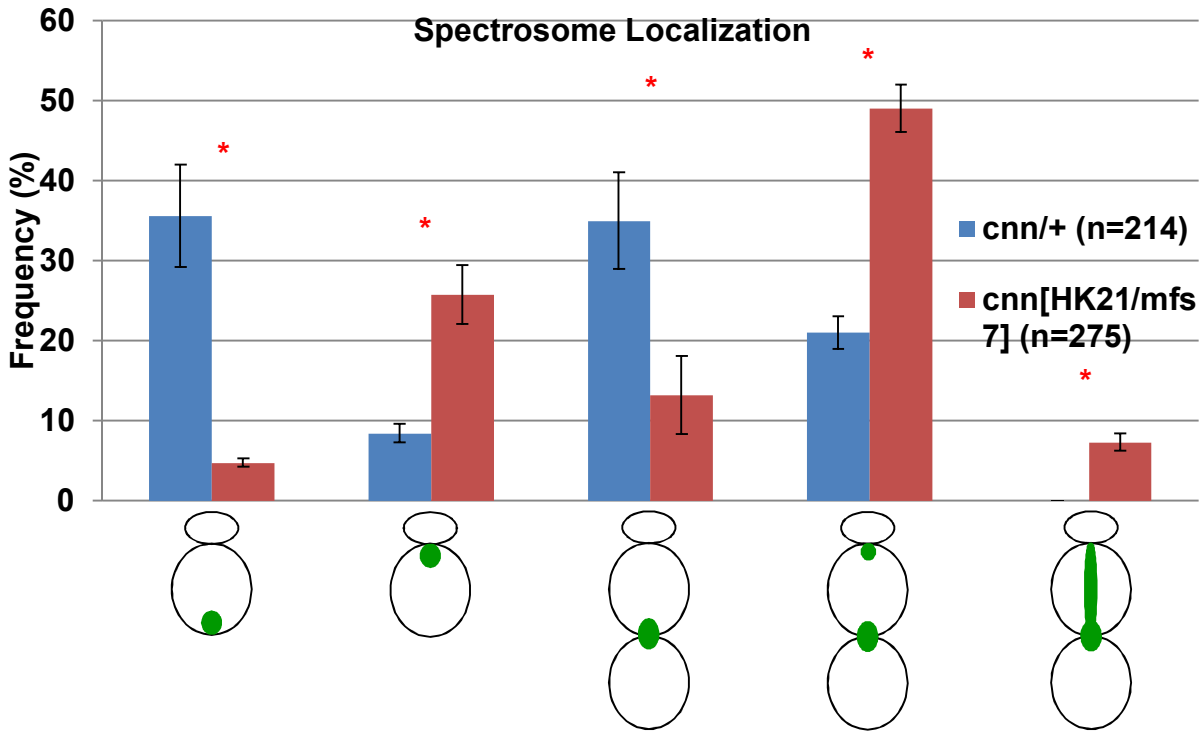
Spectrosome Localization
Frequency (%)
60
50
40
30
20
10
0
cnn/+ (n=214)
cnn[HK21/mfs 7] (n=275)
*

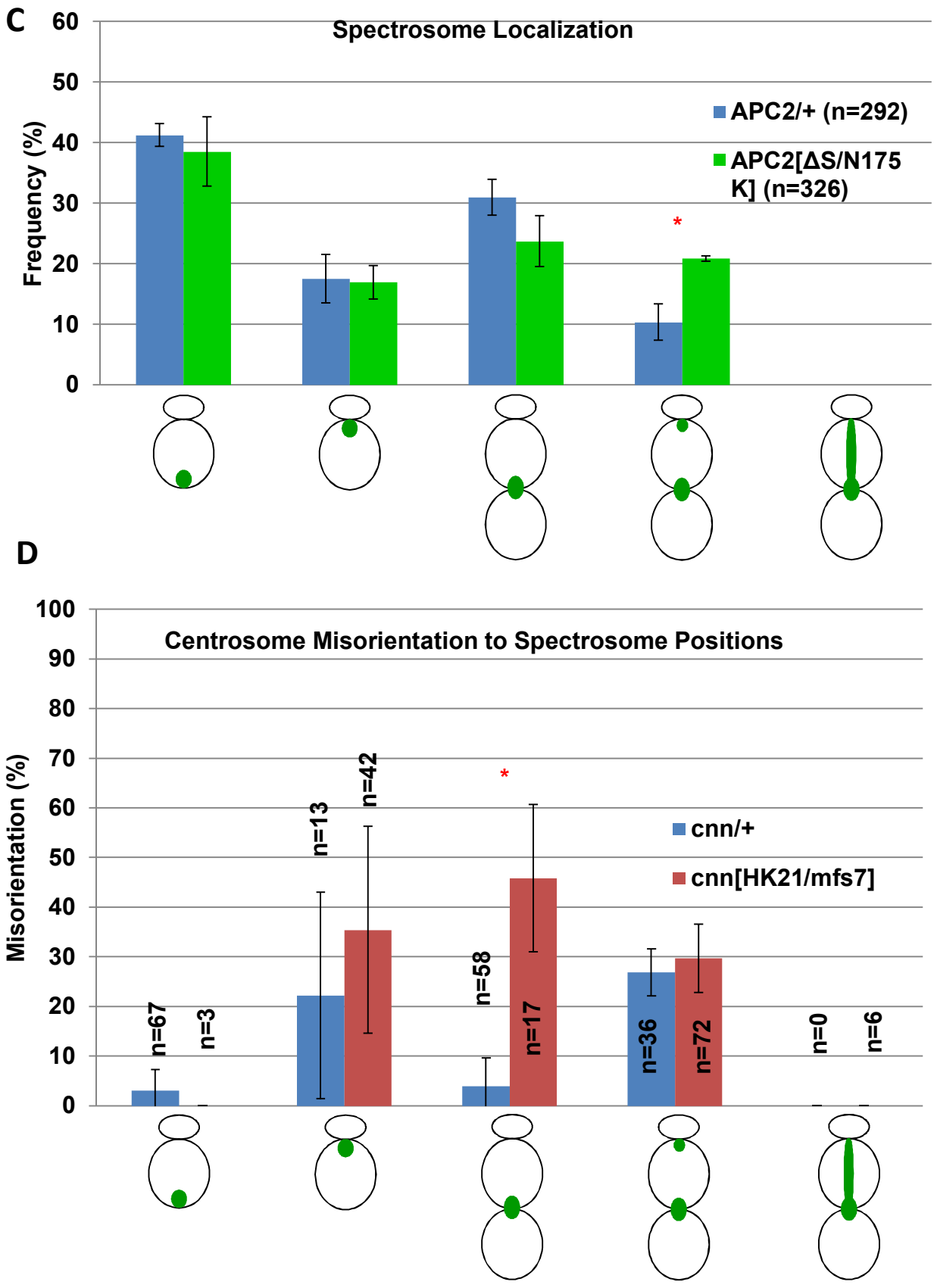
C
Spectrosome Localization
Frequency (%)
60
50
40
30
20
10
0
APC2/+ (n=292)
APC2[ΔS/N175 K] (n=326)
*
D
Centrosome Misorientation to Spectrosome Positions
Misorientation (%)
100
90
80
70
60
50
40
30
20
10
0
cnn/+
cnn[HK21/mfs7]
n=67
n=3
n=13
n=42
n=58
n=17
n=36
n=72
n=0
n=6
*

E

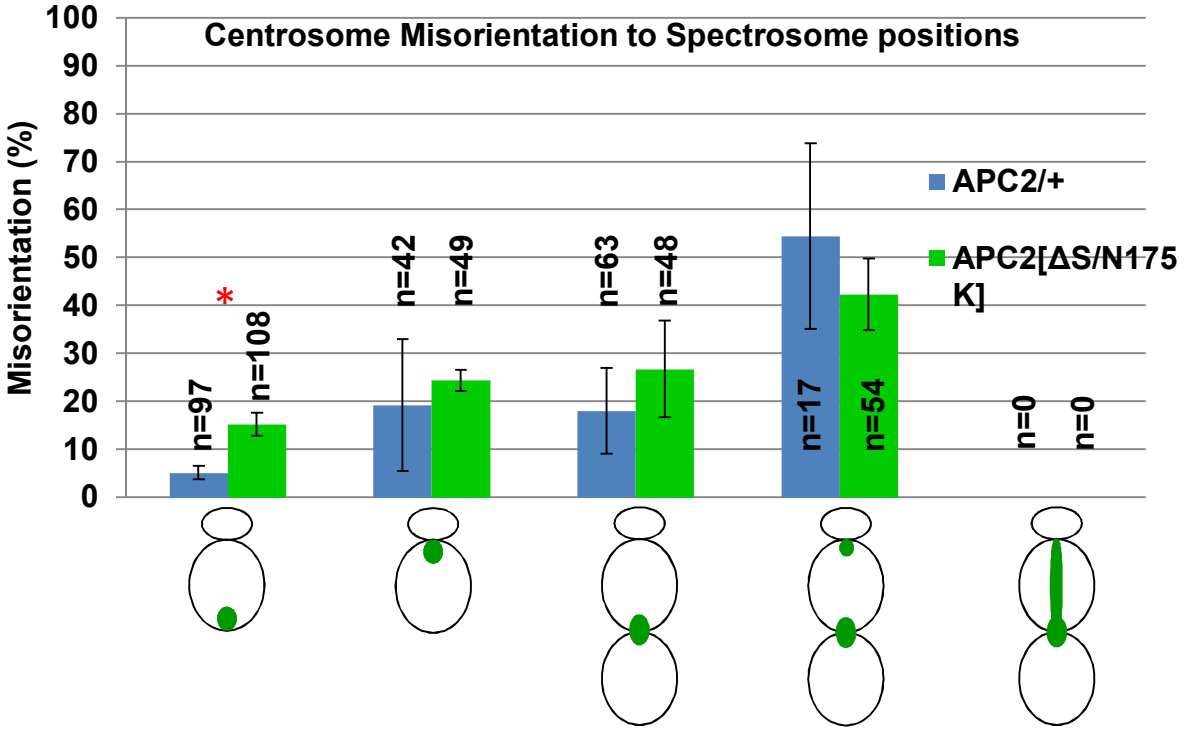
Centrosome Misorientation to Spectrosome positions
Misorientation (%)
100
90
80
70
60
50
40
30
20
10
0
APC2/+
APC2[ΔS/N175K]
*
n=97
n=108
n=42
n=49
n=63
n=48
n=17
n=54
n=0
n=0

Figure 18: Spectrosome velocity and distance to hub-GSC interface for the *cnn-mut* were compared with wild type GSCs. Based on the spectrosome tracking analysis of live-image sequences, the **(A)** interphase spectrosome velocity histograms are shown for both *cnn-mut* and wild type GSCs ($p<0.01$), and the **(B)** interphase spectrosome distance to the hub-GSC histograms are shown for the *cnn-mut* and wild type GSCs ($p<0.001$ between *cnn-mut* and wild type). The p-values were obtained using the Wilcoxon rank sum test.

A

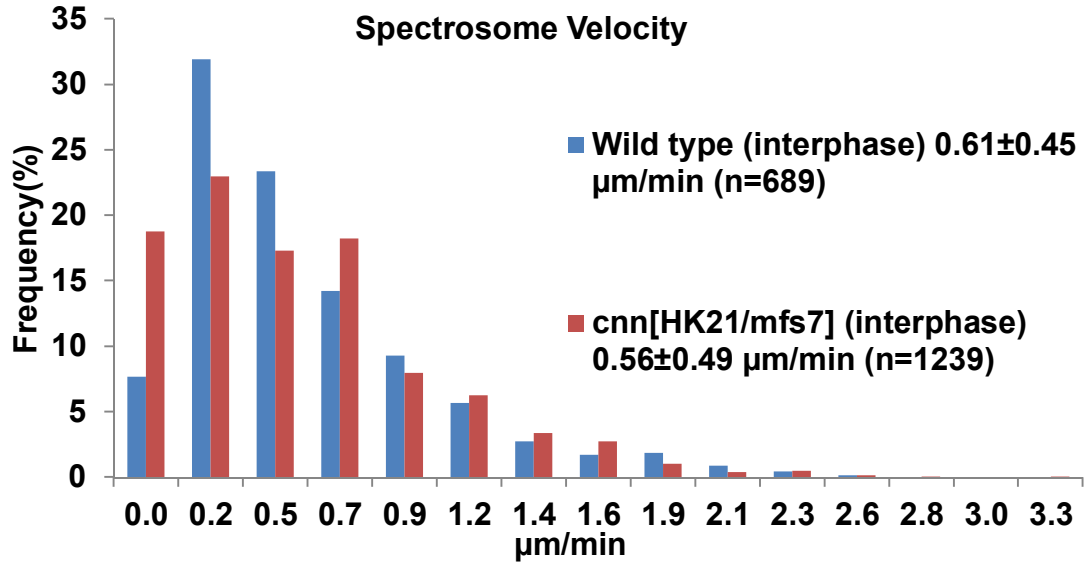
Spectrosome Velocity
Frequency(%)
35
30
25
20
15
10
5
0
Wild type (interphase) 0.61±0.45 µm/min (n=689)
cnn[HK21/mfs7] (interphase) 0.56±0.49 µm/min (n=1239)
0.0 0.2 0.5 0.7 0.9 1.2 1.4 1.6 1.9 2.1 2.3 2.6 2.8 3.0 3.3
µm/min

B

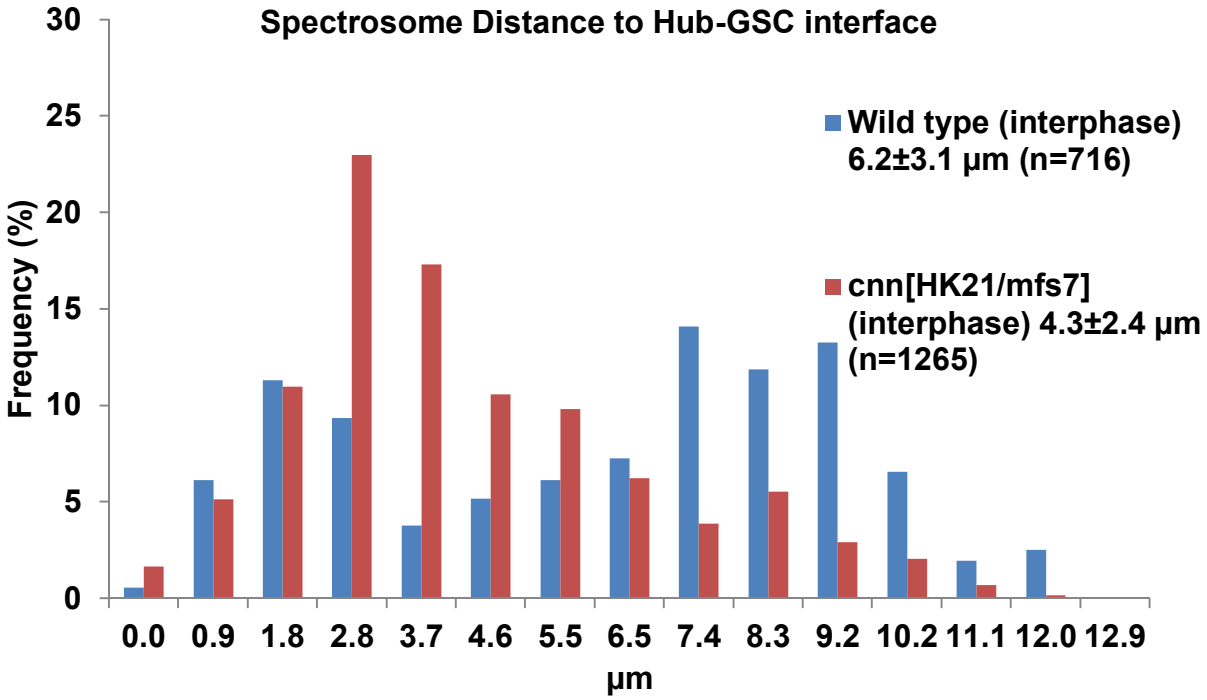
Spectrosome Distance to Hub-GSC interface
Frequency (%)
30
25
20
15
10
5
0
Wild type (interphase) 6.2±3.1 µm (n=716)
cnn[HK21/mfs7] (interphase) 4.3±2.4 µm (n=1265)
0.0 0.9 1.8 2.8 3.7 4.6 5.5 6.5 7.4 8.3 9.2 10.2 11.1 12.0 12.9
µm

Figure 19: Centrosome velocities and distances to hub-GSC interface for the *cnn-mut* and *APC2-mut* were compared with wild type GSCs. Based on the centrosome tracking analysis of live-image sequences, the **(A)** interphase GSC-inherited centrosome velocity histograms are shown for the *cnn-mut*, *APC2-mut*, and wild type GSCs ($p<0.028$ between *cnn-mut* and wild type, $p<0.001$ between *APC2-mut* and wild type), and the **(B)** interphase GB-inherited centrosome velocity histograms are shown for both *cnn-mut* and wild type GSCs ($p<0.001$). In addition, the **(C)** interphase GSC-inherited centrosome distance to the hub-GSC interphase histograms are shown for both *APC2-mut* and wild type GSCs ($p<0.001$), and the **(D)** interphase GB-inherited centrosome distance to the hub-GSC interphase histograms are shown for the *cnn-mut*, *APC2-mut*, and wild type GSCs ($p<0.001$ between *cnn-mut* and wild type, $p<0.001$ between *APC2-mut* and wild type). The p-values were obtained using the Wilcoxon rank sum test.

A

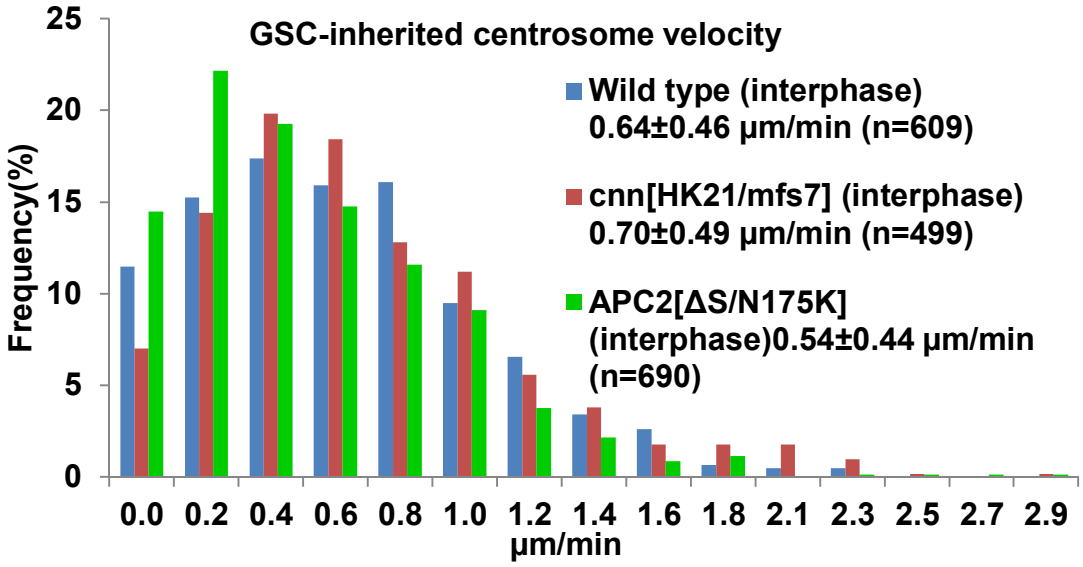
GSC-inherited centrosome velocity
Wild type (interphase)
0.64±0.46 μm/min (n=609)
cnn[HK21/mfs7] (interphase)
0.70±0.49 μm/min (n=499)
APC2[ΔS/N175K]
(interphase)0.54±0.44 μm/min
(n=690)
Frequency(%)
25
20
15
10
5
0
0.0 0.2 0.4 0.6 0.8 1.0 1.2 1.4 1.6 1.8 2.1 2.3 2.5 2.7 2.9
μm/min

B

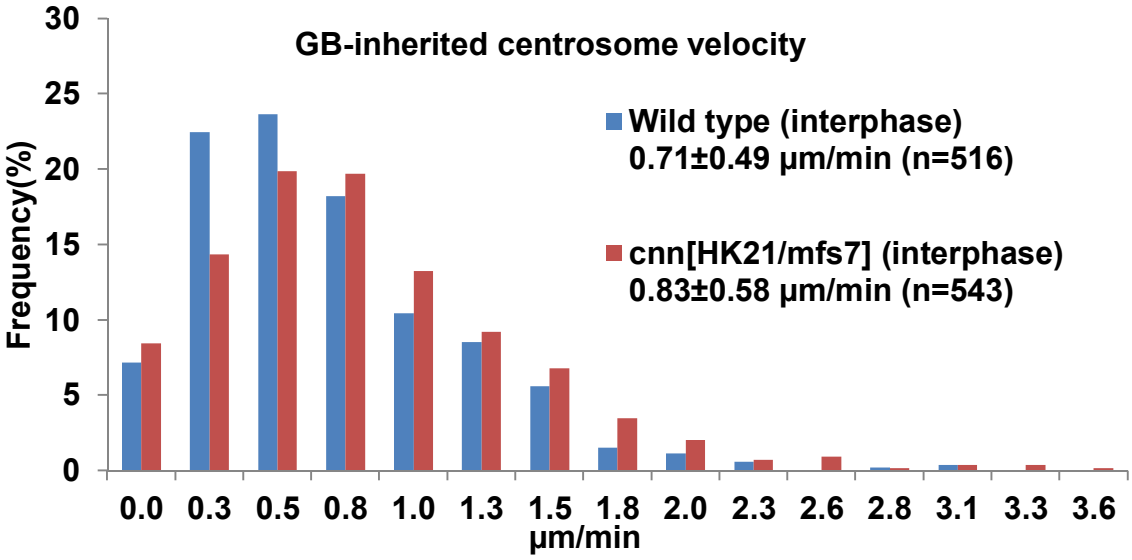
GB-inherited centrosome velocity
Wild type (interphase)
0.71±0.49 μm/min (n=516)
cnn[HK21/mfs7] (interphase)
0.83±0.58 μm/min (n=543)
Frequency(%)
30
25
20
15
10
5
0
0.0 0.3 0.5 0.8 1.0 1.3 1.5 1.8 2.0 2.3 2.6 2.8 3.1 3.3 3.6
μm/min

C

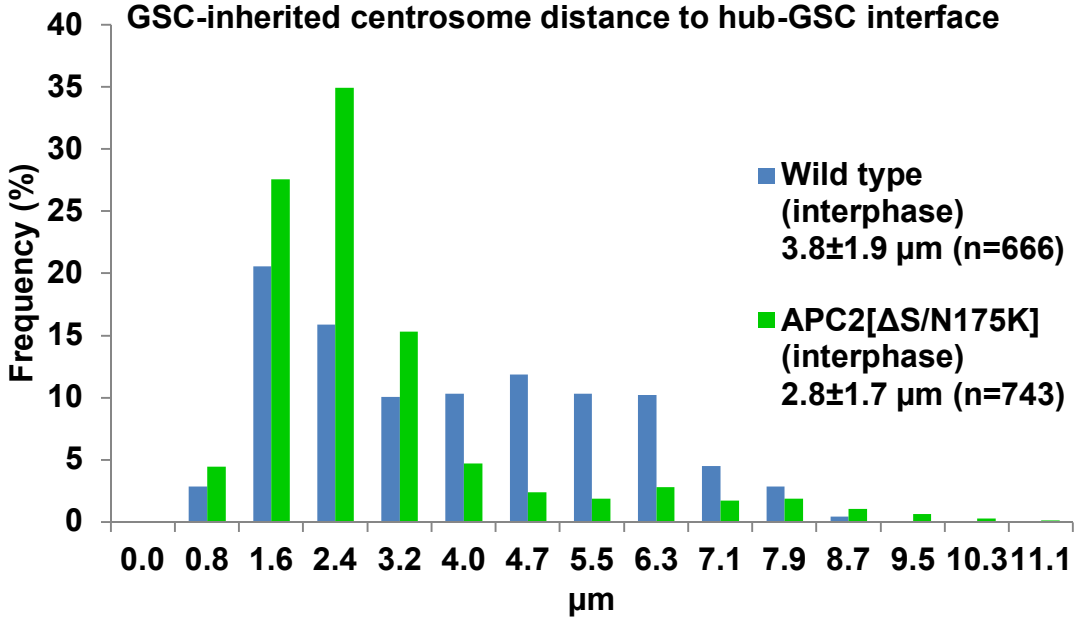
GSC-inherited centrosome distance to hub-GSC interface
Frequency (%)
40
35
30
25
20
15
10
5
0
0.0 0.8 1.6 2.4 3.2 4.0 4.7 5.5 6.3 7.1 7.9 8.7 9.5 10.3 11.1
μm
Wild type (interphase) 3.8±1.9 μm (n=666)
APC2[ΔS/N175K] (interphase) 2.8±1.7 μm (n=743)

D

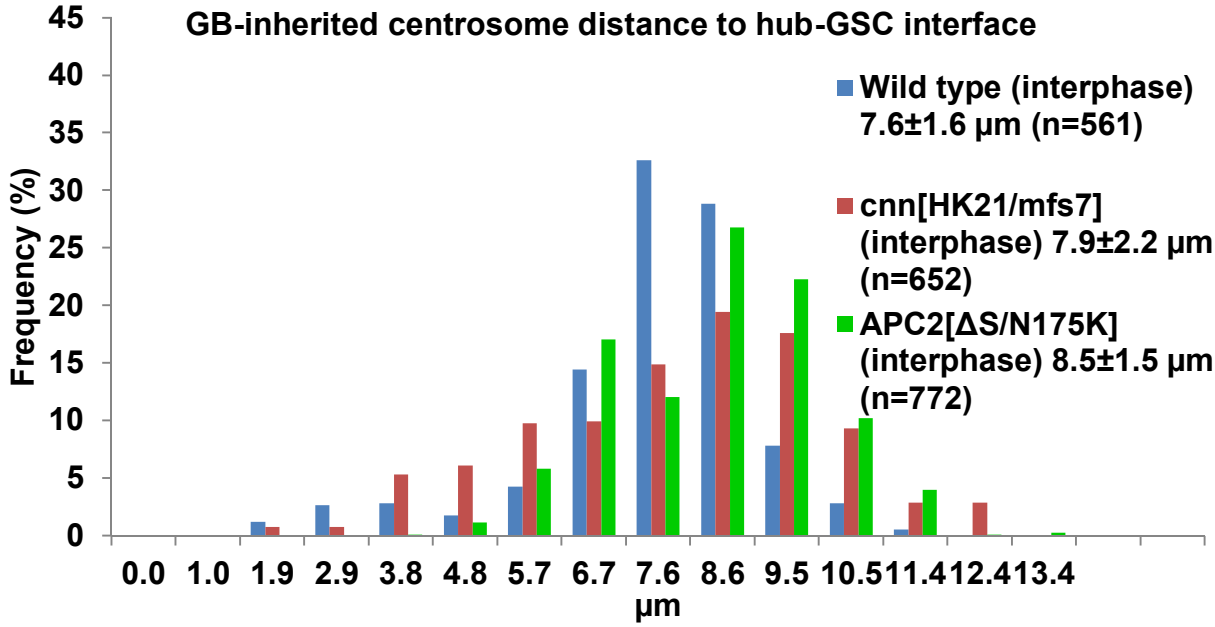
GB-inherited centrosome distance to hub-GSC interface
Frequency (%)
45
40
35
30
25
20
15
10
5
0
0.0 1.0 1.9 2.9 3.8 4.8 5.7 6.7 7.6 8.6 9.5 10.5 11.4 12.4 13.4
μm
Wild type (interphase) 7.6±1.6 μm (n=561)
cnn[HK21/mfs7] (interphase) 7.9±2.2 μm (n=652)
APC2[ΔS/N175K] (interphase) 8.5±1.5 μm (n=772)

Figure 20: Spindle angles and spindle angular velocities for the *cnn-mut* and *APC2-mut* were compared with wild type GSCs. Based on the centrosome tracking analysis of live-image sequences, the spindle angles and spindle angular velocities are calculated. **(A)** Spindle angle histograms are shown for both *cnn-mut* and wild type GSCs ($p<0.001$). **(B)** Spindle angular velocity histograms are shown for the *APC2-mut* and wild type GSCs ($p<0.0258$ between *APC2-mut* and wild type). The p-values were obtained using the Wilcoxon rank sum test.

A

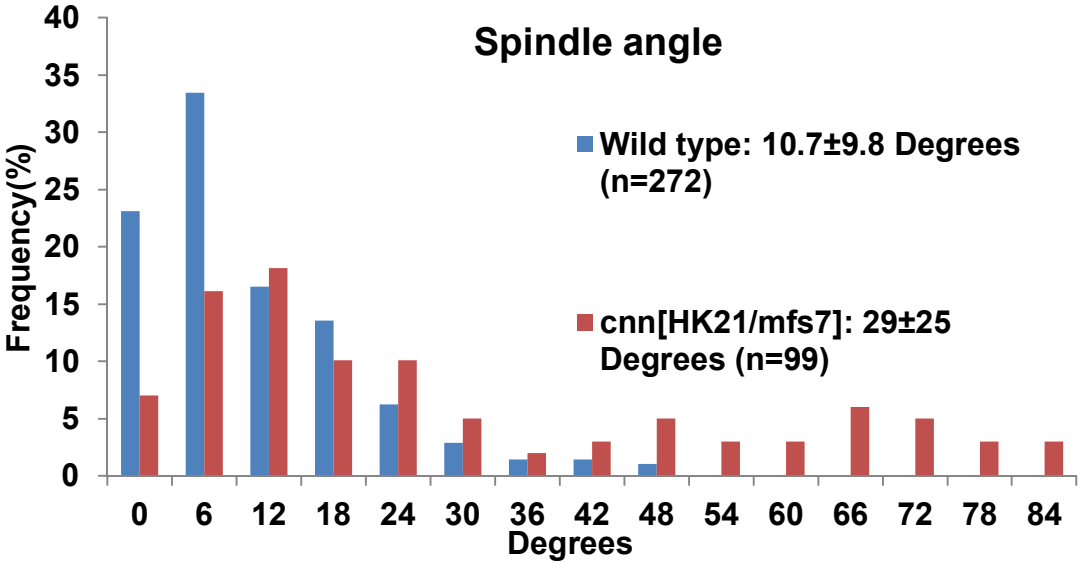
Spindle angle
Frequency(%)
40
35
30
25
20
15
10
5
0
0 6 12 18 24 30 36 42 48 54 60 66 72 78 84
Degrees
Wild type: 10.7±9.8 Degrees (n=272)
cnn[HK21/mfs7]: 29±25 Degrees (n=99)

B

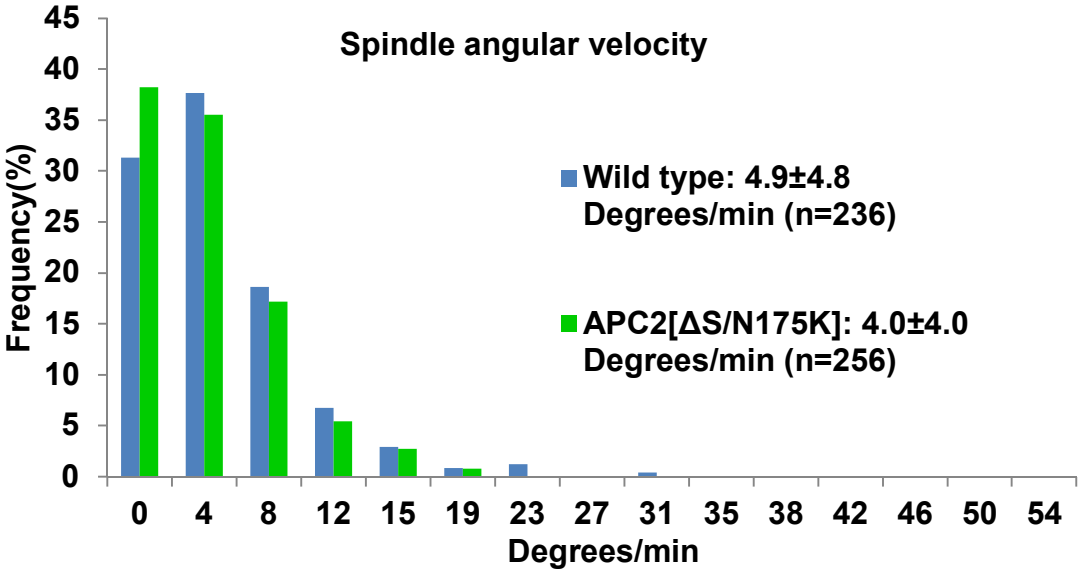
Spindle angular velocity
Frequency(%)
45
40
35
30
25
20
15
10
5
0
0 4 8 12 15 19 23 27 31 35 38 42 46 50 54
Degrees/min
Wild type: 4.9±4.8 Degrees/min (n=236)
APC2[ΔS/N175K]: 4.0±4.0 Degrees/min (n=256)

IV. DISCUSSIONS

A. Dynamic Interplay of Spectrosome and Centrosome Organelles in Asymmetric Stem Cell Divisions

(Parts of this chapter were previously published as Bang, C. and J. Cheng (2015). "Dynamic Interplay of Spectrosome and Centrosome Organelles in Asymmetric Stem Cell Divisions." PLoS ONE 10(4): e0123294.)

Centrosome is known as the microtubule organization center, facilitating mitotic spindle formation during mitosis. Our and previous results show most spindle in male GSCs were still properly oriented despite of lack of centrosome, implying, when centrosome is knocked out, another regulatory mechanism would ensure proper spindle orientation. One intriguing discovery is that, the spectrosome migrates from basal to apical in most acentrosomal GSCs, which is the stereotypical location for female GSCs where spectrosome has been shown to play an important role in orienting mitotic spindles (Deng and Lin 1997). In the wild type GSCs, the spectrosomes were seen to be about half mobile and half stationary, but when the centrosomes were knocked out, close to 71% of spectrosome became stationary, and stationary spectrosomes locating at the apical end increased dramatically. The higher frequency of stationary spectrosome locating closer to the apical region would imply they may interact with the apical mitotic spindle pole and/or the apical cortex. Spectrosome organelle itself physically anchors or provides components necessary to orient the spindle (Deng and Lin 1997), and thus it migrates to the apical in male GSCs when centrosome is absent. Additionally, it is reported previously that

spectrosome and fusome (elongated structure with similar components as spectrosome in 4-cell spermatogonia or later) have transport capability for various proteins (Lin, Yue et al. 1994, Lin and Spradling 1995, Lighthouse, Buszczak et al. 2008, Yuan, Chiang et al. 2012). Moreover, based on live imaging observations, most *DSas-4-mut* GSCs still end up dividing asymmetrically even when their spindles are not properly oriented. Consistent with this observation, the GSC number per testis in *DSas-4-mut* is not significantly different compared to that in wild type. Nevertheless, absence of centrosome significantly prolonged the GSC mitosis duration.

In female GSCs, the spectrosome is mostly found in the apical position during interphase, and is unequally cleaved and segregated during telophase (Lin, Yue et al. 1994, Lin and Spradling 1995, Deng and Lin 1997, de Cuevas and Spradling 1998). However, the growth and migration of spectrosome in male GSCs had not been reported. Here, we observed the spectrosome growth and migration in live male GSCs, and found that no cleavage of the spectrosome occurred at early stages during mitosis in wild type GSCs. Instead, our live imaging data in male GSCs (both wild type and *DSas-4-mut*) show that spectrosomes initially retained in either GSC daughter or GB daughter based on its initial position, most moved and conjoined with the ring canal prior to cytokinesis completion, segregated together with the ring canal structure when the two daughter cells detached from each other. It is an interesting finding that spectrosome eventually transfers into both GSC and GB regardless of initial positions (apical or basal).

We were naturally curious how the spectrosome coordinate with centrosome in terms of orienting mitotic spindle. The live imaging study with spectrosome knockout provides valuable hints to the centrosomes migration pattern (mostly in G2-M cell cycle phases). There are significant differences in the centrosome velocities of GSC-inherited centrosomes and GB-

inherited centrosomes in wild type compared to the *hts-mut*. The slower GSC-inherited centrosome can be interpreted by more robust microtubule arrays around GSC-inherited centrosome (Yamashita, Mahowald et al. 2007). Also, this may imply that the GSC-inherited centrosome in general might contain different composition materials (Januschke, Llamazares et al. 2011), contributing to smaller centrosome mobility. These results suggest spectrosome coordinates with centrosomes to ensure centrosome orientation, but without the spectrosome, another fail safe mechanism intervenes to ensure centrosome orientation.

Consistent to the results reported by Yuan et al., 2012, we observed insignificant changes in the interphase centrosome orientation and almost no spindle orientation change in spectrosome knockout GSCs. In addition, spectrosome knockout does not affect the mitotic duration. To better understand the spectrosomes' role in the absence of centrosomes, we tried to employ the MARCM method to create the double knockout in GSC clones. This MARCM method was a promising alternative to the actual double mutant animal model since an attempt to generate double knockout adult flies failed previously. Due to the technical challenges, we were unable to observe any mitotic GSCs albeit examining 65 double-knockout GSC clones, implying that double mutant GSCs have an extremely low mitotic activity.

In summary, we characterized the dynamic movement of centrosome and spectrosome during asymmetric GSC divisions in wild type, and showed how the dynamics changed when either centrosome or spectrosome is knocked out. Based on our results, we propose that the dynamic interplay of spectrosome and centrosome is part of the regulatory mechanisms of the GSCs, to compensate for the loss of function of the knocked out organelles, which were intended to ensure an asymmetric division of the GSCs.

B. Effects of Centrosomin and Adenomatous Polyposis Coli Protein 2 on Spectrosome Recruitment and Asymmetric Stem Cell Divisions

In a recent publication it was hypothesized that the spectrosome plays a complementary role in orienting the spindle, and thus the asymmetric division outcome of the GSCs when the centrosome is compromised (Yuan, Chiang et al. 2012, Bang and Cheng 2015). In our spindle orientation result, we found, similar to the acentrosomal GSCs (*DSas-4-mut*), that most GSCs with non-functional centrosome with intact centrioles (*cnn-mut*) and microtubule binding protein knockout (*APC2-mut*) had still properly oriented spindles. This raised two interesting questions for us to investigate: 1) Would the compromise in the PCM/astral microtubules around the centrioles (*cnn-mut*) or compromise in the microtubule binding protein (*APC2-mut*) initiate the complementary role of the spectrosome; 2) How the compromise in the PCM/astral microtubules around the centrioles (*cnn-mut*) or compromise in the microtubule binding protein (*APC2-mut*) affect dynamical properties that would shed further insight into potential asymmetric division mechanisms. Intriguing discovery of *cnn-mut* GSC is that spectrosome migrates from basal to apical cortex positions as previously seen in *DSas-4-mut* GSCs (Yuan, Chiang et al. 2012, Bang and Cheng 2015). In *APC2-mut* GSCs, however, the apical localization of spectrosome is not observed, which hints that PCM matrix/astral microtubules (in this case, lack thereof) may be responsible for the recruitment of spectrosomes to the apical cortex region instead of the APC2 protein. It is hypothesized that APC2 plays a regulatory role in controlling the centrosome orientation through binding of the centrosomal MT at the apical cortex (Inaba, Yuan et al. 2010). Moreover, we observed increased frequencies of apical and stationary spectrosomes in *cnn-mut* GSCs compared to wild type, which has high frequencies basal and mobile spectrosomes. This

result is similar to the acentrosomal data (*DSas-4-mut*) previously reported, which suggest that the stationary and apically localized spectrosome may interact with the apical mitotic spindle pole and/or the apical cortex. Furthermore, since it has been reported that the spectrosome itself physically anchors or provides components necessary to orient the spindle in female GSCs (Deng and Lin 1997), it may be likely that the spectrosome migration to the apical region and becoming immobilized would help align the spindle orientation.

Interestingly, the centrosome misorientation is both significantly increased in both *cnn-mut* and *APC2-mut* GSCs compared to their respective controls (one way student t-test). The centrosome orientation is important as centrosome positions prior to mitosis define the microtubule organizing center positions and subsequently the directionality of the spindle formation (Yamashita 2009, Tang and Marshall 2012, Inaba, Venkei et al. 2015). In addition, the centrosome orientation is important for the checkpoint of the cell cycle progression, and it only allows the progression of mitosis when the centrosomes are oriented(Cheng, Turkel et al. 2008). As both *cnn-mut* and *APC2-mut* increase the centrosome misorientation, it is not surprising to see the mitotic duration time increase for both *cnn-mut* and *APC2-mut* GSCs as regulatory mechanisms delay the cell cycle progression until the precise orientation conditions are met. These results reveal that the cnn and APC2 are important for timely divisions. One perplexing finding is how the GSC number per testis for the *APC2-mut* is significantly larger than the control when the spindle misorientation is very low. Normally, the increased GSC count per testis could be used to correlate increased incidence of spindle misorientation as higher frequencies of misorientation is expected to increase the probability of symmetric stem cell division. In this case, it is possible other signaling mechanism may play a part in increasing the GSC number, such as the Wnt/β-catenin signaling pathway (Bienz and Clevers 2010) . The *cnn-*

mut on the other hand, had increased spindle misorientation correlated to higher GSC number per testis.

Spectrosome orientation in fixed *cnn-mut* and *APC2-mut* GSCs were quantified using quantification criteria similar to the fixed *DSas-4-mut* results in the Yuan et al., 2012 manuscript. Covering all the ranges of the GSC cell cycle states, the *cnn-mut* differed from the control in every spectrosome localization category, which may indicate the spectrosome localization may depend on microtubule networks or lack thereof. On the other hand, the APC2-mut spectrosome localizations were similar to the control except for the apical and ring canal localization category. This seems to indicate that the microtubule binding APC2 proteins do not play much role in recruitment of the spectrosome. Our centrosome misorientation data (Fig. 15B) and previously reported data have shown that the centrosomes are significantly misoriented in both *cnn-mut* and *APC2-mut* GSCs (Yamashita, Jones et al. 2003, Inaba, Yuan et al. 2010). Here we quantified further at which spectrosome localization category we observe the most misorientation. In *cnn-mut* GSCs, the centrosome misorientation difference was significant in the ring canal localization category. Based on the previous evidence that (Bang and Cheng 2015) each spectrosome localization category belong to certain stages of the cell cycle (basal and apical categorization belong to the same stages of the cell cycle), the marked difference of centrosome misorientation in the ring canal category for the *cnn-mut* seem to suggest that the centrosomes are likely to freely migrate without robust microtubules during this stage of the cell cycle. Alternative possibility is the lack of directional motor proteins that may be causing the misorientation in the *cnn-mut*. For the basal localization category of the *cnn-mut* GSCs, the centrosome misorientation could not be compared statistically with the control due to the very small population size. For the *APC2-mut* GSCs, the basal spectrosome localization category showed

the most marked centrosome misorientation difference compared to the control, which may be partly due to APC2 molecules not being able to properly secure the centrosome to the apical cortex region. Alternatively, it may also be possible that the missing APC2 maybe altering the motor protein localization that may be altering centrosome localization. It has been shown that centrosome movement and positioning is regulated by motor proteins localized to the cortex such as cortical dynein and MT dynamics (Brodsky, Burakov et al. 2007, Wu, Misra et al. 2011, Laan, Pavin et al. 2012, Sitaram, Anderson et al. 2012). Nevertheless, for both *cnn-mut* and *APC2-mut* GSCs, it is interesting to note that the centrosome misorientation is considerably higher when the spectrosome is localized to the apical region compared to the basal region. Inversely observing the data, we may deduce that the spectrosomes may be recruited to the apical area when the centrosomes are misoriented for the mutants.

Quantifying spectrosome migration dynamics via live imaging of *cnn-mut* and *APC2-mut* is an interesting topic because it is the first time that such topic was explored. The spectrosome velocity histogram distribution of *cnn-mut* compared to the wild type shows significantly slower movement in velocity during interphase. There maybe two possibilities for making the spectrosome movement slower: firstly, the spectrosome anchorage to the apical region of the GSCs in *cnn-mut* limits movement and may lower the overall spectrosome movement speed; or secondly, there may be overall shift in the transport dynamics due to the cnn mutation that in turn alter the spectrosome migration. The membrane characteristics of spectrosome best describes endoplasmic reticulum (de Cuevas, Lilly et al. 1997). Since the spectrosome has close similarity to the endoplasmic reticulum, it may be probable that its transport mechanism share similarity as well. In the endoplasmic reticulum, the vesicles are transferred to the Golgi apparatus for further packaging and processing via network of microtubule and microtubule

motor proteins. It has been previous reports that microtubule motor proteins such as kinesin, dynein, dynein-dynactin complex are involved in the transport process of the endoplasmic reticulum vesicles (Burkhardt 1998, Dorner, Ciossek et al. 1998, Palmer, Watson et al. 2005, Watson and Stephens 2005, Hirokawa, Noda et al. 2009, Lord, Ferro-Novick et al. 2013). Most of the known kinesin motors move towards the plus end of microtubules and the dynein motors move toward the negative end of the microtubules (Ikuta, Kamisetty et al. 2014). It would be interesting to see if both motors are involved in spectrosome movement and if same microtubule tracks can be used by both motor proteins. No significant change in *APC2-mut* spectrosome average velocity seems to suggest that APC2 is not involved in regulating the overall dynamic movement of spectrosomes. These results show interesting indirect/direct interplays of spectrosome to APC2 and cnn proteins.

Centrosome dynamics of *cnn-mut* and *APC2-mut* GSCs are also intriguing part of the results that was not previously explored. Firstly, the GSC-inherited centrosome velocity for the *cnn-mut* was significantly faster while *APC2-mut* was significantly slower than the wild type. The faster *cnn-mut* centrosome velocity may be interpreted as the centrosome devoid of proper connections to the PCM matrix (Lucas and Raff 2007) or lack of robust microtubule surrounding the centrosome due to the cnn mutation may have caused affected over all GSC-inherited centrosome mobility. Furthermore, the faster average GB-inherited *cnn-mut* centrosome velocity also seems to indicate that the cnn mutation also affects the GB-inherited centrosomes similarly to the GSC-inherited centrosomes. On the other hand, the slower *APC2-mut* GSC-inherited centrosome velocity may be an effect of another unexplored fail-safe mechanism, affecting the centrosome movement in the absence of APC2. It is interesting to note that *APC2-mut* GB-inherited centrosome velocity is not much different than the wild type while the GSC-inherited

centrosome velocity is significantly different than the wild type, which raises the question if the GB-inherited centrosome recognition maybe regional to where the APC2 proteins localize (mainly to the hub-GSC interface). Here, it is be possible that APC2 knockout may be affecting the motor proteins located near the cortex of the GSCs. In addition, in APC2-mut GSCs, the GSC-inherited centrosomes were significantly closer to the hub-GSC interface than the wild type. There is no clear biological meaning that we can infer from this result but we may speculate that perhaps a compensation mechanism is drawing the centrosomes closer to the hub-GSC interface. Moreover, we can observe that the GB-inherited centrosome distance for *cnn-mut* and *APC2-mut* GSCs were significantly farther out from the huh-GSC interface when compared to the wild type. Biologically, we may infer from this result that change in the GSC cell shape or size may have occurred as reported previously (Yamashita, Jones et al. 2003).

Although spindle dynamics through live imaging have been reported previously by many groups on various number of stem cell types (Siller, Serr et al. 2005, Basto, Lau et al. 2006, Dix and Raff 2007, Lucas and Raff 2007, Siller and Doe 2008), we have examined previously undiscovered aspects of the spindle angle and the spindle angular velocity in *APC2-mut* and *cnn-mut* GSCs. The spindle angle for the *cnn-mut* is significantly different than the wild type. This data includes additional spindle angle data from pro-metaphase to telophase than compared to the anaphase angle measurement discussed in Fig. 15A. We can observe from the data that the *cnn-mut* GSC spindle angle is also misoriented in other stages of the mitosis as in Anaphase. Other intriguing finding is the spindle angular velocity. We can observe from the spindle angular velocity data that the average *APC2-mut* GSC is slower than the wild type. Although spindle misorientation has been reported previously in several stem cell types (Yamashita, Jones et al. 2003, Siller and Doe 2008, Inaba, Yuan et al. 2010), the spindle angular velocity has largely not

been explored previously. The reduced *APC2-mut* spindle angular velocity may be caused by alteration of apically localized motor proteins and complexes impacted by missing APC2. There are few known regulators of spindle orientation and spindle movement, including Lis-1/dynactin, dynein/dynactin, and Kip3p kinesin/Kar9p (Miller and Rose 1998, Lee, Tirnauer et al. 2000, Siller, Serr et al. 2005, Siller and Doe 2008). Elucidating how the APC2 interact with these regulators would be most useful. Alternatively, there may be a competing mechanism that is causing the stabilization of the spindle movement at the cortex. There is one such protein shown to stabilize the microtubules at the cell cortex that associates with APC2. Known as disheveled (Dvl), about ~70kDa protein, it acts as a key component in the wingless signaling pathway; interacts with, Frizzled, Axin, Plk1, among others; and regulates β-catenin accumulation level (Yanagawa, van Leeuwen et al. 1995, Habas and Dawid 2005, Wallingford and Habas 2005, Gao and Chen 2010, Kikuchi, Niikura et al. 2010). The Dvl has been implicated in asymmetric cell division in early embryos (Walston, Tuskey et al. 2004). In previous studies, it has been shown that cortical localization of Dvl accentuates disassembly of complexes containing APC, Axin, and β-catenin; controls spindle orientation and alignment within the wingless pathway; and stabilize the microtubules (Ciani, Krylova et al. 2004). So, when the APC2 is knocked out, it may shift the dynamics Dvl and influence the spindle alignment and orientation.

In summary, we characterized the effects the *cnn-mut* and *APC2-mut* have on the interplay of centrosome and spectrosome as well as the asymmetric stem cell division in *Drosophila* GSCs. Firstly, the *cnn-mut* similarly recruited spectrosomes to the apical cortex as observed previously in acentrosomal (*DSas-4-mut*) GSCs. It was previously hypothesized that the apically positioned spectrosome would properly orient the spindles when the centrosome is compromised (Yuan, Chiang et al. 2012, Bang and Cheng 2015). By comparing the *cnn-mut*

and *DSas-4-mut*, we gained further understanding that the intact PCM/astral microtubule, as compared to centrioles alone, plays important roles in maintaining the centrosome orientation, spindle orientation, and the maintenance of the GSC number. Contrary to the *Cnn-mut*, the *APC2-mut* did not change the spindle orientation or the apical spectrosome localization, but altered the centrosome orientation and homeostasis of the GSCs slightly. These results suggest that the APC2 do not associate with spectrosomes but affect the centrosome orientation during interphase. The APC2 protein was previously proposed to function as a microtubule binding protein to regulate the centrosome orientation, and ultimately regulate the outcome of the asymmetric stem cell division (Yamashita, Jones et al. 2003, Inaba, Yuan et al. 2010). Intriguingly, the lack of microtubule binding APC2 proteins produced increased frequency of misoriented centrosomes, however produced correctly oriented spindles, which may be caused by a possible competing mechanism that would regulate the spindle orientations. Contrary to the GSCs, on different cell types, the *APC2-mut* caused spindle misorientation (Caldwell, Green et al. 2007, Fleming, Zajac et al. 2007, Quyn, Appleton et al. 2010). Despite no general defect in the spindle orientation, APC2-mut GSCs exhibited dynamical differences such as slower centrosome velocity and slower spindle angular velocity.

V. CONCLUSIONS

A. Key findings

(Parts of this chapter were previously published as Bang, C. and J. Cheng (2015). "Dynamic Interplay of Spectrosome and Centrosome Organelles in Asymmetric Stem Cell Divisions." PLoS ONE 10(4): e0123294.)

This study was conducted to elucidate regulatory mechanisms of asymmetric stem cell division in male GSCs. To better understand the regulation of asymmetric stem cell divisions, movement pattern of centrosome and spectrosome, spindle orientations, and spindle dynamics were quantified under APC2, cnn, DSas-4, and hts mutant background conditions. It was hypothesized that the spectrosome plays a complimentary role in regulating the spindle orientation when the centrosome are compromised in male GSCs. The cnn and APC2 mutant conditions were designed to answer whether changes in the spectrosome positions were caused by the improper attachment of PCM/Astral MT to the cortex of the GSCs due to missing APC2 or simply caused by the absence of fully functional PCM/Astral MT. In addition, the MARCM experiment was designed to double knock out centrosomes and spectrosomes to show that spectrosome has a fail-safe role in orienting the spindle when the centrosome is compromised in male GSCs.

The expected result of the MARCM study in the male GSCs was to observe randomly oriented spindles when both centrosomes and spectrosomes are knocked out, which would show that spectrosomes have complementary roles in orienting the spindle when the centrosomes are

compromised. Unfortunately, due to reduced mitotic activity, MARCM results could not be obtained directly to show the spectrosomes' fail-safe function. However, several clues have been found which suggest that the spectrosomes play a role in orienting the spindle when centrosomes or PCM/Astral MTs are compromised, giving rise to the asymmetric stem cell division outcome. Important key findings (clues) are shown:

- Majority of spectrosome localization in *DSas-4-mut* (centrosome knockout) male GSCs changed from the basal to the apical side. In previous studies, it is in the apical location the spectrosomes have been observed to anchor the mitotic spindle poles to the apical cortices to orient the spindles in female GSCs.
- Majority of apically localized spectrosomes in *DSas-4-mut* (centrosome knockout) male GSCs became stationary. This result shows that the spectrosome is anchored to the apical region of the GSCs. This evidence suggests that the spectrosomes maybe anchoring the mitotic spindle poles to the apical cortices to orient the spindles.
- Spectrosome knockout study reveals that in male GSCs, the centrosome orientation, spindle orientation, mitosis duration, and stem cell numbers remain unchanged. These results show that in the presence of centrosomes, the role of spectrosome appear rather dispensable.
- Dynamically, however, the centrosome distance to the hub-GSC interphase and the centrosome velocities have changed significantly when spectrosome was knocked out. This shows that even though the role of spectrosome may not appear important when the centrosomes are present, there exist communication between the spectrosome and centrosomes.

- When cnn was knocked out, majority of spectrosome localization changed from the basal to the apical side in male GSCs, similar to when the centrosomes were knocked out via DSas-4 mutation. This shows that disruption of the PCM/Astral MT recruits the spectrosome to the apical region of the GSCs.
- In fixed GSCs, the localization of spectrosome throughout the whole cell cycle was drastically different in the *cnn-mut* than the wild type, which suggests that the cnn is important for the spectrosome localizations.
- When APC2 was knocked out, the spectrosomes were mainly localized to the basal side similar to the wild type GSCs. This shows that the improper attachment of the PCM/Astral MT to the apical cortex due to missing APC2 does not recruit the spectrosome to the apical area.
- In fixed GSCs, the localization of spectrosome throughout the whole cell cycle was unchanged in the *APC2-mut* compare to the wild type, which suggests that the APC2 is not important for the spectrosome localizations.

B. Application/Translation

Asymmetric stem cell division is important for maintaining tissue homeostasis and needs intricate positioning within the stem cell niche and internal cellular machinery mechanisms to achieve asymmetry. There are currently many different stem cell types that are known to go through asymmetric stem cell divisions, including: mouse and *Drosophila* neuronal stem cells, mammalian intestinal stem cells, mammalian skin stem cells, mammalian satellite cells, and mammalian lymphocytes. The resident stem cells communicate to the nearby cells through cell-cell signaling (e.g. adherent junction and paracrine signaling) and regulate the asymmetrical stem

cell division outcome by localizing polarity proteins and orienting mitotic spindles. Although our current knowledge on stem cell division maybe far from complete, there exist striking resemblances between the *Drosophila* and mammalian systems, which suggest that asymmetric stem cell division is a well conserved evolutionary process. The knowledge gained from both the external cues and the internal cellular regulations of the GSCs may be used to serve as a model for the mammalian stem cells that have polarity guiding stem cell niche and divide asymmetrically. In addition, the knowledge gained from the studies may be used for potential tissue engineering application or new cancer therapies via manipulating stem cell self-renewal or differentiation fates.

The current study investigated regulatory functions of APC2, cnn, spectrosomes, and centrosomes on asymmetric stem cell divisions, which are all part of the internal cellular machinery in the GSCs. The cnn and centrosomes are involved in the mitotic spindle orientation and assembly of mitotic spindles, PCM, and astral MT. Currently, full understanding of centrosome orientation, centrosome movement, and spindle orientation regulations are far from complete, and the results gained from the investigations would be useful in manipulating centrosome movement and placement. The APC2 and spectrosomes are hypothesized to be involved in the attachment of centrosome microtubules and mitotic spindle pole to the apical cortices of the GSCs to regulate spindle orientation. In general, the attachment and interaction of mitotic spindle poles to the apical cortices of the GSCs is spindle poles is not fully understood. The investigation results will most likely be useful in manipulating attachment of centrosomes and spindle poles to the apical cortices. One caveat of using GSCs as a model system for other mammalian stem cell types is that the spectrosomes exist uniquely in Drosophila GSCs with an exception of mammalian lymph stem cells, where usage would still suffice. Although the

translational knowledge of spectrosome to other stem cell system may be somewhat limited, spectrosomes still contain many homologous proteins found on other mammal stem cells. The spectrosome results would be useful to broader range of stem cell types once the link between the asymmetric stem cell divisions to the spectrosome components have been found.

The dynamics results such as centrosome velocity and angular spindle velocity can be useful for gaining insights on how the APC2, hts, and non-functional centrosomes (*cnn-mut*) interact with mediators such as motor proteins and microtubules. Centrosome movement and spindle angular movements are results of microtubule dynamics and motor protein interactions occurring inside the cells (Tsai, Bremner et al. 2007, Smith, Hégarat et al. 2011, Collins, Balchand et al. 2012, Kotak, Busso et al. 2012, Raaijmakers, van Heesbeen et al. 2012, Longoria and Shubeita 2013, McNally 2013).

There are various microtubule motor proteins involved in the centrosome movement, and their effects differ in different the stage of the cell cycle (Smith, Hégarat et al. 2011, Raaijmakers, van Heesbeen et al. 2012). The microtubule motor proteins involved in the centrosome separation include nuclear envelope-associated dynein (NE-dynein), motor protein kinesin-5 (Eg5), and polo-like kinase 1 (Plk1). The Eg5 is mainly activated by the cyclin-dependent kinase 1 and 2, (cdk1 and 2) and moves the centrosomes quickly. On the other hand, the Plk1 triggers the centrosome movement at a very slow rate independent of cdk1 (Smith, Hégarat et al. 2011). However, the Plk1 can trigger fast centrosome movement when the interphase microtubules destabilize. In chicken DT40 cells, when both Eg5 and Plk1 are active, the average centrosome velocity is 1.1μm/min and Eg5 alone is 0.5 μm/min. Normal GSC centrosome velocity during interphase is around 0.5 μm/min. In addition, the NE-dynein motor has been shown to mobilize centrosome around prophase in conjunction with Eg5. Although the activity

of NE-dynein is not required but its role become more evident as Eg5 activity is inhibited (Raaijmakers, van Heesbeen et al. 2012). On another study, it was shown that dynein also plays an important role in centrosome mobilization. Using rat neuronal cells, the centrosome movements were measured with and without lissencephalygene (Lis1), a regulator that inhibits dynein activity. When Lis1 was present, centrosome velocity decreased to almost 0 μm/min 0.21 μm/min (control) (Tsai, Bremner et al. 2007). Through there are differences in average centrosome velocities from one cell type to the other, trends can be compared to gain insights into how the motor proteins interact with the regulatory proteins/organelles (APC2, hts, non-functional centrosomes).

Spindle dynamics is an important event that occurs during cellular division. Particularly, the spindle positioning and correction determines the spindle orientation, which in turn controls the asymmetrical stem cell division outcome. It's been shown that cortical dynein and dynactin complex plays an important role in positioning of mitotic spindles (Collins, Balchand et al. 2012, Kotak, Busso et al. 2012, McNally 2013). The dynein and dynactin has been shown to localize to the membrane in patches beginning from the metaphase (Collins, Balchand et al. 2012, Kiyomitsu and Cheeseman 2012), localize further during anaphase, and delocalize back during telophase (Collins, Balchand et al. 2012). It has been postulated that the astral microtubules extend to the cortical dynein and position the mitotic spindle. Therefore, depending on the localization of the cortical dynein, the mitotic spindle orientation can be corrected (Collins, Balchand et al. 2012). Furthermore, it has been directly shown that the spindle oscillations are dynein dependent and disruptions of the dynein activity (Kotak, Busso et al. 2012). The change in *APC2-mut* angular spindle velocity can perhaps be used to gain insight into how the cortical dynein and dynein-dynactin complex are affected.

C. Future directions

1. Ultra-fast laser microsurgery study

Traditional way of producing the double knockouts of centrosomes and spectrosomes yielded no surviving progeny. It is interesting to note that single knockouts survived, but both knockouts did not survive. This hints that the presences of both organelles are essential for the development and survival of the organism. Furthermore, the double knockouts/knockdown of centrosomes and spectrosomes using the MARCM and RNAi (preliminary results not shown) methods have also failed. This suggests that there is a need for different knockout methods aside from genetic methods. A structural knock-out method using ultra-fast laser microsurgery is an option to implement the double knockouts of centrosomes and spectrosomes. In previous studies, centrosome ablations on mammalian cells had mixed results; one study showed that centrosome ablated cells went through mitosis successfully while other study showed strange numerous de-novo centrosome formations over a 24 hour period. Currently, we can utilize the ultra-fast laser microsurgery to successfully ablate centrosomes and spectrosomes (see preliminary result Fig. 21) in the male GSCs, however, long term affects study have not yet been performed. For the next sets of experiments, we can ablate centrosomes on an *hts-mut* background or ablate spectrosomes on a *DSas4-mut* background and record the spindle orientation using time-lapse live-cell imaging. Perhaps using the structural knockout method may be able to discover regulative roles of spectrosome on asymmetric stem cell division.

2. Aging Study

Aging deteriorates the intricate balance of tissue homeostasis. Previous studies have shown that aging decreases the stem cell numbers and increases misorientation of centrosomes.

However, despite of the centrosome misorientation, the spindles remain oriented. It is uncertain whether the spectrosome may be involved in the spindle orientation process during aging. A spectrosome migration study can be conducted in the GSCs to observe possible migration pattern changes similar to the *DSas4-mut* and *Cnn-mut* studies during aging. A link between aging and spectrosome migration pattern changes would bring one step closer to understanding how mechanistically aging affect asymmetric stem cell divisions and how the stem cells respond to such changes.

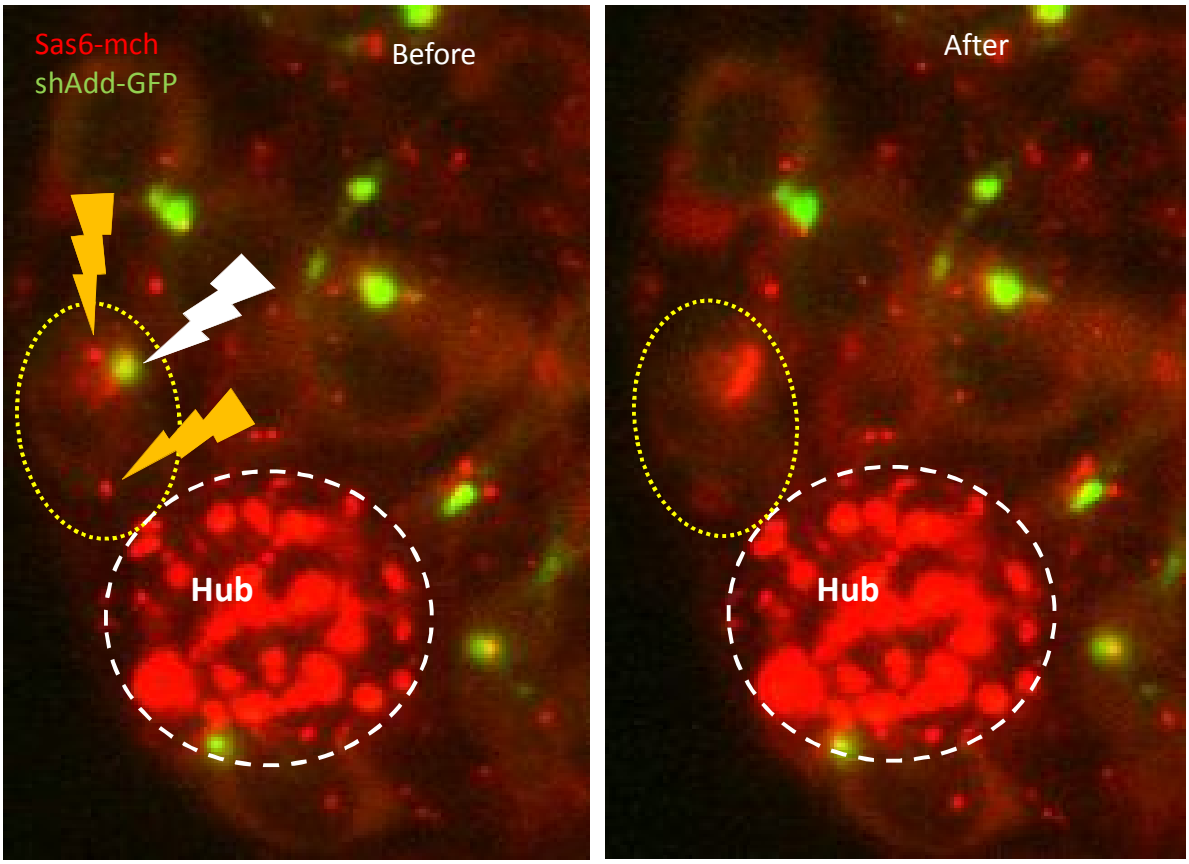

Figure 21: Preliminary result of spectrosome and centrosome ablation in a male *Drosophila* GSC via ultrafast laser microsurgery. Successful ablation of centrosomes (shown by Sas6-mch) and a spectrosome (shown by shAdd-GFP) via ultrafast laser microsurgery can be visualized by comparing the before and after images. The formation of cloudy halo around the region where the centrosome used to be suggests that the centrosome was successfully disintegrated by the laser ablation. Yellow lightening: laser targeted centrosome. White lightening: laser targeted spectrosome. Yellow dashed-line: GSC. White dashed-line: hub cells.

VI. CITED LITERATURE

Ahmed, Y., A. Nouri and E. Wieschaus (2002). "Drosophila Apc1 and Apc2 regulate Wingless transduction throughout development." Development **129**(7): 1751-1762.

Akong, K., E. E. Grevengoed, M. H. Price, B. M. McCartney, M. A. Hayden, J. C. DeNofrio and M. Peifer (2002). "Drosophila APC2 and APC1 play overlapping roles in wingless signaling in the embryo and imaginal discs." Dev Biol **250**(1): 91-100.

Avasthi, S., R. N. Srivastava, A. Singh and M. Srivastava (2008). "STEM CELL: PAST, PRESENT AND FUTURE- A REVIEW ARTICLE." Internet Journal of Medical Update **3**(1): 22-30.

Bang, C. and J. Cheng (2015). "Dynamic Interplay of Spectrosome and Centrosome Organelles in Asymmetric Stem Cell Divisions." PLoS ONE **10**(4): e0123294.

Basto, R., J. Lau, T. Vinogradova, A. Gardiol, C. G. Woods, A. Khodjakov and J. W. Raff (2006). "Flies without Centrioles." Cell **125**(7): 1375-1386.

Bausek, N. (2013). "JAK-STAT signaling in stem cells and their niches in Drosophila." JAK-STAT **2**(3): e25686.

Berrueta, L., S. K. Kraeft, J. S. Tirnauer, S. C. Schuyler, L. B. Chen, D. E. Hill, D. Pellman and B. E. Bierer (1998). "The adenomatous polyposis coli-binding protein EB1 is associated with cytoplasmic and spindle microtubules." Proc Natl Acad Sci U S A **95**(18): 10596-10601.

Bienz, M. and H. Clevers (2010). "Linking Colorectal Cancer to Wnt Signaling." Cell **103**(2): 311-320.

Biteau, B., C. E. Hochmuth and H. Jasper (2011). "Maintaining tissue homeostasis: dynamic control of somatic stem cell activity." Cell Stem Cell **9**(5): 402-411.

Blanpain, C. and E. Fuchs (2009). "Epidermal homeostasis: a balancing act of stem cells in the skin." Nat Rev Mol Cell Biol **10**(3): 207-217.

Brinster, R. L. (2002). "Germline stem cell transplantation and transgenesis." Science **296**(5576): 2174-2176.

Brodsky, I. B., A. V. Burakov and E. S. Nadezhdina (2007). "Microtubules' interaction with cell cortex is required for their radial organization, but not for centrosome positioning." Cell Motility and the Cytoskeleton **64**(6): 407-417.

Brunet, A. and T. A. Rando (2007). "Ageing: From stem to stern." Nature **449**(7160): 288-291.

Burkhardt, J. K. (1998). "The role of microtubule-based motor proteins in maintaining the structure and function of the Golgi complex." Biochimica et Biophysica Acta (BBA) - Molecular Cell Research **1404**(1–2): 113-126.

Caldwell, C. M., R. A. Green and K. B. Kaplan (2007). "APC mutations lead to cytokinetic failures in vitro and tetraploid genotypes in Min mice." The Journal of Cell Biology **178**(7): 1109-1120.

Chen, H., X. Chen and Y. Zheng (2013). "The nuclear lamina regulates germline stem cell niche organization via modulation of EGFR signaling." Cell Stem Cell **13**(1): 73-86.

Chen, M., M. Przyborowski and F. Berthiaume (2009). "Stem cells for skin tissue engineering and wound healing." Crit Rev Biomed Eng **37**(4-5): 399-421.

Cheng, J. and A. J. Hunt (2009). Time-Lapse Live Imaging of Stem Cells in Drosophila Testis. Current Protocols in Stem Cell Biology, John Wiley & Sons, Inc. **11:** 2E.2.1-2E.2.8.

Cheng, J., N. Turkel, N. Hemati, M. T. Fuller, A. J. Hunt and Y. M. Yamashita (2008). "Centrosome misorientation reduces stem cell division during ageing." Nature **456**(7222): 599-604.

Ciani, L., O. Krylova, M. J. Smalley, T. C. Dale and P. C. Salinas (2004). "A divergent canonical WNT-signaling pathway regulates microtubule dynamics: Dishevelled signals locally to stabilize microtubules." The Journal of Cell Biology **164**(2): 243-253.

Clarke, M. F. and M. Fuller (2006). "Stem Cells and Cancer: Two Faces of Eve." Cell **124**(6): 1111-1115.

Collins, E. S., S. K. Balchand, J. L. Faraci, P. Wadsworth and W.-L. Lee (2012). "Cell cycle–regulated cortical dynein/dynactin promotes symmetric cell division by differential pole motion in anaphase." Molecular Biology of the Cell **23**(17): 3380-3390.

Cox, D. N., S. A. Seyfried, L. Y. Jan and Y. N. Jan (2001). "Bazooka and atypical protein kinase C are required to regulate oocyte differentiation in the Drosophila ovary." Proceedings of the National Academy of Sciences of the United States of America **98**(25): 14475-14480.

de Cuevas, M., M. A. Lilly and A. C. Spradling (1997). "Germline cyst formation in Drosophila." Annu Rev Genet **31**: 405-428.

de Cuevas, M. and E. L. Matunis (2011). "The stem cell niche: lessons from the Drosophila testis." Development **138**(14): 2861-2869.

de Cuevas, M. and A. C. Spradling (1998). "Morphogenesis of the Drosophila fusome and its implications for oocyte specification." Development **125**(15): 2781-2789.

Demarco, R. S., Å. H. Eikenes, K. Haglund and D. L. Jones (2014). "Investigating spermatogenesis in Drosophila melanogaster." Methods **68**(1): 218-227.

Deng, W. and H. Lin (1997). "Spectrosomes and Fusomes Anchor Mitotic Spindles during Asymmetric Germ Cell Divisions and Facilitate the Formation of a Polarized Microtubule Array for Oocyte Specification in Drosophila." Developmental Biology **189**(1): 79-94.

Dix, C. I. and J. W. Raff (2007). "Drosophila Spd-2 Recruits PCM to the Sperm Centriole, but Is Dispensable for Centriole Duplication." Current Biology **17**(20): 1759-1764.

Dorner, C., T. Ciossek, S. Müller, N. P. H. Møller, A. Ullrich and R. Lammers (1998). "Characterization of KIF1C, a New Kinesin-like Protein Involved in Vesicle Transport from the Golgi Apparatus to the Endoplasmic Reticulum." Journal of Biological Chemistry **273**(32): 20267-20275.

Dubielecka, P. M., K. Stebelska, B. Jazwiec and A. F. Sikorski (2003). Cystocyte and lymphocyte derived fusomes/spectrosomes: analogies and differences: a mini-review. **8:** 221-229.

Eggert, U. S., T. J. Mitchison and C. M. Field (2006). "Animal cytokinesis: from parts list to mechanisms." Annu Rev Biochem **75**: 543-566.

Fabian, L. and J. A. Brill (2012). "Drosophila spermiogenesis: Big things come from little packages." Spermatogenesis **2**(3): 197-212.

Fleming, E. S., M. Zajac, D. M. Moschenross, D. C. Montrose, D. W. Rosenberg, A. E. Cowan and J. S. Tirnauer (2007). "Planar Spindle Orientation and Asymmetric Cytokinesis in the Mouse Small Intestine." Journal of Histochemistry & Cytochemistry **55**(11): 1173-1180.

Fu, J. and D. M. Glover (2012). "Structured illumination of the interface between centriole and peri-centriolar material." Open Biology **2**(8): 120104.

Fuller, M. T. and A. C. Spradling (2007). "Male and Female Drosophila Germline Stem Cells: Two Versions of Immortality." Science **316**(5823): 402-404.

Gao, C. and Y.-G. Chen (2010). "Dishevelled: The hub of Wnt signaling." Cellular Signalling **22**(5): 717-727.

Greenspan, R. J. (2004). Fly pushing : the theory and practice of Drosophila genetics. Cold Spring Harbor, N.Y., Cold Spring Harbor Laboratory Press.

Groden, J., A. Thliveris, W. Samowitz, M. Carlson, L. Gelbert, H. Albertsen, G. Joslyn, J. Stevens, L. Spirio, M. Robertson and et al. (1991). "Identification and characterization of the familial adenomatous polyposis coli gene." Cell **66**(3): 589-600.

Gumbiner, B. M. (1998). "Propagation and localization of Wnt signaling." Curr Opin Genet Dev **8**(4): 430-435.

Habas, R. and I. Dawid (2005). "Dishevelled and Wnt signaling: is the nucleus the final frontier?" Journal of Biology **4**(1): 2.

Hamada, F. and M. Bienz (2002). "A Drosophila APC tumour suppressor homologue functions in cellular adhesion." Nature Cell Biology **4**(3): 208-213.

He, S. H., D. Nakada and S. J. Morrison (2009). Mechanisms of Stem Cell Self-Renewal. Annual Review of Cell and Developmental Biology. Palo Alto, Annual Reviews. **25:** 377-406.

Hennig, W. (1996). "Spermatogenesis in Drosophila." Int J Dev Biol **40**(1): 167-176.

Herrera, S. C., R. Martin and G. Morata (2013). "Tissue homeostasis in the wing disc of Drosophila melanogaster: immediate response to massive damage during development." PLoS Genet **9**(4): e1003446.

Hinchcliffe, E. H., F. J. Miller, M. Cham, A. Khodjakov and G. Sluder (2001). "Requirement of a centrosomal activity for cell cycle progression through G1 into S phase." Science **291**(5508): 1547-1550.

Hirokawa, N., Y. Noda, Y. Tanaka and S. Niwa (2009). "Kinesin superfamily motor proteins and intracellular transport." Nat Rev Mol Cell Biol **10**(10): 682-696.

Hsu, Y.-C., L. Li and E. Fuchs (2014). "Emerging interactions between skin stem cells and their niches." Nat Med **20**(8): 847-856.

Ikuta, J., N. K. Kamisetty, H. Shintaku, H. Kotera, T. Kon and R. Yokokawa (2014). "Tug-of-war of microtubule filaments at the boundary of a kinesin- and dynein-patterned surface." Sci. Rep. **4**: srep05281.

Inaba, M., Z. G. Venkei and Y. M. Yamashita (2015). "The polarity protein Baz forms a platform for the centrosome orientation during asymmetric stem cell division in the Drosophila male germline." Elife **4**: eLife.04960.

Inaba, M., H. Yuan, V. Salzmann, M. T. Fuller and Y. M. Yamashita (2010). "E-Cadherin Is Required for Centrosome and Spindle Orientation in *Drosophila* Male Germline Stem Cells." PLoS ONE **5**(8): e12473.

Januschke, J., S. Llamazares, J. Reina and C. Gonzalez (2011). "Drosophila neuroblasts retain the daughter centrosome." Nat Commun **2**: 243.

Joglekar, A. P., H.-h. Liu, E. Meyhöfer, G. Mourou and A. J. Hunt (2004). "Optics at critical intensity: Applications to nanomorphing." Proceedings of the National Academy of Sciences of the United States of America **101**(16): 5856-5861.

Ke, K., J. Cheng and A. J. Hunt (2009). "The distribution of polar ejection forces determines the amplitude of chromosome directional instability." Curr Biol **19**(10): 807-815.

Kellogg, D. R., M. Moritz and B. M. Alberts (1994). "The Centrosome and Cellular Organization." Annual Review of Biochemistry **63**(1): 639-674.

Khodjakov, A., R. W. Cole, B. R. Oakley and C. L. Rieder (2000). "Centrosome-independent mitotic spindle formation in vertebrates." Curr Biol **10**(2): 59-67.

Khodjakov, A., C. L. Rieder, G. Sluder, G. Cassels, O. Sibon and C. L. Wang (2002). "De novo formation of centrosomes in vertebrate cells arrested during S phase." J Cell Biol **158**(7): 1171-1181.

Kiger, A. A., D. L. Jones, C. Schulz, M. B. Rogers and M. T. Fuller (2001). "Stem Cell Self-Renewal Specified by JAK-STAT Activation in Response to a Support Cell Cue." Science **294**(5551): 2542-2545.

Kikuchi, K., Y. Niikura, K. Kitagawa and A. Kikuchi (2010). "Dishevelled, a Wnt signalling component, is involved in mitotic progression in cooperation with Plk1." The EMBO Journal **29**(20): 3470-3483.

Kirkwood, T. B. (2005). "Understanding the odd science of aging." Cell **120**(4): 437-447.

Kiyomitsu, T. and I. M. Cheeseman (2012). "Chromosome and spindle pole-derived signals generate an intrinsic code for spindle position and orientation." Nature cell biology **14**(3): 311-317.

Kotak, S., C. Busso and P. Gönczy (2012). "Cortical dynein is critical for proper spindle positioning in human cells." The Journal of Cell Biology **199**(1): 97-110.

Kuang, S., K. Kuroda, F. Le Grand and M. A. Rudnicki (2007). "Asymmetric Self-Renewal and Commitment of Satellite Stem Cells in Muscle." Cell **129**(5): 999-1010.

Kunttas-Tatli, E., M.-N. Zhou, S. Zimmerman, O. Molinar, F. Zhouzheng, K. Carter, M. Kapur, A. Cheatle, R. Decal and B. M. McCartney (2012). "Destruction Complex Function in the Wnt Signaling Pathway of Drosophila Requires Multiple Interactions Between Adenomatous Polyposis Coli 2 and Armadillo." Genetics **190**(3): 1059-1075.

Laan, L., N. Pavin, J. Husson, G. Romet-Lemonne, M. van Duijn, M. P. López, R. D. Vale, F. Jülicher, S. L. Reck-Peterson and M. Dogterom (2012). "Cortical Dynein Controls Microtubule Dynamics to Generate Pulling Forces that Reliably Position Microtubule Asters." Cell **148**(3): 502-514.

Lechler, T. and E. Fuchs (2005). "Asymmetric cell divisions promote stratification and differentiation of mammalian skin." Nature **437**(7056): 275-280.

Lee, L., J. S. Tirnauer, J. Li, S. C. Schuyler, J. Y. Liu and D. Pellman (2000). "Positioning of the Mitotic Spindle by a Cortical-Microtubule Capture Mechanism." Science **287**(5461): 2260-2262.

Lee, T. and L. Luo (1999). "Mosaic analysis with a repressible cell marker for studies of gene function in neuronal morphogenesis." Neuron **22**(3): 451-461.

Lee, T. and L. Luo (2001). "Mosaic analysis with a repressible cell marker (MARCM) for Drosophila neural development." Trends Neurosci **24**(5): 251-254.

Li, D. Q., Z. Wang, K. C. Yoon and F. Bian (2014). "Characterization, isolation, expansion and clinical therapy of human corneal epithelial stem/progenitor cells." J Stem Cells **9**(2): 79-91.

Li, M., Y. Zhao, H. Hao, W. Han and X. Fu (2015). "Mesenchymal stem cell based therapy for non-healing wounds: Today and tomorrow." Wound Repair Regen: wrr.12304.

Lighthouse, D. V., M. Buszczak and A. C. Spradling (2008). "New components of the Drosophila fusome suggest it plays novel roles in signaling and transport." Developmental Biology **317**(1): 59-71.

Lin, H. (2002). "The stem-cell niche theory: lessons from flies." Nat Rev Genet **3**(12): 931-940.

Lin, H. and A. C. Spradling (1995). "Fusome asymmetry and oocyte determination in Drosophila." Dev Genet **16**(1): 6-12.

Lin, H., L. Yue and A. C. Spradling (1994). "The Drosophila fusome, a germline-specific organelle, contains membrane skeletal proteins and functions in cyst formation." Development **120**(4): 947-956.

Liu, L. and T. A. Rando (2011). "Manifestations and mechanisms of stem cell aging." The Journal of Cell Biology **193**(2): 257-266.

Longoria, R. A. and G. T. Shubeita (2013). "Cargo Transport by Cytoplasmic Dynein Can Center Embryonic Centrosomes." PLoS ONE **8**(7): e67710.

López-Onieva, L., A. Fernández-Miñán and A. González-Reyes (2008). "Jak/Stat signalling in niche support cells regulates dpp transcription to control germline stem cell maintenance in the Drosophila ovary." Development **135**(3): 533-540.

Lord, C., S. Ferro-Novick and E. A. Miller (2013). "The Highly Conserved COPII Coat Complex Sorts Cargo from the Endoplasmic Reticulum and Targets It to the Golgi." Cold Spring Harbor Perspectives in Biology **5**(2): a01336.

Lucas, E. P. and J. W. Raff (2007). "Maintaining the proper connection between the centrioles and the pericentriolar matrix requires Drosophila Centrosomin." The Journal of Cell Biology **178**(5): 725-732.

Marthiens, V., I. Kazanis, L. Moss, K. Long and C. ffrench-Constant (2010). "Adhesion molecules in the stem cell niche - more than just staying in shape?" Journal of Cell Science **123**(10): 1613-1622.

Matsuoka *, Y., X. Li and V. Bennett (2000). "Adducin: structure, function and regulation." Cellular and Molecular Life Sciences **57**(6): 884-895.

McCartney, B. M., H. A. Dierick, C. Kirkpatrick, M. M. Moline, A. Baas, M. Peifer and A. Bejsovec (1999). "Drosophila Apc2 Is a Cytoskeletally-Associated Protein That Regulates Wingless Signaling in the Embryonic Epidermis." The Journal of Cell Biology **146**(6): 1303-1318.

McCartney, B. M., D. G. McEwen, E. Grevengoed, P. Maddox, A. Bejsovec and M. Peifer (2001). "Drosophila APC2 and Armadillo participate in tethering mitotic spindles to cortical actin." Nat Cell Biol **3**(10): 933-938.

McKearin, D. (1997). "The Drosophila fusome, organelle biogenesis and germ cell differentiation: if you build it." Bioessays **19**(2): 147-152.

McNally, F. J. (2013). "Mechanisms of spindle positioning." The Journal of Cell Biology **200**(2): 131-140.

Megraw, T. L., L.-R. Kao and T. C. Kaufman (2001). "Zygotic development without functional mitotic centrosomes." Current Biology **11**(2): 116-120.

Megraw, T. L., S. Kilaru, F. R. Turner and T. C. Kaufman (2002). "The centrosome is a dynamic structure that ejects PCM flares." Journal of Cell Science **115**(23): 4707-4718.

Megraw, T. L., K. Li, L. R. Kao and T. C. Kaufman (1999). "The centrosomin protein is required for centrosome assembly and function during cleavage in Drosophila." Development **126**(13): 2829-2839.

Miller, R. K. and M. D. Rose (1998). "Kar9p Is a Novel Cortical Protein Required for Cytoplasmic Microtubule Orientation in Yeast." The Journal of Cell Biology **140**(2): 377-390.

Morrison, E. E., B. N. Wardleworth, J. M. Askham, A. F. Markham and D. M. Meredith (1998). "EB1, a protein which interacts with the APC tumour suppressor, is associated with the microtubule cytoskeleton throughout the cell cycle." Oncogene **17**(26): 3471-3477.

Morrison, S. J. and J. Kimble (2006). "Asymmetric and symmetric stem-cell divisions in development and cancer." Nature **441**(7097): 1068-1074.

Morrison, S. J., N. M. Shah and D. J. Anderson (1997). "Regulatory Mechanisms in Stem Cell Biology." Cell **88**(3): 287-298.

Morrison, S. J. and A. C. Spradling (2008). "Stem Cells and Niches: Mechanisms That Promote Stem Cell Maintenance throughout Life." Cell **132**(4): 598-611.

Munemitsu, S., B. Souza, O. Muller, I. Albert, B. Rubinfeld and P. Polakis (1994). "The APC gene product associates with microtubules in vivo and promotes their assembly in vitro." Cancer Res **54**(14): 3676-3681.

Nadig, R. R. (2009). "Stem cell therapy – Hype or hope? A review." Journal of Conservative Dentistry : JCD **12**(4): 131-138.

Neumüller, R. A. and J. A. Knoblich (2009). "Dividing cellular asymmetry: asymmetric cell division and its implications for stem cells and cancer." Genes & Development **23**(23): 2675-2699.

Ottone, C., B. Krusche, A. Whitby, M. Clements, G. Quadrato, M. E. Pitulescu, R. H. Adams and S. Parrinello (2014). "Direct cell-cell contact with the vascular niche maintains quiescent neural stem cells." Nat Cell Biol **16**(11): 1045-1056.

Palmer, K. J., P. Watson and D. J. Stephens (2005). "The role of microtubules in transport between the endoplasmic reticulum and Golgi apparatus in mammalian cells." Biochem Soc Symp(72): 1-13.

PARDAL, R., A. V. MOLOFSKY, S. HE and S. J. MORRISON (2005). "Stem Cell Self-Renewal and Cancer Cell Proliferation Are Regulated by Common Networks That Balance the Activation of Proto-oncogenes and Tumor Suppressors." Cold Spring Harbor Symposia on Quantitative Biology **70**: 177-185.

Pariser, H., G. Herradon, L. Ezquerra, P. Perez-Pinera and T. F. Deuel (2005). "Pleiotrophin regulates serine phosphorylation and the cellular distribution of β-adducin through activation of protein kinase C." Proceedings of the National Academy of Sciences of the United States of America **102**(35): 12407-12412.

Pariser, H., P. Perez-Pinera, L. Ezquerra, G. Herradon and T. F. Deuel (2005). "Pleiotrophin stimulates tyrosine phosphorylation of β-adducin through inactivation of the transmembrane receptor protein tyrosine phosphatase β/ζ." Biochemical and Biophysical Research Communications **335**(1): 232-239.

Petrella, L. N., T. Smith-Leiker and L. Cooley (2007). "The Ovhts polyprotein is cleaved to produce fusome and ring canal proteins required for Drosophila oogenesis." Development **134**(4): 703-712.

Quyn, A. J., P. L. Appleton, F. A. Carey, R. J. C. Steele, N. Barker, H. Clevers, R. A. Ridgway, O. J. Sansom and I. S. Näthke (2010). "Spindle Orientation Bias in Gut Epithelial Stem Cell Compartments Is Lost in Precancerous Tissue." Cell Stem Cell **6**(2): 175-181.

Raaijmakers, J. A., R. G. H. P. van Heesbeen, J. L. Meaders, E. F. Geers, B. Fernandez-Garcia, R. H. Medema and M. E. Tanenbaum (2012). "Nuclear envelope-associated dynein drives prophase centrosome separation and enables Eg5-independent bipolar spindle formation." The EMBO Journal **31**(21): 4179-4190.

Rabelink, T. J. and M. H. Little (2013). "Stromal cells in tissue homeostasis: balancing regeneration and fibrosis." Nat Rev Nephrol **9**(12): 747-753.

Radtke, F. and H. Clevers (2005). "Self-Renewal and Cancer of the Gut: Two Sides of a Coin." Science **307**(5717): 1904-1909.

Rattis, F. M., C. Voermans and T. Reya (2004). "Wnt signaling in the stem cell niche." Curr Opin Hematol **11**(2): 88-94.

Rattner, J. B. and S. G. Phillips (1973). "INDEPENDENCE OF CENTRIOLE FORMATION AND DNA SYNTHESIS." The Journal of Cell Biology **57**(2): 359-372.

Raymond, K., M. A. Deugnier, M. M. Faraldo and M. A. Glukhova (2009). "Adhesion within the stem cell niches." Curr Opin Cell Biol **21**(5): 623-629.

Riparbelli, M. G. and G. Callaini (2011). "Male gametogenesis without centrioles." Developmental Biology **349**(2): 427-439.

Roberts, D. M., M. I. Pronobis, K. M. Alexandre, G. C. Rogers, J. S. Poulton, D. E. Schneider, K.-C. Jung, D. J. McKay and M. Peifer (2012). "Defining Components of the ßcatenin Destruction Complex and Exploring Its Regulation and Mechanisms of Action during Development." PLoS ONE **7**(2): e31284.

Sacco, A. and P. L. Puri (2015). "Regulation of Muscle Satellite Cell Function in Tissue Homeostasis and Aging." Cell Stem Cell **16**(6): 585-587.

Sheng, X. R., T. Posenau, J. J. Gumulak-Smith, E. Matunis, M. Van Doren and M. Wawersik (2009). "Jak–STAT regulation of male germline stem cell establishment during Drosophila embryogenesis." Developmental Biology **334**(2): 335-344.

Shivdasani, A. A. and P. W. Ingham (2003). "Regulation of stem cell maintenance and transit amplifying cell proliferation by tgf-beta signaling in Drosophila spermatogenesis." Curr Biol **13**(23): 2065-2072.

Siller, K. H. and C. Q. Doe (2008). "Lis1/dynactin regulates metaphase spindle orientation in Drosophila neuroblasts." Developmental Biology **319**(1): 1-9.

Siller, K. H., M. Serr, R. Steward, T. S. Hays and C. Q. Doe (2005). "Live Imaging of Drosophila Brain Neuroblasts Reveals a Role for Lis1/Dynactin in Spindle Assembly and Mitotic Checkpoint Control." Molecular Biology of the Cell **16**(11): 5127-5140.

Simons, Benjamin D. and H. Clevers (2011). "Strategies for Homeostatic Stem Cell Self-Renewal in Adult Tissues." Cell **145**(6): 851-862.

Singh, S. R. (2012). "Stem cell niche in tissue homeostasis, aging and cancer." Curr Med Chem **19**(35): 5965-5974.

Sitaram, P., M. A. Anderson, J. N. Jodoin, E. Lee and L. A. Lee (2012). "Regulation of dynein localization and centrosome positioning by Lis-1 and asunder during Drosophila spermatogenesis." Development **139**(16): 2945-2954.

Smith, E., N. Hégarat, C. Vesely, I. Roseboom, C. Larch, H. Streicher, K. Straatman, H. Flynn, M. Skehel, T. Hirota, R. Kuriyama and H. Hochegger (2011). "Differential control of Eg5-dependent centrosome separation by Plk1 and Cdk1." The EMBO Journal **30**(11): 2233-2245.

Smith, K. J., D. B. Levy, P. Maupin, T. D. Pollard, B. Vogelstein and K. W. Kinzler (1994). "Wild-type but not mutant APC associates with the microtubule cytoskeleton." Cancer Res **54**(14): 3672-3675.

Snapp, E. L., T. Iida, D. Frescas, J. Lippincott-Schwartz and M. A. Lilly (2004). "The Fusome Mediates Intercellular Endoplasmic Reticulum Connectivity in Drosophila Ovarian Cysts." Molecular Biology of the Cell **15**(10): 4512-4521.

Spradling, A., M. T. Fuller, R. E. Braun and S. Yoshida (2011). "Germline Stem Cells." Cold Spring Harbor Perspectives in Biology **3**(11): a002642.

Spradling, A. C., T. Nystul, D. Lighthouse, L. Morris, D. Fox, R. Cox, T. Tootle, R. Frederick and A. Skora (2008). "Stem Cells and Their Niches: Integrated Units That Maintain Drosophila Tissues." Cold Spring Harbor Symposia on Quantitative Biology **73**: 49-57.

Stevens, N. R., A. A. Raposo, R. Basto, D. St Johnston and J. W. Raff (2007). "From stem cell to embryo without centrioles." Curr Biol **17**(17): 1498-1503.

Su, L. K., M. Burrell, D. E. Hill, J. Gyuris, R. Brent, R. Wiltshire, J. Trent, B. Vogelstein and K. W. Kinzler (1995). "APC binds to the novel protein EB1." Cancer Res **55**(14): 2972-2977.

Tanentzapf, G., D. Devenport, D. Godt and N. H. Brown (2007). "Integrin-dependent anchoring of a stem-cell niche." Nat Cell Biol **9**(12): 1413-1418.

Tang, N. and W. F. Marshall (2012). "Centrosome positioning in vertebrate development." Journal of Cell Science **125**(21): 4951-4961.

Trounson, A., R. Thakar, G. Lomax and D. Gibbons (2011). "Clinical trials for stem cell therapies." BMC Medicine **9**(1): 52.

Tsai, J.-W., K. H. Bremner and R. B. Vallee (2007). "Dual subcellular roles for LIS1 and dynein in radial neuronal migration in live brain tissue." Nat Neurosci **10**(8): 970-979.

Tulina, N. and E. Matunis (2001). "Control of Stem Cell Self-Renewal in Drosophila Spermatogenesis by JAK-STAT Signaling." Science **294**(5551): 2546-2549.

Vaizel-Ohayon, D. and E. D. Schejter (1999). "Mutations in centrosomin reveal requirements for centrosomal function during early Drosophila embryogenesis." Current Biology **9**(16): 889-898.

Van Zant, G. and Y. Liang (2003). "The role of stem cells in aging." Exp Hematol **31**(8): 659-672.

Wallingford, J. B. and R. Habas (2005). "The developmental biology of Dishevelled: an enigmatic protein governing cell fate and cell polarity." Development **132**(20): 4421-4436.

Walston, T., C. Tuskey, L. Edgar, N. Hawkins, G. Ellis, B. Bowerman, W. Wood and J. Hardin (2004). "Multiple Wnt Signaling Pathways Converge to Orient the Mitotic Spindle in Early C. elegans Embryos." Developmental Cell **7**(6): 831-841.

Watson, P. and D. J. Stephens (2005). "ER-to-Golgi transport: Form and formation of vesicular and tubular carriers." Biochimica et Biophysica Acta (BBA) - Molecular Cell Research **1744**(3): 304-315.

Watt, F. M., Hogan and B. L. M. (2000). "Out of Eden: Stem Cells and Their Niches." Science **287**(5457): 1427-1430.

Wu, J., G. Misra, R. J. Russell, A. J. C. Ladd, T. P. Lele and R. B. Dickinson (2011). "Effects of dynein on microtubule mechanics and centrosome positioning." Molecular Biology of the Cell **22**(24): 4834-4841.

Wu, J. S. and L. Luo (2007). "A protocol for mosaic analysis with a repressible cell marker (MARCM) in Drosophila." Nat. Protocols **1**(6): 2583-2589.

Xie, T., E. Kawase, D. Kirilly and M. D. Wong (2005). "Intimate relationships with their neighbors: Tales of stem cells in Drosophila reproductive systems." Developmental Dynamics **232**(3): 775-790.

Yamashita, Y. M. (2009). "Regulation of asymmetric stem cell division: spindle orientation and the centrosome." Frontiers in bioscience : a journal and virtual library **14**: 3003-3011.

Yamashita, Y. M. (2010). "Cell adhesion in regulation of asymmetric stem cell division." Current Opinion in Cell Biology **22**(5): 605-610.

Yamashita, Y. M., M. T. Fuller and D. L. Jones (2005). "Signaling in stem cell niches: lessons from the Drosophila germline." Journal of Cell Science **118**(4): 665-672.

Yamashita, Y. M., D. L. Jones and M. T. Fuller (2003). "Orientation of asymmetric stem cell division by the APC tumor suppressor and centrosome." Science **301**(5639): 1547-1550.

Yamashita, Y. M., A. P. Mahowald, J. R. Perlin and M. T. Fuller (2007). "Asymmetric inheritance of mother versus daughter centrosome in stem cell division." Science **315**(5811): 518-521.

Yamashita, Y. M., H. Yuan, J. Cheng and A. J. Hunt (2010). "Polarity in Stem Cell Division: Asymmetric Stem Cell Division in Tissue Homeostasis." Cold Spring Harbor Perspectives in Biology **2**(1): a001313.

Yanagawa, S., F. van Leeuwen, A. Wodarz, J. Klingensmith and R. Nusse (1995). "The dishevelled protein is modified by wingless signaling in Drosophila." Genes & Development **9**(9): 1087-1097.

Yuan, H., C. Y. Chiang, J. Cheng, V. Salzmann and Y. M. Yamashita (2012). "Regulation of cyclin A localization downstream of Par-1 function is critical for the centrosome orientation checkpoint in Drosophila male germline stem cells." Dev Biol **361**(1): 57-67.

Zebrowski, D. C. and F. B. Engel (2013). "The cardiomyocyte cell cycle in hypertrophy, tissue homeostasis, and regeneration." Rev Physiol Biochem Pharmacol **165**: 67-96.

VII. APPENDIX

Copyright Permission: Authors are the copy right holders (see underlined texts) & Creative Commons 4.0

PLOS.ORG PLOS JOURNALS ABOUT CONTACT LOGIN

PLOS | BLOGS

Wednesday, July 15, 2015 | The PLOS ONE Community Blog

Home STAFF BLOGS ↓ BLOGS NETWORK ↓ COMMUNITY ↓ Search RSS FEED

EveryONE

PLOS | ONE community blog

OPEN ACCESS

www.plosone.org

Home About EveryONE Frequently Asked Questions Media Conferences

← Next Steps in Reproducibility

Our 200,000-Year-Old Ancestors: Neanderthal Bones in Northern France →

The Rights Stuff: Copyright, Scientific Debate, and Reuse

By Damian Pattinson and Cameron Neylon
Posted: November 19, 2014

Hello there! If you enjoy the content on EveryONE, consider subscribing for future posts via **email** or **RSS feed**.

We've all monkeyed around trying to sort out the ownership of published content. In the scientific community, copyright and its (mis)application in publishing has authors, publishers, and readers grappling with questions of what is legally possible, what is desirable, and what is "allowable" by any particular party.

The most recent example of these challenges can be found in a *PLOS ONE* article published yesterday by Stirling et al., which focuses on a re-analysis of images used by other research groups as evidence for the creation of "striped nanoparticles". The scientific controversy is fascinating and has been covered on blogs and in social media, but the copyright issues that cropped up during the paper's publication process are also noteworthy.

In the study, the authors re-analyzed key results from previous work written up in the literature by other researchers and wanted to share their findings by publishing them, formally adding to the scientific literature on nanoparticles. To provide context and more effectively discuss the data, the authors of the re-analysis included figures (images) from previous studies in their own paper. However, the original figures were published in journals that owned the copyright of all the written content. And here is where we ran into a problem, and one that was far from simple.

Search EveryONE

Search

Recent Posts

- PLOS ONE's Top 5 Videos of 2015 (So Far)
- PLOS Recommended Data Repositories
- I Know What You Think: Collective Intelligence in Online Communication
- Flight of the Bats: Exploring Head Shape and Aerodynamics
- Small Talk: When Bacterial Chatter Gets Invasive
- Zoom-Enhance: Identifying Trends in Article-Level Metrics
- Biting Off What They Can Chew: Scientists Use 3D Reconstructions to Study Animal Jaw Mechanics
- PLOS ONE Update on Peer Review Process
- Fun(d) with Science
- Earth Day 2015: Celebrating Our Awe Inspiring World

Categories

- Aggregators
- Article-Level Metrics
- Ask EveryONE
- Author Spotlight
- Awards
- Blog Pick of the Month
- Collections
- Conferences

Stay Connected

PLOS ONE on Twitter
Article E-mail Alerts
PLOS ONE Articles RSS
Visit PLOSONE.org
PLOS on Twitter
PLOS on Facebook
PLOS on LinkedIn
Get PLOS.org Updates

Tags

Academic Editor Help Aggregators animal behavior archaeology Article-Level Metrics AskEveryONE Author Help author spotlight Awards Awareness bacteria Behavior blogging Blog Pick of the Month Blogs cancer citizen science climate change Collections conservation ecology Editor's choice Editorial Manager FAQ Featured Image fish fossils Functionality Halloween how to insects language Media music new species Open Access paleontology Peer review peer reviewers PLoS ONE PLoS ONE Video Shorts

Copyright Permission (Ctd…)

Clearing rights for republication

These journals generally hold a copyright status of "all rights reserved". With this restriction, there are three possible ways that these figures *could be* incorporated into a newly published article.

1) The authors could declare that the reproduction is "fair use" or "fair dealing":

Traditionally, this hasn't been done for reproduction of single images from papers. The problem from a publisher's (and author's) perspective with this approach is that it isn't totally clear whether it applies in this case. Publishers are pretty risk averse about this kind of claim (as fair use is a defense against infringement rather than a license itself), so we usually prefer to ask permission.

2) The copyright holder could authorize a *specific* use under a *limited* license:

This is the traditional approach—the author would be responsible for negotiating a single use license from the rights holder. This will be a familiar experience to many authors who have written reviews that incorporate figures from other papers. It's common enough that there are online tools to speed up this kind of transaction.

3) The rights holder could authorize the image to be republished under an open license that allows extensive reuse, with the authors as the copyright holder:

PLOS uses a Creative Commons Attribution License (CC BY 4.0) specifically to cover this issue. With the Stirling, et al. paper, we worked with the authors and the publishers on taking this approach, and we want to say thank you to The Royal Society of Chemistry, Nature Publishing Group (NPG), Wiley Blackwell, and the American Chemical Society for working with us to enable the republication of the material. NPG has a standing policy that they will authorize re-publication of images under the same license as the rest of the article, something they've done for us in the past. The other publishers worked hard to make it possible on this occasion, giving approval a few weeks ago. We are very grateful for their efforts.

Why the fuss?

So why did PLOS push for option three when the second was more traditional? As Kevin Smith at Duke has pointed out, it's not a legal question or a problem with the Creative Commons licenses. It is perfectly possible to mark part of an article as being made available under a different copyright license. But as a question of *policy*, we make every effort to avoid mixing different licenses within articles.

We do this because, at the heart of PLOS's work on Open Access, is enabling re-use. Every day people grab newly published articles for various kinds of processing. Some are mining text for information, some are collecting images for use in other projects, and some are working on new forms of display and article presentation. Each of these depends on the downstream user having the rights to copy, store, and transmit the articles. All the articles. And all the pieces of the articles.

- Creative re-use
- Ecology
- Events
- Featured Image
- Fun
- Images
- Internet/Blogging
- Interviews
- Manuscript submission and peer review system
- Media
- Open Access
- Paleontology
- Peer review
- PLoS Editorial Manager
- Service improvements
- Social Media
- Submissions
- Topic Focus
- Worth A Thousand Words

Copyright Permission (ctd…)

On any given day, PLOS might publish a few hundred articles. It is certainly possible in principle to add a copyright statement to a single image. But downstream users would need to check every figure legend of every paper *by hand* to identify single images they aren't allowed to use. By insisting on a uniform CC BY license throughout, we give the downstream users clarity and confidence in their rights.

In a perfect world, there would be a clear and consistent machine-readable way of designating sections of an article and differing copyrights within them. But such a standard doesn't yet exist, and even if it did, there is still a clear advantage to the downstream user to have a uniform policy that grants largely unrestricted reuse.

This case has been both interesting and challenging for us and the authors (who we thank for their patience while we have addressed the licensing issues!). It has highlighted the need for publishers to be willing to authorize onward publication rights with reasonable flexibility as to the licensing arrangements. As the industry moves away from copyright assignment to "license to publish" arrangements, it is important that we get the details of those licenses right. There could be immense value in shared model "license to publish" agreements that would help consistency and support smaller publishers. Most importantly, we have learned the need for clear presentation of our legal and policy obligations when it comes to copyright and reuse.

About Damian Pattinson

Editorial Director, PLOS ONE

View all posts by Damian Pattinson →

About Cameron Neylon

View all posts by Cameron Neylon →

This entry was posted in Aggregators. Bookmark the permalink.

← Next Steps in Reproducibility

Our 200,000-Year-Old Ancestors: Neanderthal Bones in Northern France →

Copyright Permission (ctd…)

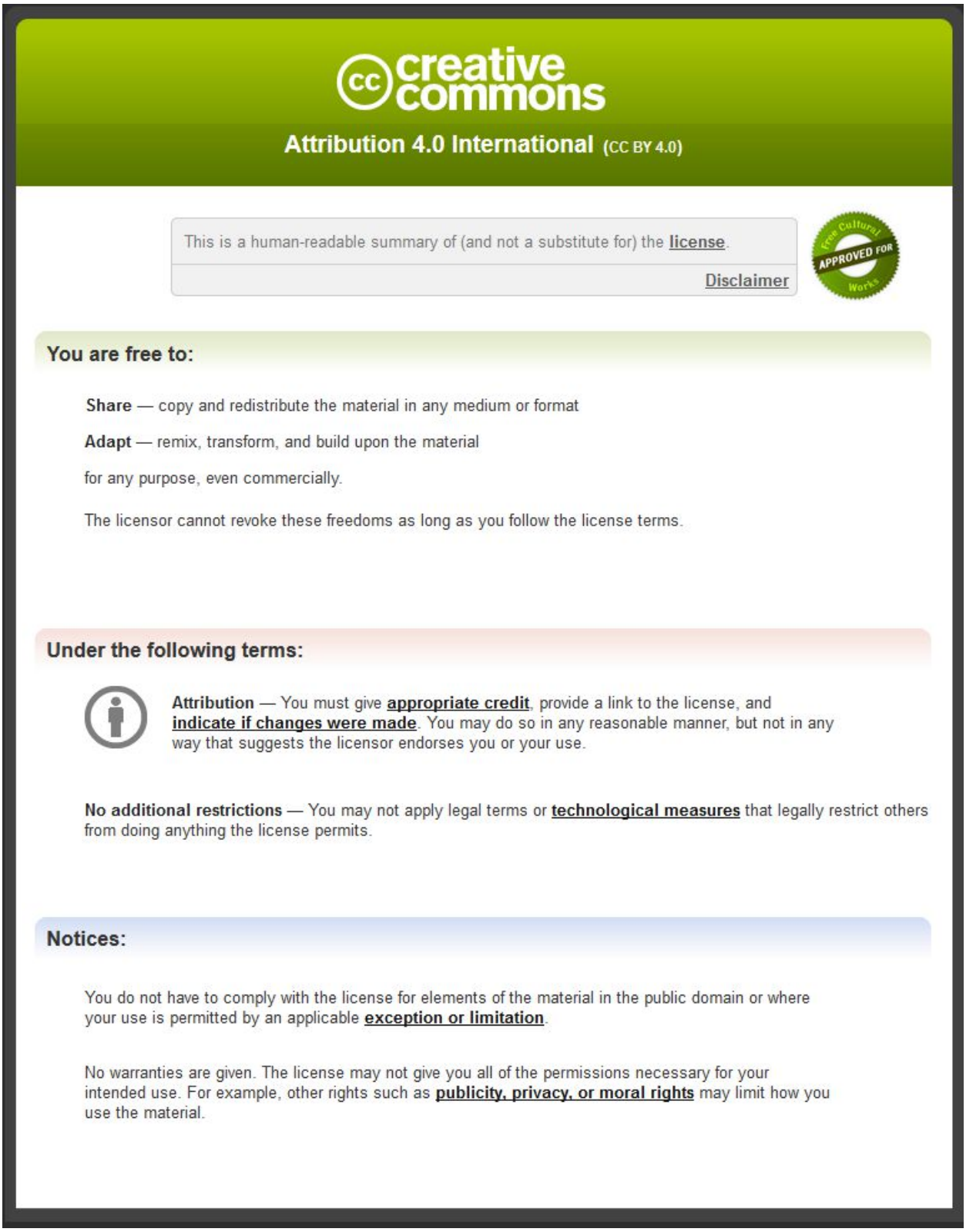

creative commons

Attribution 4.0 International (CC BY 4.0)

This is a human-readable summary of (and not a substitute for) the license.

Disclaimer

Free Cultural APPROVED FOR Works

You are free to:

Share — copy and redistribute the material in any medium or format

Adapt — remix, transform, and build upon the material

for any purpose, even commercially.

The licensor cannot revoke these freedoms as long as you follow the license terms.

Under the following terms:

Attribution — You must give **appropriate credit**, provide a link to the license, and **indicate if changes were made**. You may do so in any reasonable manner, but not in any way that suggests the licensor endorses you or your use.

No additional restrictions — You may not apply legal terms or **technological measures** that legally restrict others from doing anything the license permits.

Notices:

You do not have to comply with the license for elements of the material in the public domain or where your use is permitted by an applicable **exception or limitation**.

No warranties are given. The license may not give you all of the permissions necessary for your intended use. For example, other rights such as **publicity, privacy, or moral rights** may limit how you use the material.

VIII. VITA

Chi Bang

EDUCATION

BS, Bioengineering (ABET), December 2003
University of California, San Diego (UCSD)

MS, Biomedical Engineering, September 2004-2006
City College of New York (CCNY), GPA: 3.77/4.0

Ph.D Candidate, Bioengineering, Fall 2009-Present
University of Illinois at Chicago (UIC), GPA: 3.71/4.0

RESEARCH EXPERIENCE

Graduate Research Assistant, Lab of Dr. Jun Cheng at UIC, Chicago, IL, 5/11-present

Studied how spectrosomes and centrosomes regulate asymmetric stem cell division, which direct self-renewal and differentiation in *Drosophila* male gonads.

- Utilized genetic manipulation techniques to generate desirable genotypes in drosophila(mutants, knockouts, UAS-tagged systems, RNAi systems, fluorescent protein genes, Mosaic analysis with a repressible cell marker methods).
- Utilized ultrafast laser microsurgery to ablate subcellular structures.
- Utilized live-cell imaging (with epi-fluorescence) and confocal imaging modalities.
- Developed image processing and tracking programs to quantify structural details and migration pattern, respectively, for both confocal and time-lapse images (Labview & Matlab).
- Developed and tested Ultrafast laser microsurgery platform for intercellular organelles such as centrosome and spectrosome.

Graduate Research Assistant, Lab of Dr. Brenda Russell at UIC, Chicago, IL Supported by the National Institutes of Health grants T32 HL007692, R.J. Solaro (PI) 6/10-4/11

Quantified how stiffness and microprojections regulate micromechanical cell properties of Neonatal Rat Ventricular Myocyte (NRVM) such as beat frequency and shortening velocity.

Research Associate III, Biosite-Inverness, Inc., San Diego, CA, 1/07-11/08

- Assisted in diagnostic assay development and testing for High Sensitivity Troponin I and Myeloperoxidase.
  - Selected antibodies (through standard ELISA and Triage device testing) and analyzed data for quantitative assay performance.

- Characterized Triage device platform and performed failure mode analysis for possible trouble shooting.
  - Characterized flow and diffusion patterns to observe how these phenomena affect assay performance.
  - Characterized the effect of all possible blood/device contained chemicals/antigens/proteins that may potentially become problems.
  - Tested for temperature dependence, stability, reproducibility, and assembly settings.

Graduate Research Assistant (MS), City College of New York, New York, NY, 9/05-9/06

Developed and computed multi-physics mathematical models that predict fluid and solute transport across capillaries: revised Starling hypothesis.

Intern, Mount Sinai School of Medicine-Nephrology, New York, NY, 6/05-9/05

Observed affects the erb binding heregulin has on maturation and proliferation of the urothelium in in-vitro organ cultured kidneys.

Undergraduate Research Assistant, UCSD Vascular Molecular Bioengineering Laboratory, La Jolla, CA,3/03-7/04

Investigated the role mechanical forces have on proliferation and apoptosis molecular pathways of vascular smooth muscle cells and endothelial cells (aortic).

TEACHING EXPERIENCE (University of Illinois at Chicago)

Fall 2009	Teaching Assistant BioE 240: Physiologic Data and Modeling
Spring 2010	Teaching Assistant BioE 456: Cell & Tissue Engineering Laboratory
Spring 2012, 2013	Teaching Assistant BioE 430: Bioinstrumentation
Fall 2011, 2014 2015	Teaching Assistant BioE 525: Physiological and Cellular Effects of Biomechanical Forces

RESEARCH MENTORSHIP EXPERIENCE (University of Illinois at Chicago)

2011-2012 Nikhil Bommakanti (BioE Undergraduate Student)

Development of image processing programs to quantify the spectrosome size across multiple tissue layers.

2012-2013 Emerald Fikejs (Illinois Mathematics and Science Academy Student)

Development of tracking programs to track the migration pattern of spectrosome and centrosomes.

2013 Danielle Madsen (Illinois Mathematics and Science Academy Student)
Quantifying Locations of Centrosomes and Spectrosomes in APC2-mut Drosophila melanogaster during Asymmetrical Germline Stem Cell Division.

2014 Shilpa Colachina (UIC undergraduate student)
Quantified centrosome and spectrosome positioning in Cnn-mut Germline Stem Cells.

SKILLS AND TECHNIQUES

Molecular Biology and Protein Biochemistry Techniques

- Western blotting
- ELISA
- Paraffin tissue section
- Primer Design
- RNA Isolation
- 2-D Gel
- Immunoprecipitation
- PCR
- Agarose/PAGE-Gel
- HPLC

Cell Culture Techniques

- Rat Myocyte isolation and culture
- Embroynic Kidney Cultivation and In-vitro culture
- Drosophila male gonad isolation and culture
- BAEC isolation and culture
- RASMC, hMSC, HUVEC, hMSC culture
- Bacterial culture

Microscopy Techniques

- Confocal Microscopy
- Time-lapse live imaging
- Ultrafast laser microsurgery

Fabrication Methods

- Soft lithography techniques: SU-8, Parylene, and PDMS topography fabrication; PDMS micro-channel fabrication and testing.

Mechanical Stimulation

- Lateral flow shear stress chamber
- Customized mechanical strain device (uniaxial, biaxial, radial strain)
- Flexcell strain device (uniaxial, biaxial, radial strain)

Design and Mathematical Modeling

- Mathematical modeling and modeling programs (Partial differential equation, Finite difference methods, COMSOL Multiphysics, and Pro-Mechanica)
- Programming (Labview, Matlab, Maple, Mathematica, and FORTRAN)
- Technical Drawing (Auto-CAD and Pro-Engineer)

Data Acquisitions

- Statistics/statistics software (Excel, Sigma Plot,JMP, R, Analyze-It)
- Working knowledge of laboratory data acquisitions (Undergraduate Lab, Labview)

EXTRACURRICULAR ACTIVITIES

Member St. Columba Church Choir, CA: Bass 2003-2004, 2006-2009
Member St. Francis Assissi Church Choir, NY: Bass 2004-2006
Member Korean Martyr's Church, IL: Bass and Tenor 2009-2015

LEADERSHIP POSITIONS

Member, Graduate Student Council, Univ Illinois at Chicago 2013-2014

AWARDS and HONORS

- Fall 2011 Outstanding TA Award (Dept. of Bioengineering at Univ Illinois at Chicago)
- National Institute of Health T32 Institutional National Research Service Award Fellowship, 20 10-2011 (Univ Illinois at Chicago)
- Executive management's special discretionary bonus, 2007 (Biosite Inc., $3000)
- Tau Beta Pi Honor's Society: NY Eta, 2006 (Engineering, City College of New York)
- Provost's List, 2003: (Univ California at San Diego)

PRESENTED ABSTRACTS

- **Chi Bang** and Jun Cheng. "Spectrosome Dynamics in Asymmetric Stem Cell Division" Abstracts for the UIC College of Medicine Research 2014, Nov. 21th, 2014, Chicago, Illinois, USA
- **Chi Bang** and Jun Cheng. "Time-lapse Imaging Reveals the Role of Spectrosome and Centrosome in Asymmetric Stem Cell Division" Abstracts for the AAAS 2014 Annual Meeting, Feb. 13-17th, 2014, Chicago, Illinois, USA
- **Chi Bang** and Jun Cheng. "Time-lapse Imaging Reveals the Role of Spectrosome and Centrosome in Asymmetric Stem Cell Division" Abstracts for the UIC College of Medicine Research 2013, Nov. 20th, 2013, Chicago, Illinois, USA
- **Chi Bang** and Jun Cheng. "Time-lapse Imaging Reveals the Role of Spectrosome and Centrosome in Asymmetric Stem Cell Division" Abstracts for the BMES 2013 Annual Meeting, Sept. 25-28th, 2013, Seattle, Washington, USA
- **Chi Bang** and Jun Cheng. "Interplay of Spectrosome Organelle in Asymmetric Stem Cell Division" Abstracts for the 6th Annual Stem Cell and Regenerative Medicine Program, Sept. 20th, 2013, Chicago, Illinois, USA
- **Chi Bang** and Jun Cheng. "Role of Spectrosome and Centrosome Proteins in Asymmetric Stem Cell Division" Abstracts for the BMES Midwest Biomedical Engineering Career

Conference, 2013, April 19th, 2013, Chicago, Illinois, USA

- **Chi Bang** and Jun Cheng. "Living Tissue Microscope System Reveals Spectrosome's Role in Asymmetric Stem Cell Division" Abstracts for the UIC College of Medicine Research 2012, November 16th, 2012, Chicago, Illinois, USA
- **Chi Bang** and Jun Cheng. "Role of Spectrosome and Centrosome Proteins in Asymmetric Stem Cell Division" Abstracts for the 5th Annual Stem Cell and Regenerative Medicine Program, May 10th, 2012, Chicago, Illinois, USA
- **Chi Bang**, Zhinan Wang, Wei Shen, Jun Cheng. "The Biomedical Application of Ultrafast Laser Microsurgery and Time-Lapse Live-Imaging" Abstracts for the 9th Annual Chicago Biomedical Consortium Symposium (Engineering Biology: From Tools to Insights), October 21, 2011, Chicago, Illinois, USA
- X. Zhang, **C. Bang**, R. H. Adamson, F. E. Curry, S. Weinbaum. "Transient Regulation of Transport by Pericytes in Post Capillary Venules" Abstracts for the 8th World Congress for Microcirculation, August 15-19, 2007 Milwaukee, Wisconsin, USA

INVITED TALKS

- Chi Bang, Zhinan Wang, Wei Shen, Jun Cheng. 'Data Blitz', featuring short talks by selected poster presenter. "The Biomedical Application of Ultrafast Laser Microsurgery and Time-Lapse Live-Imaging" Abstracts for the 9th Annual Chicago Biomedical Consortium Symposium (Engineering Biology: From Tools to Insights), October 21, 2011, Chicago, Illinois, USA

PUBLICATIONS

- **Bang, C.** and J. Cheng (2015). "Dynamic Interplay of Spectrosome and Centrosome Organelles in Asymmetric Stem Cell Divisions." PLoS ONE **10**(4): e0123294.

- Yao, L.-H., Y. Rao, **C. Bang**, S. Kurilova, K. Varga, C.-Y. Wang, B. D. Weller, W. Cho, J. Cheng and L.-W. Gong (2013). "Actin Polymerization Does Not Provide Direct Mechanical Forces for Vesicle Fission during Clathrin-Mediated Endocytosis." The Journal of Neuroscience 33(40): 15793-15798.